Master's thesis

NTNU
Norwegian University of Science and Technology
Faculty of Natural Sciences
Department of Materials Science and Engineering

Tristan Petrus Maria Van Kaam

Effects of Pre-Oxidation on the Hydrogen Reduction of Ilmenite

Master's thesis in Materials Science and Engineering
Supervisor: Merete Tangstad
Co-supervisor: Stephen Lobo, Faan Du Preez
July 2023

NTNU
Norwegian University of
Science and Technology

Tristan Petrus Maria Van Kaam

Effects of Pre-Oxidation on the Hydrogen Reduction of Ilmenite

Master's thesis in Materials Science and Engineering
Supervisor: Merete Tangstad
Co-supervisor: Stephen Lobo, Faan Du Preez
July 2023

Norwegian University of Science and Technology
Faculty of Natural Sciences
Department of Materials Science and Engineering

NTNU
Norwegian University of
Science and Technology

Acknowledgements

First, I would like to thank my supervisors. Merete Tangstad, for giving me the opportunity and trust to write my thesis in South-Africa at HySA Infrastructure. She has always given valuable input and insight into the work conducted for the duration of the project. I would also like to thank Stephen Lobo, whom I have worked with on both my bachelor's thesis and now also my master's thesis. He has provided great discussion about results and given explanations for things I have had difficulty in understanding. Finally, I would like to thank my South-African supervisor Faan Du Preez for accommodating me at HySA Infrastructure and being a gracious host. He has allowed me to test my academic understanding and helped me throughout the entire project. All my best wishes go out to him and his family.

During my 6 month stay in South-Africa, I've been assisted by multiple individuals in conducting analysis and general discussion. I would like to thank Xolisa Goso for accommodating me at Mintek and my co-workers whom I met during my stay there. For conducting the analysis, I would like to thank René Bekker for ICP and particle size analysis, Innocent Shuro for allowing me to use the SEM, Makatu and Thabo for assistance with preparation, and Belinda Venter for the XRD and Rietveld analysis. As well as Adamantia Lazou for her feedback on the report. I would also like to thank all the people I've had the opportunity to meet and spend time with both in and outside of HySA.

Finally, I would like to thank my ever-expanding family, Meggie, Pierre, Minou, Sara, Jessie, Remco, Alex, Zandra, Linea, Chris, and my boiz Daniel and Lin, for supporting me and cheering me on.

-Tristan Petrus Maria van Kaam

"Slegs met die skouer aan die wiel, kan berge versit word"

-Unknown

Abstract

The pressure to make metallurgical processes more environmentally friendly is ever-increasing. This has led to research into replacing carbon monoxide as a reducing agent with other options. One gas that has shown potential as a replacement is hydrogen. Before the step can be taken in industry, it needs to be better understood which is where this master's thesis enters the stage.

This thesis examined the effects of oxidation on the hydrogen reduction of ilmenite. Two types of sand-ilmenite were used. One was obtained from Senegal, supplied by Eramet Titanium and Iron AS(GCO), and the other from KwaZulu-Natal(KZN) South-Africa, supplied by Mintek. Three oxidation temperatures were chosen to obtain different oxidation degrees, 700, 800, and 1000°C. GCO ilmenite was reduced at three temperatures to study the effect of reduction temperature, 800, 900, and 1000°C. KZN ilmenite was reduced at 800°C. Both were reduced under a hydrogen atmosphere in a horizontal alumina tube furnace with a flow rate of 2.4 l/min. The starting points, oxidized- and reduced samples, were examined with XRD, SEM, and ICP. The weight change occurring during oxidation and reduction was reported and formed the basis of the conclusions. The oxidized material was sent for XRF and wet chemical analysis at Eramet Titanium and Iron AS.

The GCO ilmenite showed little effect of pre-oxidation. The samples reduced at 800°C and oxidized at 700 and 800°C followed a similar reduction path to the as-received sample, while the sample oxidized at 1000°C showed signs of improved kinetics. At a reduction temperature of 900°C, the difference in the reduction path grew smaller. At 1000°C, the as-received sample reached the highest reduction degree with an O:Fe ratio of -0.25 compared to approximately -0.16 for the oxidized samples. The negative value corresponds to more oxygen being removed than what is connected to iron. From the Rietveld analysis, it became clear that initially, after 5 minutes of reduction, the ilmenite content increased before decreasing as the reduction time increased. The iron and rutile content increased with increasing reduction times. During SEM analysis, the iron distribution differed from no oxidation to the highest oxidation degree. Going from connected metallic iron to distributed throughout the grain in small globules.

The KZN ilmenite showed a greater difference in reduction progression depending on the oxidation degree. For the as-received sample and the 700°C oxidation, the sample had an O:Fe ratio of 0.39 and 0.46, respectively, after 60 minutes of reduction. The samples oxidized at 800, and 1000°C showed signs of complete reduction with an O:Fe ratio of 0.05. The oxidation at higher temperatures, 800 and 1000°C, was seen to improve reduction kinetics. The non-complete reduction was also reflected in the Rietveld analysis where ilmenite was found for both the as-received sample and the sample oxidized at 700°C. Similar trends were found in the KZN ilmenite as the GCO sample reduced at 800°C, where the ilmenite content initially increases before decreasing for longer reduction times. The iron and rutile content was observed to increase for all reduction times. The iron distribution depended on the oxidation temperature similar to the GCO ilmenite.

The GCO and KZN sample reduced at 800°C were dissolved with sulfuric acid and analyzed with ICP. The main difference found in the GCO sample was the iron and titanium concentration after 5 minutes of reduction. It was found to increase with increasing oxidation degree. As the reduction time increased the titanium dissolution decreased while the iron dissolution increased. The same could be said for the KZN sample. The main difference between the two types of ilmenite was that the KZN sample showed a greater effect of oxidation on the dissolution of iron compared to the GCO sample.

Contents

Acknowledgements **ii**

Abstract **iv**

Figure list **viii**

Symbol list **xii**

1 Introduction **1**
1.1 The Tyssedal process . . . 1
1.2 Scope of work . . . 2

2 Theory **3**
2.1 A literature study . . . 3
2.2 Fe-O system . . . 3
2.3 Iron oxidation and reduction . . . 4
2.3.1 Reaction progression . . . 4
2.3.2 Particle size dependency . . . 4
2.3.3 Effect of reducing agent on Fe-O reduction . . . 5
2.3.4 Morphology . . . 7
2.4 Ilmenite and its oxides . . . 9
2.4.1 Ilmenite(M_2O_3) . . . 10
2.4.2 Pseudobrooktite(M_3O_5) . . . 10
2.4.3 Titanium oxides(Ti_nO_{2n-1}) . . . 11
2.4.4 Pseudorutile/H239($Fe_2Ti_3O_9$) . . . 14
2.5 Ilmenite oxidation . . . 16
2.5.1 Chemical reactions . . . 16
2.5.2 Temperature dependence . . . 17
2.5.3 Morphology changes . . . 20
2.5.4 Particle size dependence . . . 23
2.6 Ilmenite reduction . . . 24
2.6.1 Reduction progression . . . 24
2.6.2 Parameters dependency . . . 26
2.6.3 Morphology . . . 28
2.7 Impurities . . . 31
2.7.1 Reduction . . . 31
2.8 Sulfuric acid leaching and the sulfate process . . . 33
2.9 Summary . . . 35

3 Method and Materials **36**
3.1 Materials . . . 36
3.1.1 Ilmenite concentrate . . . 36
3.1.2 Crucibles . . . 37
3.2 Methodology . . . 37
3.2.1 Oxidation . . . 37

3.2.2 Reduction . . . 38
3.2.3 X-Ray diffraction . . . 39
3.2.4 Secondary electron microscopy . . . 39
3.2.5 ICP-OES . . . 39

4 Results **41**
4.1 Starting material . . . 41
4.1.1 GCO ilmenite . . . 41
4.1.2 KZN ilmenite . . . 42
4.2 Understanding oxidation . . . 44
4.2.1 XRD and Rietveld analysis . . . 48
4.2.2 SEM and EDS analysis: Cross-section and topology . . . 49
4.3 Results from reduction . . . 56
4.3.1 Effect of oxidation temperature . . . 56
4.3.2 Effect of reduction temperature . . . 58
4.3.3 XRD and Rietveld analysis . . . 60
4.3.4 SEM and EDS . . . 62
4.3.5 Iron and titanium dissolution . . . 67
4.3.6 KZN ilmenite: Experimental data and analyses . . . 74

5 Discussion **80**
5.1 Differences in starting material . . . 80
5.2 GCO ilmenite: Discussion . . . 81
5.2.1 Micro-TGA results . . . 81
5.2.2 GCO Ilmenite oxidation . . . 82
5.2.3 Effect of oxidation temperature on reduction . . . 85
5.2.4 Effect of reduction temperature . . . 86
5.3 Analytical results for the GCO ilmenite . . . 87
5.3.1 XRD analysis . . . 88
5.3.2 SEM analysis . . . 88
5.3.3 Acid digestion . . . 90
5.4 Discussion of KZN sample and comparison to GCO ilmenite . . . 92
5.4.1 Oxidation . . . 92
5.4.2 Reduction . . . 94
5.4.3 Acid digestion . . . 95
5.5 Sources of error . . . 96
5.6 Future work . . . 97

6 Conclusion **98**

Bibliography **99**

A Hot acid leaching **104**

B XRD-analysis **106**

C SEM analysis **117**

Figure list

1.1 Flow sheet of the Tyssedal process, originally drawn by Solheim[1]. 1

2.1 Fe-Fe_2O_3 phase diagram based on results found by Darken and Gurry[9]. 3
2.2 Baur–Glässner diagram as constructed by Spreitzer and Schenk[10]. Including the Boudouard reaction, at 1 bar with carbon activity of 1. 5
2.3 Reduction of wüstite, to iron using different H_2/CO-gas mixtures at temperatures of 800°C(a), 900°C(b) and 1000°C(c)[18]. 6
2.4 Hematite(a) and magnetite(b) reduced with hydrogen gas[20]. 7
2.5 Temperature(°C) vs amount of argon in the reducing gas, (a) CO as a reducing agent, (b) H_2[21]. 8
2.6 The Ti_2O_3-Fe_2O_3 phase diagram as suggested by Rosenqvist[30], redrawn by Lobo[8]. 10
2.7 Ti_3O_5-Fe_2TiO_5 phase diagram, originally drawn by Borowiec and Rosenqvist[30], based on results found by Grey and Merritt[35], redrawn by Lobo[8]. 11
2.8 Diagram showing the equilibrium partial pressure of oxygen vs 1/T, with the equilibrium oxygen pressures for hydrogen and carbon monoxide reactant, drawn by Lobo[8]. 12
2.9 Calculated phase diagram for the Ti_2O_3-TiO_2 system, as found by Waldner and Eriksson[37]. 13
2.10 Comparison of values for oxygen potentials for different compositions of titanium oxide at 1000 degrees, given by Ketteridge[39]. 13
2.11 Schematic representation of the mechanism for ilmenite oxidation at temperatures below 900°C(a, b) and at high temperatures, above 900°C(c)[43]. 15
2.12 Chemical transformations of pseudorutile at different temperatures, as presented by Cheng and Gao[40]. 16
2.13 Simplification of oxidation path for ilmenite and pseudorutile, as presented by Gupta et. al.[27]. 17
2.14 Determination of products after oxidation at 800°C for 60 minutes, by Cheng and Gao[40]. 18
2.15 XRD result found by Choi and Parl[24] after 6 hours of oxidation. 19
2.16 Surface and cross sectional SEM image of a1), a2)ilmenite surface and cross section, b1, b2)ilmenite oxidised at 780°C surface and cross section, c1, c2) ilmenite oxidised at 900 surface and cross section[24]. 20
2.17 BET analysis of pre-oxidized ilmenite where a) is quenched upon reaching temperature and b) is calcined for three hours[25]. 21
2.18 BSE images obtained by Chen et. al.[24]. 22
2.19 BSE image and point analysis of the hematite layer that forms along the grain boundary, as found by Salehi et. al.[41]. 22
2.20 Oxidation of ilmenite at 800°C for 1-hour a) and 120 hours b), as found by Zhang et. al.[55]. 23
2.21 Weight change occurring during oxidation given a 5 gram sample, for different times and temperatures, a) 700°C, b) 850°C and c) 1000°C[26]. 24
2.22 Reduction curves for Panzhihua ilmenite at different temperatures[62]. 27

2.23 Reduction curves from Lobo[8] experiments, for pure hydrogen and pure carbon monoxide. . . . 27
2.24 Reduction curves as found by Wang et. al.[63], showing varying hydrogen content for natural ilmenite concentrate. . . . 28
2.25 Schematic drawing of the shrinking core model applied to ilmenite reduction, as drawn by Lobo[8]. . . . 28
2.26 Ilmenite from Egersund, Norway, reduced at 1100°C in a CO atmosphere for 5 minutes. Precipitated iron (white), oxide (gray)[34]. . . . 29
2.27 Micrograph as found by Östberg[34], white is metallic iron, gray is oxide. . . . 30
2.28 Two grains reduced at 1000°C in an hydrogen atmosphere[41]. . . . 31
2.29 Effects of 1wt% of different impurities compared to the as received material[49]. Reduction at conducted at 900°C. . . . 32
2.30 Total dissolution of titanium in fraction plotted against leaching time, leaching temperature of 100°C was used, varying concentrations (1) 85wt% (2) 80wt%, (3) 60wt%, (4) 50wt%[69]. . . . 34
2.31 Effect of reaction temperature, $H2SO_4$ concentration of 20 wt%, with a reaction time of 3 hours[70]. . . . 34
2.32 Extracted concentration plotted against leaching times. . . . 35

3.1 Size distribution of ilmenite samples. . . . 37

4.1 Grains in as-received GCO sample, cross-section, EDS values shown in Table 4.2. 41
4.2 Grains in as-received GCO sample, topology. . . . 42
4.3 Observed dissimilar grains present in the cross-sectioned KZN ilmenite. . . . 43
4.4 Grains in as-received KZN sample, topology. . . . 44
4.5 The change in weight plotted against temperature for different heating rates. . . . 45
4.6 The 1. derivative of %weight change as a function of temperature. . . . 45
4.7 The first derivative of %weight change as a function of time is plotted. . . . 46
4.8 Measured heat flow as a function of time for GCO and KZN ilmenite. . . . 46
4.9 The change in heat flow over the change in temperature is plotted against temperature. . . . 47
4.10 Recorded weight change after oxidation for 1 hour at different temperatures. . . . 47
4.11 Overview of iron species, given in weight percent. . . . 48
4.12 BSE images showing grains from samples oxidized at different temperatures. . . . 49
4.13 Different grains from samples oxidized at 700°C. . . . 51
4.14 Different grains from KZN samples oxidized at 700°C. . . . 52
4.15 Different grains from KZN samples oxidized at 800°C. . . . 53
4.16 Different grains from KZN samples oxidized at 1000°C. . . . 54
4.17 Topology of from both GCO(a-d) and KZN(e-h) sample for oxidation temperatures of 700 and 1000°C. . . . 55
4.18 Weight change(a) and O:Fe(b) curves for GCO sample reduced at 800°C. . . . 56
4.19 Weight change(a) and O:Fe(b) curves for GCO sample reduced at 900°C. . . . 57
4.20 Weight change(a) and O:Fe(b) curves for GCO sample reduced at 1000°C. . . . 57
4.21 Weight change(a) and conversion(b) curves for as-received GCO sample. . . . 58
4.22 Weight change(a) and conversion(b) curves for GCO sample oxidised at 700°C. . 58
4.23 Weight change(a) and conversion(b) curves for GCO sample oxidised at 800°C. . 59
4.24 Weight change(a) and conversion(b) curves for GCO sample oxidised at 1000°C. 59
4.25 BSE images of grains from the as-received GCO sample, for different reduction times, the bright phase is metallic iron. . . . 62
4.26 BSE images of grains from 700°C oxidized sample, for different reduction times, the bright phase is metallic iron. . . . 63
4.27 BSE images of samples oxidised at 1000°C, reduced at 800°C for 5 minutes. . . . 65

4.28 BSE images of grains from the as-received sample and different reduction times. The white phases are assumed to be metallic iron. 66
4.29 SE images of as-received GCO sample reduced at 800°C. 67
4.30 Iron and titanium dissolution given in % (a, b) and ppm values(c, d), reduced at 800°C. 68
4.31 Iron and titanium dissolution given in % (a, b) and ppm values(c, d), reduced at 1000°C. 69
4.32 BSE images of grains from samples oxidized at 800°C and 1000°C reduced at 800 degrees for 15 minutes and leached for 120 minutes. 71
4.33 BSE, mapping, and point analysis of samples that have been leached for 120 minutes. 72
4.34 Topology image and EDS analysis of leached grain surface from reduced samples. Values from EDS are shown in Table 4.30. 73
4.35 %Weight change curves(a) and O:Fe ratio(b) for the KZN ilmenite, reduced at 800°C. 74
4.36 Cross-section of KZN ilmenite reduced for 5 minutes, a)-c) are as-received, d)-f) are oxidised at 1000°C. EDS values given in Tables 4.35 and 4.36 respectively. . . 76
4.37 Cross-section of KZN ilmenite reduced for 60 minutes, a) and b) as-received, c) and d) oxidized at 1000°C. EDS values given in Tables 4.37 and 4.38 respectively. 77
4.38 Iron and titanium dissolution of the KZN ilmenite given in % (a, b) and ppm values(c, d), reduced at 800°C. 79

A.1 Iron and titanium dissolution after hot acid leaching of as-received GCO material for different holding times at 80°C. 104
A.2 Iron and titanium dissolution after hot acid leaching of oxidized GCO samples. Holding time was 90 minutes at 80°C. 104
A.3 Iron and titanium dissolution after hot acid leaching of as-received KZN material for different holding times at 80°C. 105
A.4 Iron and titanium dissolution after hot acid leaching of oxidized KZN samples. Holding time was 90 minutes at 80°C. 105

B.1 XRD-results analysed with the PDF-4, for the GCO sample. 106
B.2 XRD-results analyzed with the Crystallography Open Database(COD) for as-received GCO sample and different oxidation temperatures. 107
B.3 XRD-results analyzed with the PDF-4), for as-received GCO sample and different oxidation temperatures. 108
B.4 XRD-results obtained for reduction of as-received GCO sample, reduced at 800°C. 109
B.5 XRD-results obtained for reduction of GCO sample oxidised at 700°C, reduced at 800°C. 110
B.6 XRD-results obtained for reduction of GCO sample oxidised at 800°C, reduced at 800°C. 111
B.7 XRD-results obtained for reduction of GCO sample oxidised at 1000°C, reduced at 800°C. 112
B.8 XRD-results obtained for reduction of as-received GCO sample, reduced at 1000°C.113
B.9 XRD-results for reduced GCO ilmenite at 800°C for 5 minutes(Black), and leached(Red) for 120 minutes, analysed with the Crystallography Open Database(COD. 114
B.10 XRD-results for reduced GCO ilmenite at 1000°C for 5 minutes(Black), and leached(Red) for 120 minutes, analysed with the Crystallography Open Database(COD).115
B.11 XRD-results for reduced GCO ilmenite at 800°C for 60 minutes(Black), and leached(Red) for 120 minutes, analysed with the Crystallography Open Database(COD).116

C.1 Cross-section of grain in GCO ilmenite, oxidised at 1000°, reduced at 800°C for 15 minutes. 117
C.2 Cross section of grain in GCO ilmenite, oxidised at 1000°, reduced at 800°C for 28 minutes. 118
C.3 Cross section of grain in GCO ilmenite, oxidised at 1000°, reduced at 800°C for 60 minutes. 119
C.4 Topology changes for KZN ilmenite during oxidation at different temperatures. . 120

Symbol list

Symbol	**Meaning**
$FeTiO_3$	Ilmenite(M_2O_3)
Fe_2TiO_5	Ferric pseudobrookite
$FeTi_2O_5$	Ferrous pseudobrookite
$Fe_2Ti_3O_9$/H239	Pseudorutile
Ti	Titanium
TiO_2	Rutile/Titanium dioxide
Ti_nO_{2n-1}	4≤n≤10, Magneli-phases
TiC	Titanium carbide
Fe	Iron
Fe^{2+}	Ferrous iron
Fe^{3+}	Ferric iron
FeO	Wustite
Fe_3O_4	Magnetite
Fe_2O_3	Hematite
Fe_3C	Iron carbide
MgO	Magnesium oxide
SiO_2	Silicon oxide
Al_2O_3	Alumina
MnO	Manganese oxide
CaO	Calcium oxide
Na_2O	Sodium oxide
P_2O_5	Phosphorus pentoxide
V_2O_5	Vanadium(V) oxide
K_2O	Potasium oxide
Ni	Nickel
Co	Cobolt
Direct reduced iron	DRI
TPR	Temperature programmed reduction
TGA	Thermogravimetric analysis
GOD	Gas oxidation degree
C	Carbon
CO	Carbon monoxide
CO_2	Carbon dioxide
H_2	Hydrogen
H_2O	Water vapour
O_2	Oxygen
Ar	Argon

Symbol	**Meaning**
p_{H_2}	Partial pressure of hydrogen
p_{O_2}	Partial pressure of oxygen
p_{H_2O}	Partial pressure of water vapour
p_{CO}	Partial pressure of carbon monoxide
p_{CO_2}	Partial pressure of carbon dioxide
G	Gibbs free energy
H	Enthalpy
S	Entropy
K	Equilibrium constant
T	Temperature
m^2/g	Cubic meter per gram
$vol\%$	Volume percent
$mol\%$	Mol percent
$wt\%$	Weight percent
$R_{(g)}$	Reducing agent
$RO_{(g)}$	Product gas
R	Ideal gas constant
μ	Micro
XRD	X-ray diffraction
BET	Brunauer-Emmett-Teller analysis
SEM	Scanning electron microscope
BSE	Back scattered electrons
SE	Secondary electrons
SCM	Shrinking core model

1 Introduction

Ilmenite($FeTiO_3$) is commonly mined from two sources, rock- and sand-ilmenite. Rock-ilmenite contains higher concentrations of impurities(3-4 wt%), which in turn can limit the application of the products. One such mine for rock ilmenite is located in Rogaland, Norway[1]. The second source for ilmenite, sand-ilmenite is more commonly used due to its lower impurity content. The lower concentration of impurities is due to the weather effect, explained in later sections. Today the processing plant in Tyssedal is owned and operated by Eramet Titanium and Iron AS. After originally using Norwegian ore they switched the ilmenite source to sand ilmenite mined in the Grande Côte mine located in Senegal[2]. This enabled the end product of high titania slag could be used in the chloride process. Today the plant in Tyssedal is the only one in the world where pre-reduction of ilmenite is conducted.

1.1 The Tyssedal process

The process, as shown in the flow sheet drawn by Solheim in 1983[1] depicted in Figure 1.1, has remained relatively unchanged. In this process, the ilmenite concentrate is pelletized to form green pellets, which are then sintered in a traveling grate furnace. Hereafter, the pellets are fed to a counter-current rotary kiln, where they are pre-reduced using coal at a temperature of approximately 1100°C.

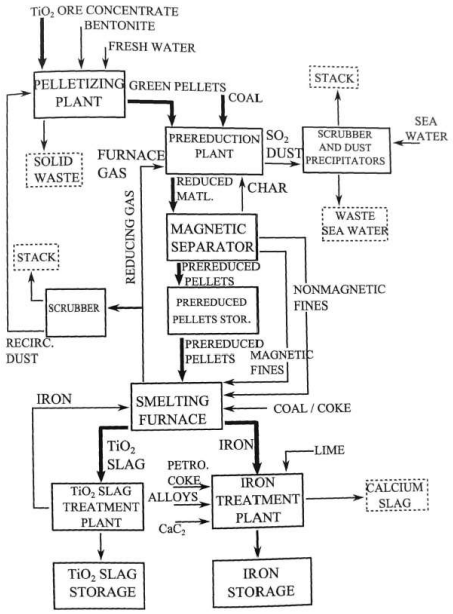

Figure 1.1: Flow sheet of the Tyssedal process, originally drawn by Solheim[1].

After the pre-reduction, the pellets undergo magnetic separation to separate the pellets from any gangue material before the pellets, along with coal, are then fed to a submerged arc furnace for smelting. The iron oxide content in the ilmenite is metalized, and two distinct liquid metal and slag phases form. The metal and slag phases comprise mainly of Fe and high titania, respectively. The Fe is tapped at a lower level than the slag and is processed further to specified qualities. The high titania slag gets crushed and prepared for shipping to the customer.

1.2 Scope of work

The use of coal as a reducing agent leads to emissions of carbon dioxide(CO_2). In 2021, Eramet Titanium and Iron AS reported CO_2 emissions of approximately 275 000 tons[3]. This gives great incentive to improve the environmental aspect of the process, which is why Eramet started investigating alternative reducing agents. Since 20 mol% of ilmenite is iron, inspiration for alternative reducing agents has been drawn from the direct reduced iron(DRI) process. The MIDREX process is the most commonly used today[4] and uses synthetic gas(syn gas) which is a mix of CO and H_2 made from natural gas. Another research project launched is Hybrit[5], which successfully produced DRI using hydrogen. By switching the coal out with hydrogen completely one can reduce the total emission of carbon dioxide by 80%[6]. Before the full potential of ilmenite reduction with hydrogen can be reached, a better understanding of the changes accompanying this switch needs to be established.

This Master's thesis looks to build upon the current knowledge of ilmenite reduction using hydrogen as a reducing agent and bring the implementation one step closer. Previously the effects of water vapor have been investigated by Canaguier[7] and the effects of different gas mixtures of CO and H_2 by Lobo[8]. The main objectives of the thesis are to look into the effects pre-oxidation has on reduction with hydrogen by using different ilmenite samples oxidized and reduced at different temperatures.

2 Theory

2.1 A literature study

In this chapter, an extensive literature will be presented. To gain a better understanding of how the different parts tie in together a summary will be given. An overview of the Fe-O system is given where changes occurring during oxidation and reduction are presented. Ilmenite concentrate can contain different types of iron oxides. It is therefore important to have an understanding of how these might change during the reduction progression. The ilmenite compound contains a substantial amount of iron and the pre-reduction is performed to metalize this iron. An underlying understanding of how iron oxides and reduces can be useful in drawing conclusions. Furthermore, the oxidation of ilmenite is inspired by the oxidation of magnetite which was seen to improve the overall reducibility of the ore, which is why these findings are presented as well. Ilmenite, pseudobrookite, and pseudorutile are compounds that can form during oxidation or reduction of ilmenite concentrate. A basic understanding of how the different compounds occur and act is crucial for following the results and the discussion. Since pseudorutile is a poorly documented compound extra attention has been given to it. The goal of the thesis is to gain a greater understanding on how oxidation affects the reduction of ilmenite with hydrogen. Hence, it is of great use to understand these mechanisms and how oxidation and reduction can differ from one concentrate to the next. Finally, one of the analytical techniques used was hot acid leaching which is closely related to the sulfate process, commonly used for ilmenite processing. A brief overview is given of the different aspects of this process.

2.2 Fe-O system

To gain a greater understanding of the phases one can expect in the iron oxygen system a study of the phase diagram can be of use. Darken and Gurry[9] characterized the iron-hematite (Fe-Fe_2O_3) system through a series of equilibrium experiments, where the atmosphere had a know partial pressure of oxygen and a total pressure of 1 atm. The phase diagram they found is shown in Figure 2.1

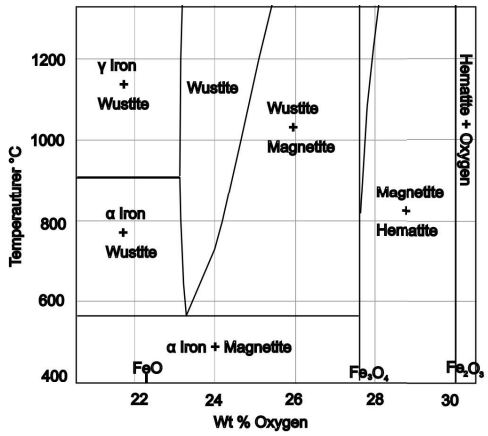

Figure 2.1: Fe-Fe_2O_3 phase diagram based on results found by Darken and Gurry[9].

As can be seen from the figure, the two endpoints of the phase diagram are hematite and oxygen on one side, and iron + wüstite or magnetite on the other. From the diagram, one can see that magnetite and wüstite both gain a greater solid solution as the temperature increases. For lower temperatures, magnetite and iron are the stable phases. At a constant temperature and a decreasing oxygen pressure, the equilibrium reaction progression would be as follows, Fe_2O_3-Fe_3O_4-FeO-Fe, for temperatures above 570°C.

2.3 Iron oxidation and reduction

Even though the iron oxygen system is one of the most explored binary systems to date, mostly due to the iron and steel industry, there is still discussion around the actual interactions that occur during the oxidation and reduction of iron and iron ore. Some of these uncertainties will be mentioned in the following section.

2.3.1 Reaction progression

As mentioned previously, thermodynamics suggests that hematite reduces to metallic iron through multiple phases. Two mechanisms have been mentioned. Firstly for temperatures below approximately 570°C, where hematite reduces to magnetite, then to metallic iron. For temperatures above 570°C, the extra step of wüstite is added before metallic iron is present, creating the reaction mechanism of Fe_2O_3-Fe_3O_4-FeO-Fe, shown in Reaction 2.1-2.3. These mechanisms are again mentioned in literature by authors like Spreitzer and Schenk[10] and Zhang et. al.[11]. The latter authors looked into the ideal and the regular reduction mechanism of hematite. They go on to mention that the final step occurring above 570°C, where wüstite reduces to metallic iron occurs over a gradient. This can be seen in the phase diagram shown in Figure 2.1, as a wide stability area of wüstite. The phases that have been observed during reduction tend to differ depending on the reducing agent present. One example of this can be found when Mondal et. al[12] reduced hematite in a pure carbon monoxide atmosphere. The reaction mechanism they suggested was that hematite reduced directly to wüstite before reducing further to metallic iron. The final step was the formation of iron carbide(Fe_3C). The temperature programmed reduction(TPR) showed only one reaction rate during reduction for temperatures above 600°C, which was why magnetite was neglected. Tahari et. al.[13] looked into the effect hydrogen and carbon monoxide had on reduction and they concluded that for hydrogen reduction the theoretical path was followed, Fe_2O_3-Fe_3O_4-FeO-Fe.

$$3Fe2O3 + R = 2Fe3O4 + RO \tag{2.1}$$

$$Fe2O3 + 3R = 2Fe + 3RO \tag{2.2}$$

$$Fe3O4 + R = FeO + RO \tag{2.3}$$

$$FeO + R = Fe + RO \tag{2.4}$$

2.3.2 Particle size dependency

The reaction progresses differs based on the particle size. For smaller particle sizes Turkdogan and Vintres[14] suggest that the hydrogen gas can diffuse into the grain and the reduction will then start throughout the grain, leaving no clear reaction interface. This type of reduction mechanism is referred to as internal reduction. It can also occur in porous ores, where reactions will start on the walls of the pores. Along with particle size and porosity, lower reduction

temperature also favors the internal reduction mechanism[14]. On the other hand, when pellets were reduced by Bondale et. al.[15], the reaction was seen to progress topochemically. The same principle applied for larger particles and higher temperatures, where reduction mainly occurred at pore openings and on the particle surface. As the particle size increases, the internal reduction ceased[16].

The reaction rate has also been found to be dependent on particle size. For a fixed mass of the sample, a reduction in the particle size is chaperoned by an increase in the reaction surface. A review conducted by Spreitzer and Schenk[10] that investigated the reduction of iron ore with hydrogen found that the decrease in particle size was found to increase the reaction rate, particularly for the initial and final stages. It was further found during a review of the kinetics of iron ore reduction with hydrogen, conducted by Heidari et. al.[17] that due to hydrogen's increased diffusivity, the reaction rate would be less dependent on particle size when compared to carbon monoxide as a reducing agent.

2.3.3 Effect of reducing agent on Fe-O reduction

Traditionally iron oxides are reduced with carbon monoxide. Due to rising environmental concerns, the steel and iron industry is looking else were for their reducing agents. Some examples of this are the direct reduced iron processes, like the Midrex process[4], which uses synthesis gas mixtures. The HYBRIT project[5] on the other hand, uses green hydrogen as a reducing agent. To gain a greater understanding of some of the differences that can occur when different reducing agents are used, some of the findings are represented here.

The two main reducing agents of interest are hydrogen and carbon monoxide. One way of comparing the two is through a Baur-Glassner diagram, as shown in Figure 2.2. In the diagram, the temperature is plotted against the gas oxidation degree(GOD), which corresponds to the partial pressure of the product gas over the total pressure. The dashed lines represent the reaction involving hydrogen while the solid line involves carbon monoxide.

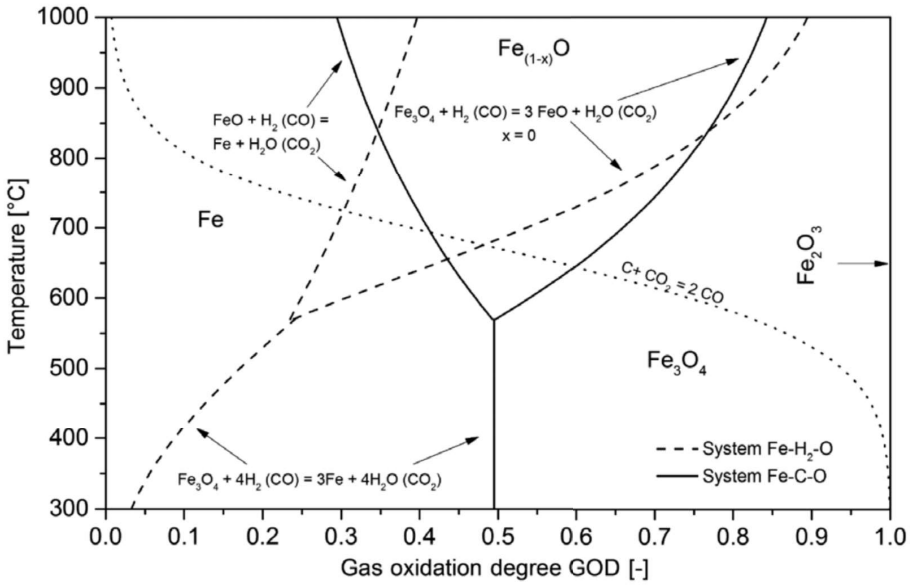

Figure 2.2: Baur–Glässner diagram as constructed by Spreitzer and Schenk[10]. Including the Boudouard reaction, at 1 bar with carbon activity of 1.

It becomes clear from Figure 2.2 that from a thermodynamic point of view, hydrogen reduction is faster at higher temperatures, and carbon monoxide reduction is faster at lower temperatures[17]. The point where the two gases intercept in reduction potential can be seen at 810°C. At this stage, hydrogen shows faster reduction kinetics due to its stronger diffusion properties[10]. It is also mentioned that even though hydrogen itself has good diffusive properties, the product gas of water vapor shows poor diffusive properties[10]. This could hinder further reactions. In this case, it was seen to hinder the reaction at 4-5% of water vapor. The final step of the reduction was affected most, while the initial step of hematite to magnetite was least affected.

Reduction with hydrogen and carbon monoxide-based gas mixtures has also been investigated. Zuo et. al.[18] investigated iron oxide reduction using H_2/CO mixtures. In Figure 2.3, one can see that for lower temperatures there is a greater dependence on hydrogen and carbon monoxide. As the temperature increases, pure hydrogen still shows a faster reduction rate. When gas mixtures with ratios of 1:1 H_2:CO were used, the same reduction level was reached after 30 minutes.

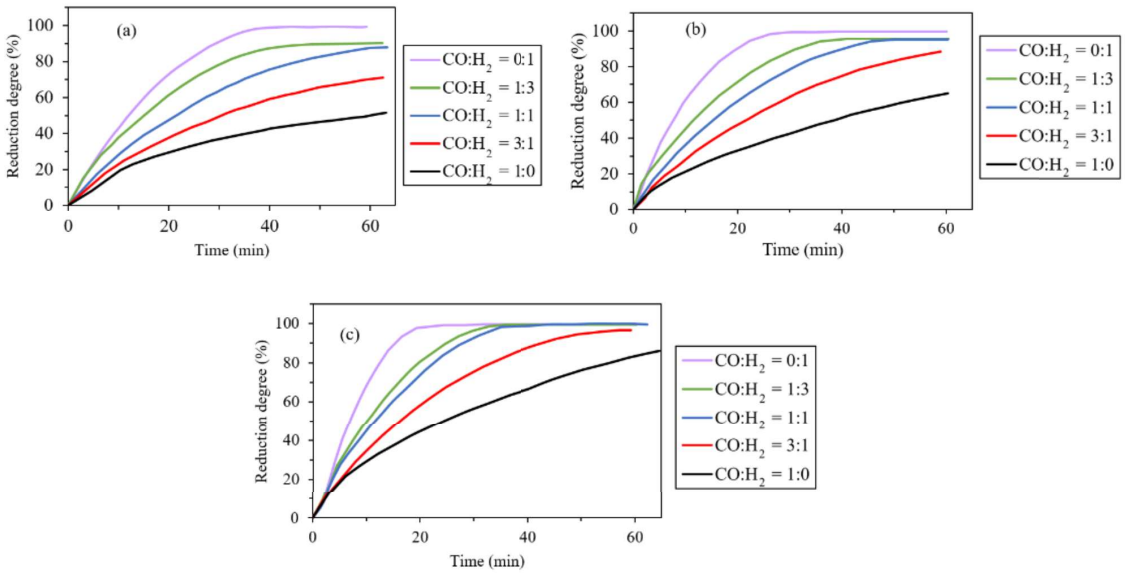

Figure 2.3: Reduction of wüstite, to iron using different H_2/CO-gas mixtures at temperatures of 800°C(a), 900°C(b) and 1000°C(c)[18].

Wang et. al.[19] conducted similar experiments on iron sand where hydrogen and argon mixtures were used. Partial pressures above 0.4 pH_2 seemed to have little effect on the reduction degree at 900°C after 50 minutes. Tahari et. al.[13] investigated the effect of gas concentrations of both hydrogen and carbon monoxide. They found that even though the reduction of iron ores started at a lower temperature when CO gas was used, the reduction with hydrogen was completed in a shorter period for concentrations above 20% H_2. The reason for this difference was believed to be due to the stronger adsorption properties of CO.

2.3.4 Morphology

Different reducing agents can lead to different morphology changes during reduction. Turkdogan and Vintres[16] did a study on the reduction and oxidation of iron oxides and iron with different gas mixtures. They found that reduction with hydrogen would produce finer pores compared to carbon monoxide reduction. They also found that when mixing product gas in the inlet the H_2/H_2O would result in a larger pore area than when CO/CO_2 gas mixtures were used. Furthermore, the pore surface of the product was also found to be widely dependent on the initial pore surface.

Along with the difference in morphology created by varying the reducing gas, the starting phase will lead to different morphologies and morphological changes. One common pre-treatment for iron ore is oxidation. For the consideration of iron sands[19], the oxidation treatment showed an improvement in the proceeding reduction, which was attributed to the separation of titanium and iron-rich phases. There was also seen a formation of micro-cracks that increased the exposed surface area of the oxide. Since magnetite has a denser grain exterior than hematite, oxidation gave an increase in following reduction rates at elevated temperatures[17][10]. This was due to oxidation helping increase the porosity and break down the exterior. In Figure 2.4 one can see hematite and magnetite reduced with hydrogen. The bright spots represent the metallic iron.

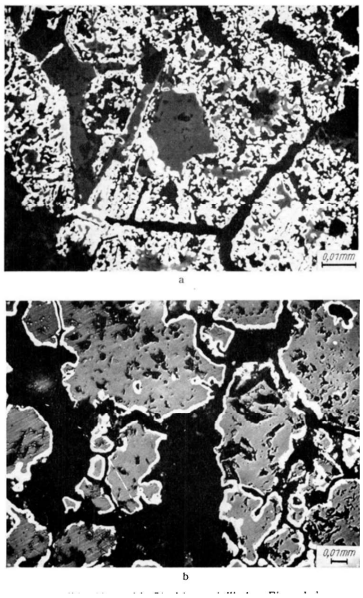

Figure 2.4: Hematite(a) and magnetite(b) reduced with hydrogen gas[20].

The formation of a solid iron layer around the grains could lead to slower reaction rates as the reducing agent needs to diffuse through the iron. For the reduction of hematite, the iron that is created has a greater chance to be porous[10], so that the reducing agent can diffuse through the pores.

It was further found that the formation of pores in the iron was dependent on the pores present in the ore[16]. One example of this was seen in experiments conducted by Turkdogan and Vinteres[16]. It was found that even though the starting material of wüstite was dense the metallic iron left after reduction was seen to be porous.

Iron distribution

Iron nucleation and agglomeration during reduction depend on starting conditions. According to Turkdogan and Vinteres[14], the mobility of Fe occurs mainly during reduction, and that further annealing had little effect on Fe movement. They also showed that as the reduction temperature increases, the iron had a tendency to become coarser. Typically, the formed Fe is of a porous or dense nature. Moujahid and Rist[21] and others [10] have mentioned a third category of fibrous or whiskers. This type of iron formation can occur at gas combinations near equilibrium.

As mentioned, dense or porous iron formation is the most common, which is why Moujahid and Rist[21] conducted a study where they classified the conditions for when the different iron types were created. They had similar findings to Turkdogan and Vinteres[14]. For lower temperatures, the pores found in the iron were fine, while increasing the temperature led to coarser pores. Furthermore, the two main parameters that affected iron nucleation were reduction temperatures and the reducing potential in the gas. The reducing potential was controlled by altering the amounts of the product gas in the inlet or vol% of argon. The temperature range was between 400 - 1100°C. They argued that the formation of dense iron could occur in lower reducing potentials, which was the case for pure carbon monoxide or hydrogen and water vapor gas mixtures. For pure hydrogen the creation of porous iron was present.

The results found by Moujahid and Rist[21], are summarized in Figure 2.5. In the figure, the circles represent the formation of porous iron. The triangles show the formation of dense iron, while the gray areas are transition areas where both types were found. From the figure, one can see that for reduction occurring at 800°C with pure carbon monoxide dense iron was found. Porous iron was created at a similar temperature range when pure H_2 was used.

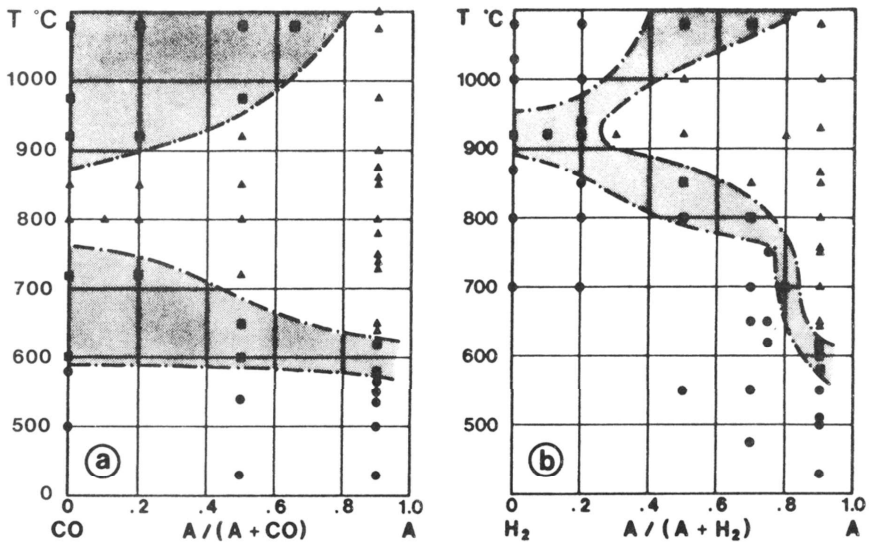

Figure 2.5: Temperature(°C) vs amount of argon in the reducing gas, (a) CO as a reducing agent, (b) H_2[21].

2.4 Ilmenite and its oxides

As mentioned, ilmenite is recovered in two forms, sand- and rock-ilmenite. The composition and type of ilmenite depends on the location it was mined. Pure ilmenite or synthetic ilmenite, like what was created during Canaguier[22] experiments contains a 1:1 mole-ratio of iron to titanium. In reality, these ratios vary greatly. Table 2.1 presents the chemical composition of ilmenite from various sources.

Table 2.1: Ilmenite compositions from different locations.

(wt%)	$\%TiO_2$	$\%Fe_{tot}$	$\%FeO$	$\%Fe_2O_3$	$\%MgO$	$\%SiO_2$	$\%Al_2O_3$	$\%MnO$	$\%CaO$
Norway[23]	44.4	35.5	34.9	11.97	5.9	2.7	0.7	0.4	0.3
China[24]	46.2	31.6	30.7	11.1*	5.1	3.4	1.1	0.6*	1.0
Australia[25] (Primary)	55.6	28.2	14.1	24.6	0.2	0.6	0.8	1.4	<0.01
Australia[25] (Secondary)	58.7	24.7	8.3	26.1	0.2	0.8	1.2	1.3	0.0
Iran[26]	44.7	35.63	35.5	11.8	1.3	3.7	1.0	0.8	1.1
USA[27]	64.9	21.3	2.2	27.9	0.2	0.2	1.0	1.3	0
KwaZulu-Natal[28]	42.4	34.9	44.9		0.6	0.2	0.1	1	0.1
Senegal[29]	53.5	30.6	19.2	22.4	0.6	0.1	0.6	1.0	0.0

As can be seen from the table, the most common impurities in ilmenite are magnesium, silicon, manganese, aluminum, and calcium oxide. The impurities that affect the Fe-Ti-O system the most are magnesium and manganese, which in turn have been studied the most by authors like Rosenqvist[30][31] and Johnson[32]. Moreover, what separates the different types of ilmenite would be the amount of Fe^{2+}. The Fe^{2+} content of rock-type ilmenite is typically higher than for sand-type ilmenite. The reason for this is due to weathering. The weathering effect will oxidize Fe^{2+} cations to Fe^{3+} in the ilmenite, due to the exposure to the atmosphere and water[33]. The Fe^{3+} atoms are then ejected from the ilmenite, decreasing the total amount of iron present. Mn^{2+} cations follows suit, while magnesium remains[33]. The reason for magnesium not being washed away is to maintain a balance in the lattice after the removal of iron and manganese cations. The difference can be seen in the Australian primary and secondary ilmenite given in Table 2.1.

2.4.1 Ilmenite(M_2O_3)

As mentioned, stoichiometric ilmenite has a Ti:Fe ratio of 1:1, but there can be a great deal of variance in the ratio, especially at higher temperatures. An example of this was presented by Borowiec and Rosenqvist[30]. In Figure 2.6 the phase diagram between hematite and ilmenite is shown. From the diagram, one can see that there is complete solubility towards the iron-rich side of the diagram, above 780°C. As one approaches the titanium side of the diagram the pseudobrookite and iron phases form complete solubility above 1346°C. The line following the 50 mol% Fe_2O_3 is stoichiometric ilmenite. Since natural ilmenite can contain hematite[34], heating the ilmenite could lead to the hematite dissolving into the ilmenite structure.

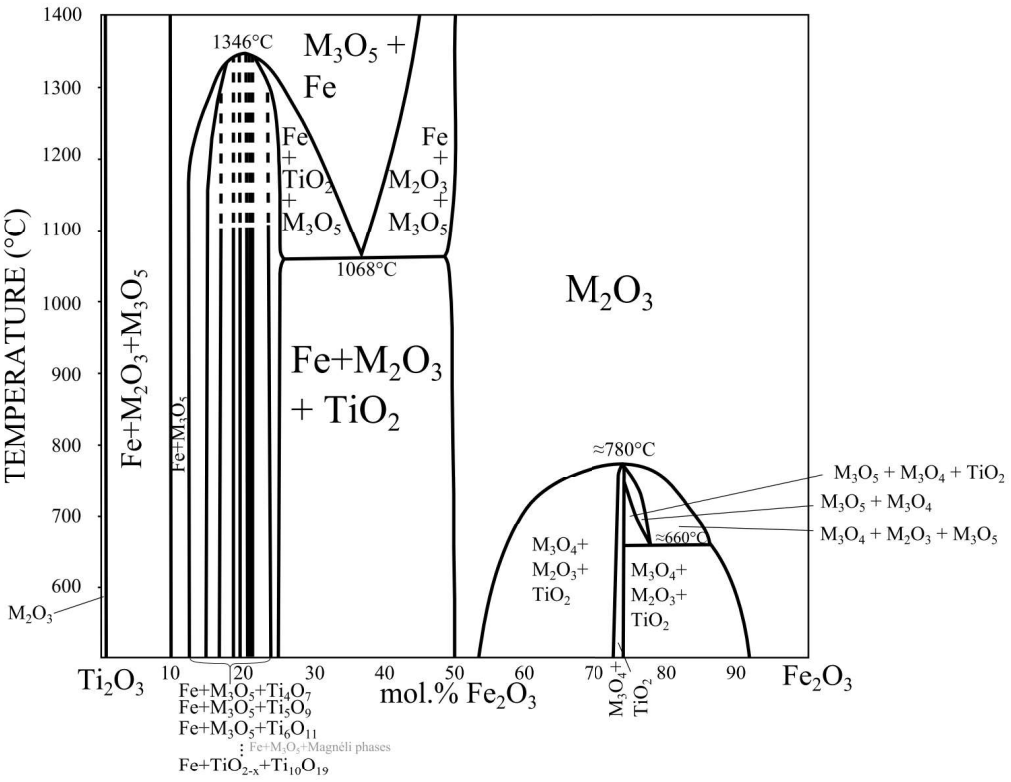

Figure 2.6: The Ti_2O_3-Fe_2O_3 phase diagram as suggested by Rosenqvist[30], redrawn by Lobo[8].

2.4.2 Pseudobrooktite(M_3O_5)

The M_3O_5 phase in the Fe-Ti-O system can form during oxidation and be present after the reduction of ilmenite. The most common occurrences during oxidation are ferric pseudobrookite (Fe_2TiO_5) and ferrous pseudobrookite ($FeTi_2O_5$). In cases where impurities like magnesium or manganese are high, the impurity atoms can replace the iron atoms in the crystal lattice. Grey and Merritt[35] conducted experiments on the stability regions of the pseudobrookite solid solution. They mention that above 1346°C there was a complete solid solution of the M_3O_5 phase. Along with the minimum temperature of 1139°C for the existence of an M_3O_5 in equilibrium with metallic iron. Borowiec and Rosenqvist[30] used their findings to generate the phase diagram shown in Figure 2.7. From the figure, one can see that as the iron content increases the M_3O_5 phase stabilizes at lower temperatures.

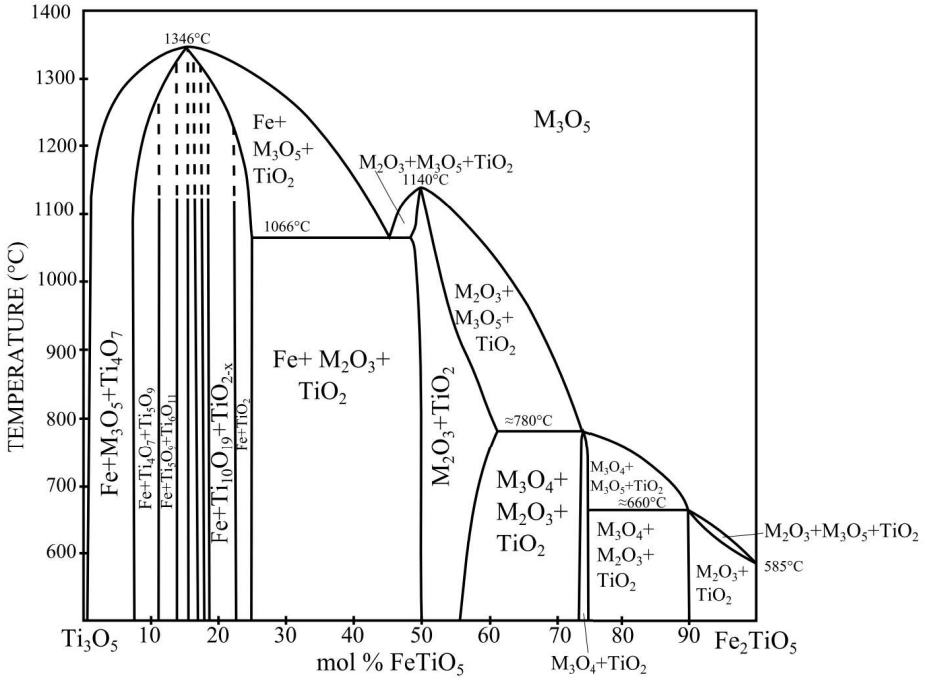

Figure 2.7: Ti_3O_5-Fe_2TiO_5 phase diagram, originally drawn by Borowiec and Rosenqvist[30], based on results found by Grey and Merritt[35], redrawn by Lobo[8].

2.4.3 Titanium oxides(Ti_nO_{2n-1})

When considering ilmenite reduction using hydrogen, the presence of lower titanium oxides needs to be taken into account. At what point rutile starts reducing to lower oxides is based on both temperature and gas composition. One example of a gas composition is given in the diagram shown in Figure 2.8. In this case, the composition is given as 99:1 vol% R:RO, for both H_2 and CO. From the figure it can be seen that the temperature required for rutile reduction would be 1080°C for hydrogen gas and around 1200°C for carbon monoxide, this corresponds well with values found by Tangstad[23]. If the gas purity were to increase the lines would shift downwards in the diagram, lowering the temperature at which rutile reduces.

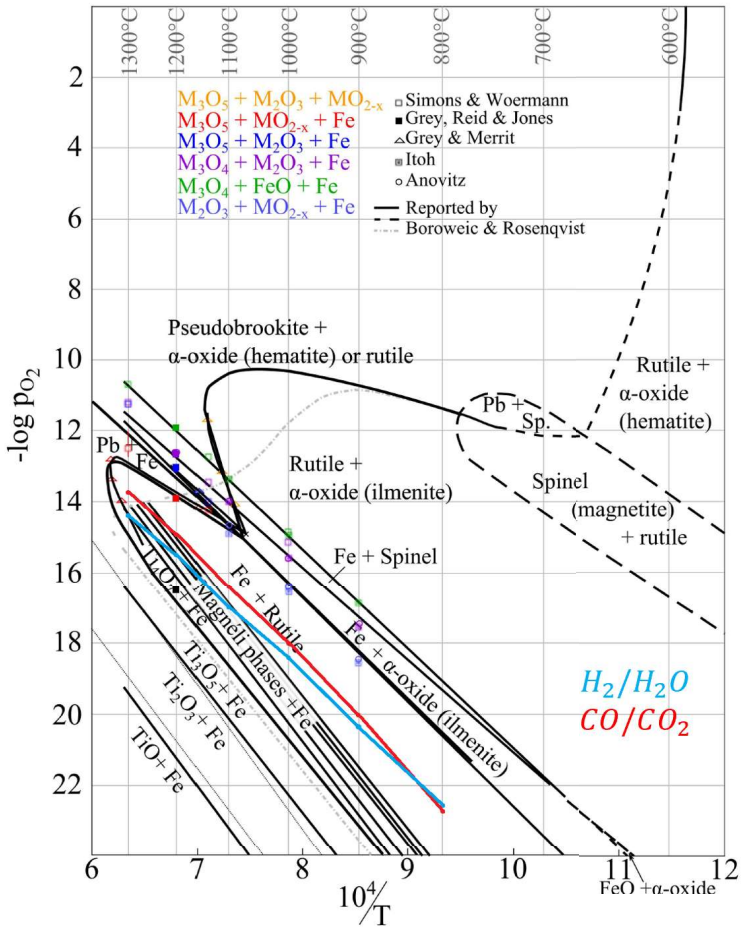

Figure 2.8: Diagram showing the equilibrium partial pressure of oxygen vs 1/T, with the equilibrium oxygen pressures for hydrogen and carbon monoxide reactant, drawn by Lobo[8].

Based on results produced by Lobo[8] and Kaam[36], given the gas purity is high enough, for temperatures as low as 900°C lower titanium oxides could be found after 2 hours of reduction. Waldner and Eriksson[37] conducted thermodynamic modeling of the titanium oxygen system. They showed that as the oxygen content decreases the rutile first enters an area of oxygen-deficient rutile, described as TiO_{2-x}, before reducing further through a set of lower titanium oxides. The phase diagram that they suggested is shown in Figure 2.9. Michaud and Pidgeon[38] showed that the end product of rutile reduction using hydrogen was a Ti_3O_5 phase, but mention little of the kinetics. When applying this to the reduction of ilmenite the most likely end product would be one of the Magnéli-phases, defined as Ti_nO_{2n-1}, where according to Waldner and Eriksson the given n values were $4 \leq n \leq 10$.

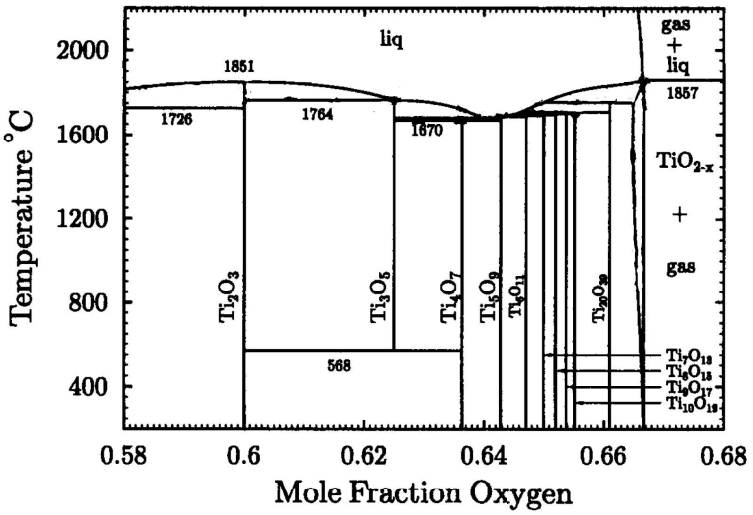

Figure 2.9: Calculated phase diagram for the Ti_2O_3-TiO_2 system, as found by Waldner and Eriksson[37].

In a thesis written by Ketteridge[39], he compared oxygen pressures for a given composition of TiO_x, for $(1.88 \leq x \leq 2)$ from given authors at 1000°C, seen in Figure 2.10. From the figure, it is clear that at this temperature the partial pressure for oxygen needs to be less than 10^{-15} for rutile to become oxygen deficient and lower than $10^{-19.5}$ for the presence of Magnéli phases to appear. If one compares these values with the values shown in Figure 2.8 the partial pressure created by 99:1 H_2:H_2O is $10^{-18.3}$, where oxygen deficient rutile should be stable.

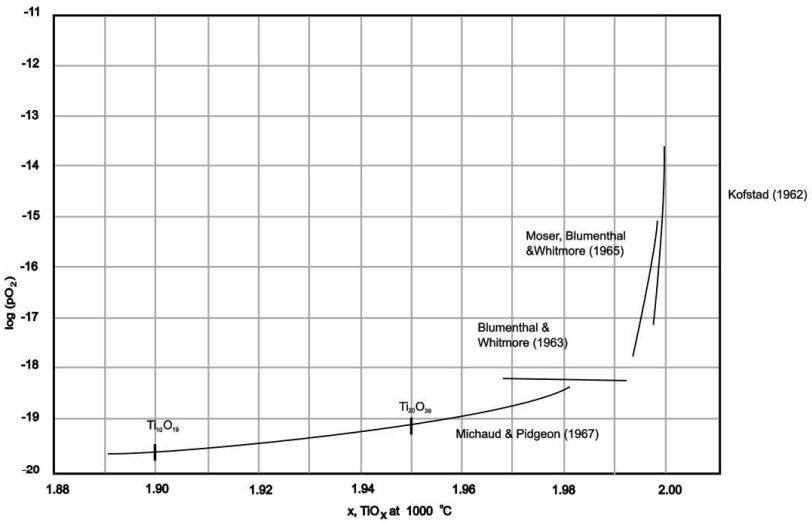

Figure 2.10: Comparison of values for oxygen potentials for different compositions of titanium oxide at 1000 degrees, given by Ketteridge[39].

2.4.4 Pseudorutile/H239($Fe_2Ti_3O_9$)

Pseudorutile($Fe_2Ti_3O_9$) can occur both naturally and as a product of ilmenite oxidation. As mentioned, sand-ilmenite can undergo weathering where some of the ferrous iron oxidizes and is washed away due to the weather[40]. A side product of this phenomenon is the creation of pseudorutile. Research conducted by Salehi et. al.[41] on the micro-structural changes during oxidation suggested that the production of pseudorutile might lead to a decrease in volume, which in turn would initiate the creation of micro-cracks and porosities. When the compound occurs during oxidation it has by multiple authors been referred to as H239[40][42][24], which will be used from this point onward.

Cheng and Gao looked into the micro-structural changes that occurred during roasting of natural ilmenite[40]. They argued that the creation of H239 was favored when the particle size was small and the oxygen pressure was high. This reconfirmed the results found by Fu et. al[42], who looked at the morphological changes of ilmenite during oxidation. They suggested that the following reactions could occur during oxidation. Where the creation of H239 was more present at smaller particle sizes and higher oxygen pressures, which was also later confirmed by Xiao et. al.[43].

$$4\,\mathrm{FeTiO_3} + \mathrm{O_2} = 2\,\mathrm{Fe_2O_3} + 4\,\mathrm{TiO_2} \tag{2.5}$$

$$12\,\mathrm{FeTiO_3} + 3\,\mathrm{O_2} = 4\,\mathrm{Fe_2Ti_3O_9} + 2\,\mathrm{Fe_2O_3} \tag{2.6}$$

Contrary to Fu et. al.'s findings Cheng and Gao stated that the reaction shown in Reaction 2.7 was correct. Here hematite reacts with rutile to form pseudorutile. To prove this reaction path they conducted experiments of first oxidizing ilmenite at 800°C to create the products of hematite and rutile and then oxidizing it further at 900°C. This showed that the reaction was favored over the oxidation of ilmenite at 900°C.

$$\mathrm{Fe_2O_3} + 3\,\mathrm{TiO_2} = \mathrm{Fe_2Ti_3O_9} \tag{2.7}$$

Phase transitions occurring during the oxidation of ilmenite were investigated by Xiao et. al[43]. Two main reactions were mentioned for the oxidation of ilmenite at lower temperatures, as shown below.

$$4\,\mathrm{FeTiO_3} + \mathrm{O_{2(g)}} = 4\,\mathrm{TiO_2} + 2\,\mathrm{Fe_2O_3} \tag{2.8}$$

$$12\,\mathrm{FeTiO_3} + 3\,\mathrm{O_{2(g)}} = 4\,\mathrm{Fe_2Ti_3O_9} \tag{2.9}$$

Since the main products at low temperatures are rutile and hematite, Reaction 2.8 has a faster rate than Reaction 2.9, hence H239 makes up a small part of the finished product. In contrast to what was mentioned by Cheng and Gao[40], Xiao et. al. concluded with that the recombination of rutile and hematite, shown in Reaction 2.7, did not occur in the temperature range of 600-700°C. Thermodynamically speaking the reverse reaction is favored in this temperature range. This led to the conclusion that H239 is an intermediate product of oxidation at low temperatures. In Figure 2.11 an overview is given of the different reaction mechanisms for high and low temperatures.

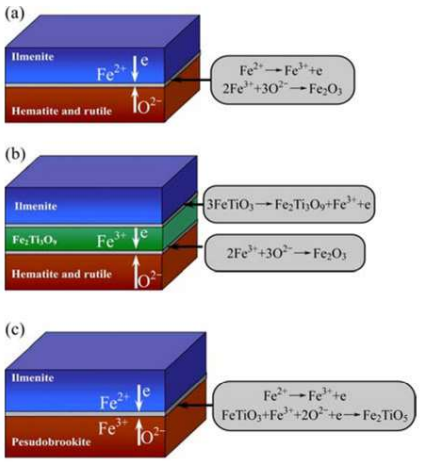

Figure 2.11: Schematic representation of the mechanism for ilmenite oxidation at temperatures below 900°C(a, b) and at high temperatures, above 900°C(c)[43].

Exactly what happens to pseudorutile during oxidation is somewhat discussed. Salehi et. al.[41] looked into the microstructural changes that occur during oxidation. They mentioned that if pseudorutile was present in the starting material it would remain mostly intact after oxidation. One did, however, see an increase in micropores and cracks where the pseudorutile was present.

Further studies have been conducted by Cheng and Gao[40]. They performed XRD analysis on ilmenite oxidized at different temperatures and different times, to see how the phase changes over time. In Figure 2.12 one can see the XRD results for pseudorutile oxidized at 600°C and 800°C at various holding times. At 600°C the pseudorutile decomposes into hematite and rutile. While if the temperature is increased further to 800°C one can see that the pseudorutile still decomposes to hematite and rutile, but recombines to form H239, before ferri pseudobrookite is formed as the stable end product of oxidation.

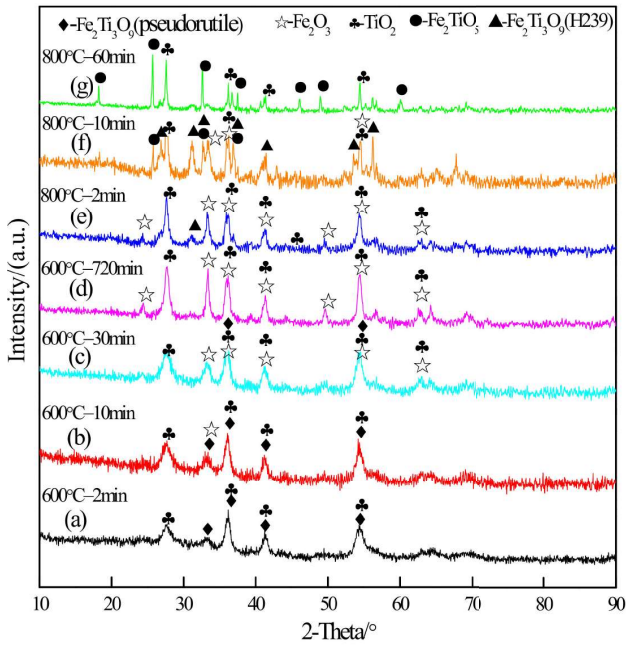

Figure 2.12: Chemical transformations of pseudorutile at different temperatures, as presented by Cheng and Gao[40].

2.5 Ilmenite oxidation

The oxidation of ilmenite and its effects on reduction is much discussed. In the following chapter, an overview of the different reactions that can occur will be given, before a broader explanation of how the different parameters might affect the oxidation process.

2.5.1 Chemical reactions

Gupta et. al. gave a good overview of the different chemical reactions that occurs during the heating of ilmenite at various temperatures[27]. In Figure 2.13 one can see that ilmenite reacts with oxygen and forms an intermediate compound, which is a mixture of hematite and rutile, $Fe_2O_3 * 2TiO_2$. before either breaking down to ferric pseudobrookite and rutile below 800°C. This in turn breaks down further to hematite and rutile. As the temperature is increased to above 800°C, ferri pseudobrookite and rutile will be the stable end products of oxidation.

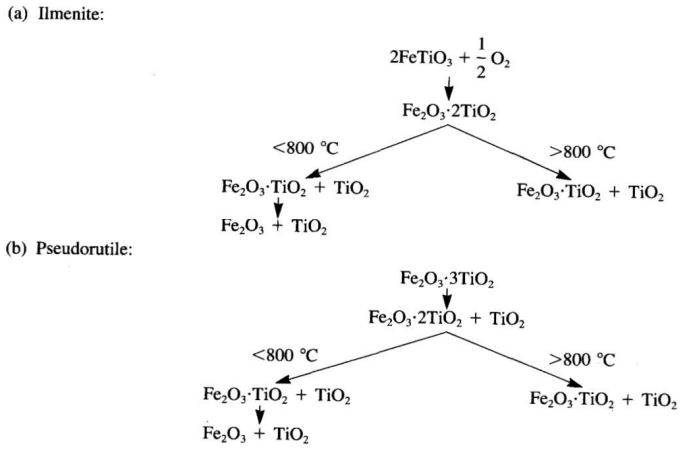

Figure 2.13: Simplification of oxidation path for ilmenite and pseudorutile, as presented by Gupta et. al.[27].

One of the phases shown in Figure 2.13 is pseudorutile. According to Gupta et. al., the compound will follow a very similar route as ilmenite, but rutile will be present in a greater amount after oxidation. In the following section, special attention is attributed to the compound and the parameters of its stability.

2.5.2 Temperature dependence

Oxidation of ilmenite is mainly temperature dependant in regards to end products and reaction rates. For the latter, the main understanding is that as the temperature of oxidation increases the reaction rate increases along with it. Due to the temperature dependency of ilmenite oxidation, it is simpler to divide the findings into three areas of interest, low-, intermediate- and high- oxidation temperature.

As seen from Figure 2.13, Gupta suggested that the end products of ilmenite oxidation at temperatures below 800°C were hematite and rutile. The same goes for the decomposition of pseudorutile. Research has been conducted on the oxidation of ilmenite in the temperature range of 500°C to 600°C[25][44][43]. Xiao et. al.[43] conducted ilmenite oxidation at both temperatures. Here the results indicated that for 500°C there was little change to the starting ilmenite after two hours. One could see indications of an H239 peak in the XRD results. The same peak was present when oxidation temperatures reached 600°C along with small amounts of hematite being created. This indicates a slow reaction rate in this temperature range, which was also concluded by the other authors[44][25]. Choi and Park[24] conducted oxidation experiments where the holding time was 6 hours. In the temperature range of 600°C, both rutile and hematite were present in the end product along with ilmenite, which gives an indication that the assumption of Gupta is valid, given enough time.

When the temperature is increased further to 700°C, the reaction rates increase along with it. Choi and Park[24] noticed an increase in the amount of hematite and rutile detected in the sample and a sharp decrease in the ilmenite content as well as the presence of the H239 phase. Another paper published by Xiao et. al.[44] mentions the same observations, along with the presence of an H239 phase in small amounts. As mentioned previously the creation of an H239 phase is favored by a smaller grain size, which in Choi and Park's case was 75 μm. This is considered to be within the range favorable for H239 creation. In Xiao's case, the particle size was not given.

An interesting observation was made by Samanta et. al.[45] on the oxidation behaviors of titaniferous magnetite ore. An overview of the composition of the ores is given in Table 2.2. From the table, it is clear that the rutile content is lower and the total iron content higher than in ilmenite. The main difference would be the presence of magnetite along with hematite and ilmenite. When the ore was oxidized for up to 24 hours at 700 degrees, a ferric pseudobrookite phase was observed.

Table 2.2: WDXRF results of the raw material used by Samanta et. al.[45].

	Fe_tot	TiO_2	SiO_2	Al_2O_3	MnO	MgO
(wt%)	48.18	22.51	1.79	3.37	0.25	1.44
Na_2O	P_2O_5	V_2O_5	K_2O	Ni	Co	CaO
0.13	0.03	0.435	0.03	0.0341	0.0188	1.12

In the temperature range of 800°C one commonly sees a transition area between two main stable compounds. Briggs and Sacco[46] argue that in this temperature area, one would see pseudobrookite and rutile as stable end products. They go on to mention that an H239 phase was not observed around this temperature range. No data on particle size was given in the article. In more recent publications Lv. et. al.[47] studied the oxidation kinetics of ilmenite concentrate powder. They mention an intermediate temperature area of 770°C to 1000°C, where pseudorutile and rutile are stable. These findings coincide well with XRD results obtained by Zhang and Ostrovski[25]. Zhang and Ostrovski looked at the effects of oxidation on the properties of ilmenite concentrate. For samples oxidized at 800°C the phases found were ilmenite, hematite, rutile, and pseudorutile. Along with trace amounts of an $Fe_2O_3 * 2TiO_2$ ($Fe_2Ti_2O_7$) phase, which was also mentioned by Gupta[27] as an intermediate product obtained during oxidation. Due to the low quantity of these phases and little data surrounding them Cheng and Gao[40] tried to distinguish between the intermediate phase and the H239 phase by using $Cr_2Ti_2O_7$ as a reference pattern for XRD analysis. This compound was used due to the similarities between the two. Their results and comparison are shown in Figure 2.14.

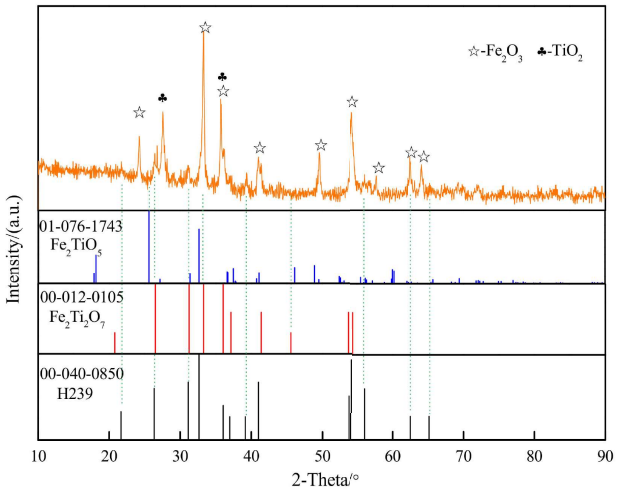

Figure 2.14: Determination of products after oxidation at 800°C for 60 minutes, by Cheng and Gao[40].

As can be seen from the figures, multiple main peaks overlap between the H239 phase and the $Fe_2Ti_2O_7$ phase, making it hard to distinguish between them by XRD alone. Furthermore, they also confirm that for their parameters a ferri pseudobrookite phase was not observed after oxidation at 800°C for 60 minutes. When oxidizing at 800°C for 6 hours, Choi and Park[24] found that the Fe_2TiO_5 phase was present, indicating that the reaction was possible at this temperature but with slow kinetics.

At higher temperatures than 800°C the remaining stable phases are ferri pseudobrookite and rutile, as can be seen by the XRD results found by Choi and Park[24] shown in Figure 2.15. As can be seen from the results, the ferri pseudobrookite phase first appears at 800°C and upon further increasing the temperature becomes the main phase along with rutile after 6 hours of oxidation.

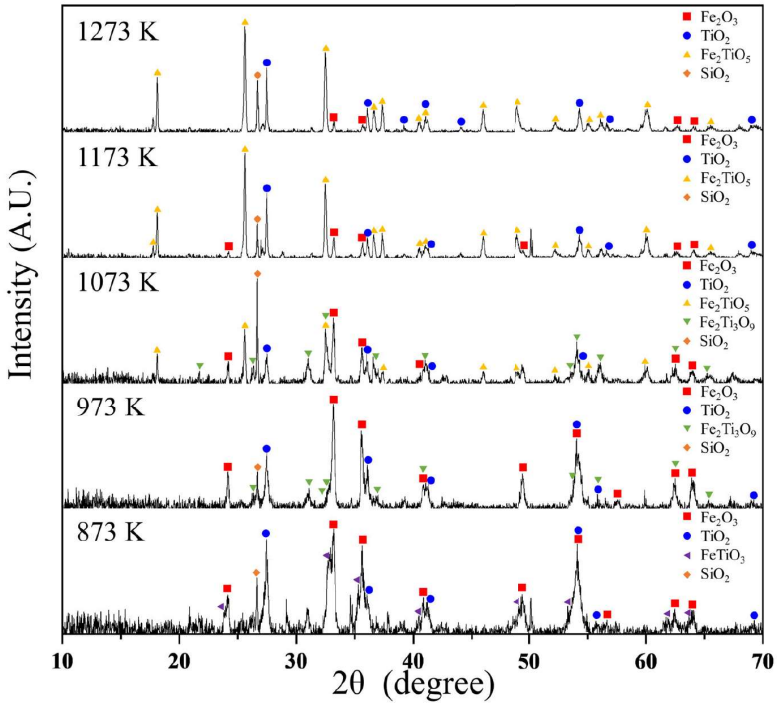

Figure 2.15: XRD result found by Choi and Parl[24] after 6 hours of oxidation.

Where the formation of the ferri pseudobrookite phase starts is somewhat discussed. Gupta et. al.[27] mention at 800°C, which coincides well with the results shown in Figure 2.15. On the other hand, when looking at pellets oxidized by S. Lobo[8] at 800°C for 2 hours the ferri pseudobrookite was not present in the XRD analysis of the end product. The ferric iron was present in a pseudorutile state.

To summarise, the oxidation temperature will determine the end products. It can be divided into three different temperature areas. For lower temperatures, 700°C and below, rutile and hematite tend to be the stable products along with pseudorutile. Given that the reaction is favored during oxidation. At high temperatures above 900°C, the only stable phase seems to be ferri pseudobrookite. Then there is an intermediate zone where the stable phases are a mixture of the four mentioned, rutile, hematite, pseudorutile, and ferri pseudobrookite.

2.5.3 Morphology changes

Untreated ilmenite tends to have a dense inner structure, and in the case of ilmenite sands, the grains tend to be smooth on the surface[24]. In this section, an overview is given of the different changes to morphology that can occur during oxidation. In similarity to the article written by Samanta et. al.[45], where they mention that oxidation helps to break down the complex structure of titaniferous magnetite ore. The same can be said about the pre-oxidation of ilmenite, where the single crystal structure of ilmenite could get turned into a polycrystalline structure[48], which in turn helps prevent the formation of an iron barrier around the grains[49] as well as sintering[50].

As the ilmenite oxidizes, the uptake of oxygen leads to volume expansion, which in turn results in crack formation throughout the oxidized grain. Both Chen et. al.[24] and Zhang et. al. argue that crack formation plays an important role as to why oxidation helps with proceeding reduction. They mention that the crack formation leads to an improvement in gas diffusion of both reactants and products[24]. The creation of cracks and micro-pores was also discussed by Xiao et. al.[44]. They mention that the formation of these cracks were temperature dependent. At lower temperatures, the micro-pores created along the surface of the ilmenite could help with oxygen diffusion and further oxidation of the sample, while at elevated temperatures, above 1050°C, the micro-pores close up and leave a sintered structure which in turn could slow down further oxidation. Along with gas diffusion, the cracks increase the active surface area where reaction can occur and can serve as nucleation sites for iron formation[51][47].

Along with the crack formation increasing the specific surface area. The surface itself undergoes changes during oxidation. According to oxidation studies performed by Zhang et. al., the surface goes from being smooth to rough and porous. This effect can be seen in Figure 2.16 where the raw material, oxidation at 780°C for three hours and 900°C for 30 minutes.

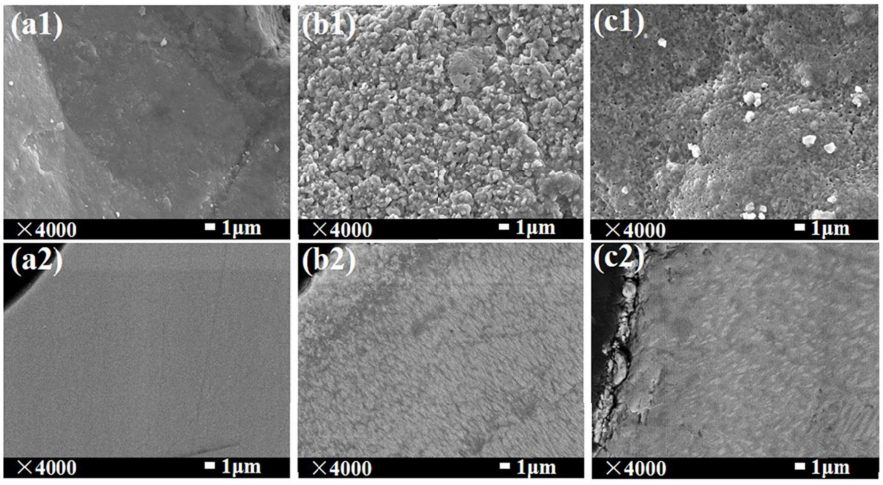

Figure 2.16: Surface and cross sectional SEM image of a1), a2)ilmenite surface and cross section, b1, b2)ilmenite oxidised at 780°C surface and cross section, c1, c2) ilmenite oxidised at 900 surface and cross section[24].

The same phenomenon was described by Zhao et. al.[52]. They mentioned that as the oxidation progressed, the surface of ilmenite grains would go from smooth to have a lot of protuberances. These protuberances would in turn increase the specific surface area of the ilmenite. Most research points towards the increase of specific surface area[47][44][53], but the research performed by Zhang and Ostrovski[25] points in the opposite direction. They looked into the effects of pre-

oxidation and sintering on the properties of ilmenite. When analyzing the specific surface area of oxidized ilmenite, both were quenched upon reaching temperature and calcined for three hours. They showed that the surface area decreased drastically as the oxidation temperature reached above 600°C, as can be seen in Figure 2.17.

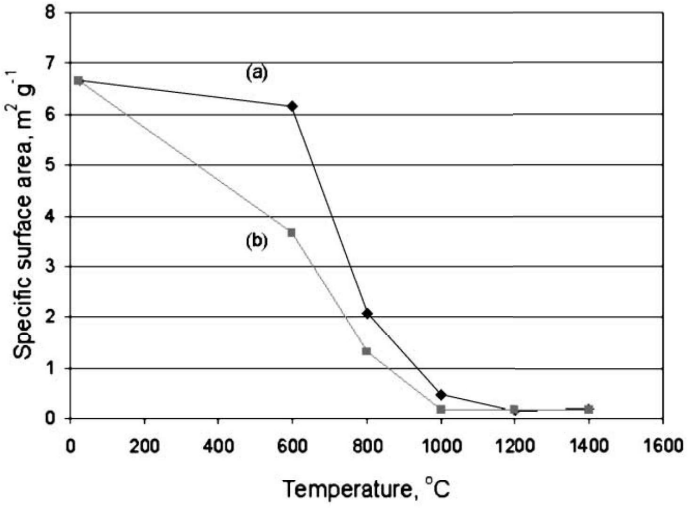

Figure 2.17: BET analysis of pre-oxidized ilmenite where a) is quenched upon reaching temperature and b) is calcined for three hours[25].

In a later article published by Lv. et. al.[54] on the effects of pre-oxidation on hydrogen reduction of ilmenite, they showed the opposite of Zhang and Ostrovski. They augured that the specific surface area of the powder increased after oxidation. For raw ilmenite, the surface area was given as 27.881 m^2/g while ilmenite that had undergone pre-oxidation at 1200°C gave a surface area of 78.841 m^2/g. Choi and Park[24] argued that one of the reasons to pre-oxidize ilmenite before the reduction was that it would increase reduction kinetics. Where the kinetics was believed to improve with the increased surface area after oxidation.

As ilmenite is oxidized, the single crystals of ilmenite break down into a poly-crystalline array[48]. Depending on the oxidizing temperature the ilmenite will either break down to rutile and hematite or pseudobrookite and rutile. Either way, the oxidation of ilmenite will lead to a change in how the iron is distributed in the oxide matrix.

One indication of the single crystal structure breaking down to a poly-crystalline array can be seen in the SEM images obtained by Chen et. al.[24], shown in Figure 2.18. From the BSE images represented in the figure one can see how in the raw ilmenite the iron agglomerates along the grain boundaries after reduction, independent of the H_2/CO ratio. While for oxidized ilmenite the metallic iron seems to be distributed throughout the grains. Similar findings were presented by Zhang et. al.[24]. They also mention that due to the greater distribution of metallic iron, it will not hinder diffusion to the same degree as if it was distributed along the grain boundaries.

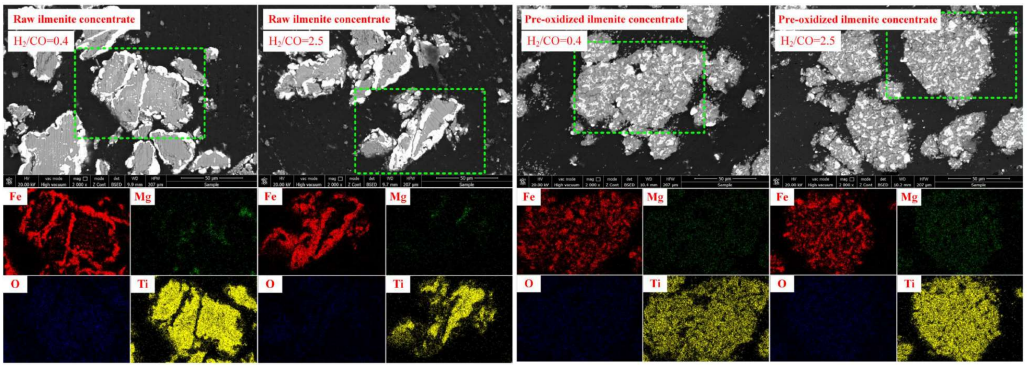

(a) Raw ilmenite reduced at different H_2/CO ratios(b) Pre-oxidised ilmenite, reduced at different H_2/CO ratios

Figure 2.18: BSE images obtained by Chen et. al.[24].

As the iron distributes itself throughout the newly formed grains, a thin layer of hematite tends to form along the grain boundaries. Salehi et. al.[41] mentioned that the layer occurs in grains where ilmenite is distributed close to the grain surface. The thickness of the hematite layer seems to stay constant throughout the oxidation, in Salehi's experiments the thickness was given as 2 μm. An example of the hematite layer formation is given in Figure 2.19. Choi and Park[24] mention the creation of the same layer around ilmenite grains.

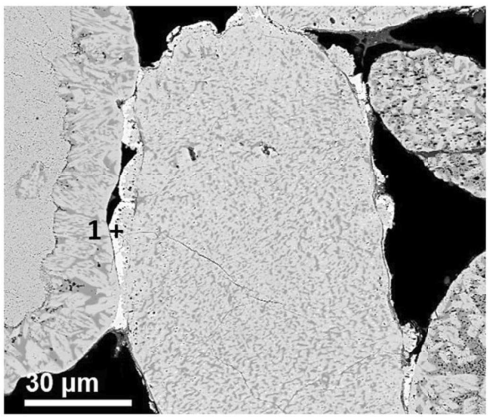

Atomic percent %

	1
Ti	4.1
Fe	46.0
O	48.3
Mn	0.6
Mg	0.4
Al	0.5
Si	0.2

Figure 2.19: BSE image and point analysis of the hematite layer that forms along the grain boundary, as found by Salehi et. al.[41].

In a study done by Zhang et. al.[55] on the morphological changes that occurred during the oxidation of Panzhihua ilmenite. They divide the reaction and changes that occur during oxidation into two temperature areas. For temperatures below 800°C, three stages occur during oxidation. In the initial stage, a hematite layer is rapidly created along the surface of the grain. Similar to the layer mentioned by Salehi et. al.[41] and Choi and Park[24]. The layer did not increase in thickness after three minutes of oxidation. Zhang et. al. mention that the creation of a hematite layer is due to the diffusion of iron drawn toward the initial reaction interface.

As the oxidation progresses, the interior of the grains changes. A hairlike rutile structure appears along with three different phases, believed to be ilmenite and hematite[55]. The progression of oxidation is believed to be due to oxygen anion diffusion inwards in the grains, which in turn oxidizes the remaining ferrous iron and separates the ilmenite into rutile and hematite. The mechanism behind this is due to the fact that titanium cations have a lower likelihood of movement, as opposed to diffusion. When the oxidation nears its end, the reaction itself stops while the rutile grains continue to grow and eventually form a continuous matrix.

For different temperatures below 800°C, the same structure appears at different times. One example given by the authors was after 24 hours of oxidation at 600°C the structure was similar to oxidation at 750°C for 20 minutes. The reason was that the oxidation was mainly controlled by ionic migration, which is heavily temperature dependent.

For temperatures above 800°C, pseudobrookite needs to be taken into account. The oxidation process is still divided into three stages. The first stage at this temperature is similar to what occurs below 800°C. Ilmenite first reacts to create rutile and hematite phases. This reaction is considered fast and may be overlooked. After the initial stage pseudobrookite starts appearing. Even though hematite, is not the stable end product at these temperatures the initial hematite layer still appears during oxidation and stays consistent throughout oxidation.

The same goes as for lower temperatures, the same morphology and phases can occur at different times of oxidation. In this temperature range, the example of 800°C is used. In Figure 2.20 one can see two cross-sections of oxidized ilmenite at 800°C. The morphology appearing after 120 hours, shown in image b) is of similar structure as what occurs at 900°C, where rutile and hematite have recombined into a pseudobrookite phase with rutile dispersed throughout the matrix.

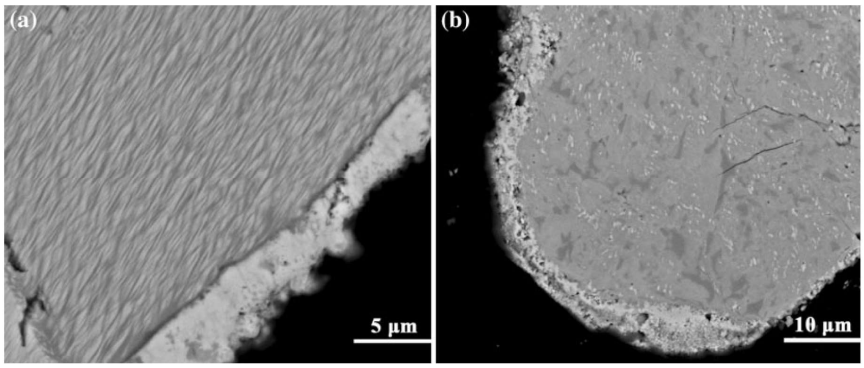

Figure 2.20: Oxidation of ilmenite at 800°C for 1-hour a) and 120 hours b), as found by Zhang et. al.[55].

2.5.4 Particle size dependence

As mentioned previously, the H239 phase is severely dependent on particle size. The smaller the particle the more likely the phase is formed during oxidation[42]. Furthermore in an article written by Salehi et. al.[26] they mentioned that after size partitioning the ilmenite powder there was seen a difference in reaction kinetics at lower temperatures. As the temperature increased above 1000°C the reaction kinetics seemed to be independent of particle size, as seen in Figure 2.21. Xiao et. al.[43] argued that this effect was due to the increase in surface area as the particle size decreased, which led to an increase in reaction kinetics.

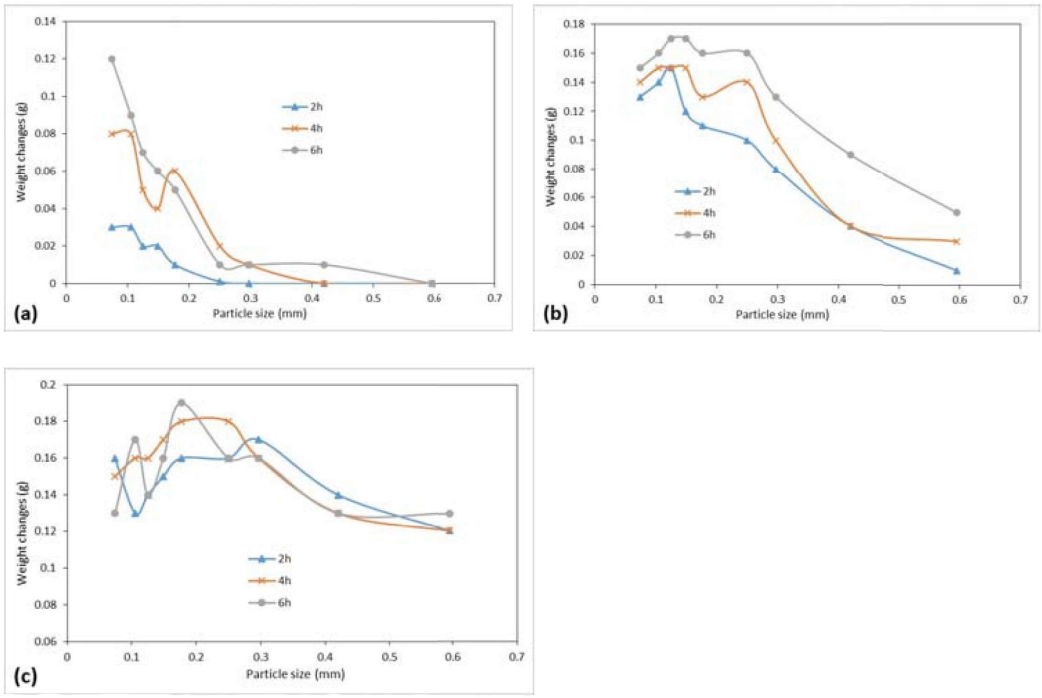

Figure 2.21: Weight change occurring during oxidation given a 5 gram sample, for different times and temperatures, a) 700°C, b) 850°C and c) 1000°C[26].

2.6 Ilmenite reduction

The steps ilmenite goes through during reduction are mainly dependent on starting material, reduction potential in the reducing gas, and the reduction temperature. The reduction progression of ilmenite and the effects of changing reducing parameters will be discussed in the following section.

2.6.1 Reduction progression

For oxidized ilmenite, three main reaction steps are commonly mentioned. The first two steps focus on the reduction of iron. Stage 1 is the reduction of ferric iron to ferrous iron. Stage 2, the ferrous iron, reduces to metallic iron, while Stage 3 encompasses the reduction of titanium oxides to lower oxides or Magnéli phases. The three stages have been mentioned by other authors, like Lobo[8] for reductions with hydrogen and carbon monoxide, Gupta and Grieveson[56] for reduction with carbon. For reduction with carbon, the Boudouard reaction should also be considered[56], Wang et. al. for reduction with hydrogen and argon gas. Building further on the division of different reactions occurring, one can divide the progression of the reaction according to a multi-layered shrinking core model as suggested by Levenspiel[57], also mentioned by Zhao and Shadman[48]. This mechanism can describe the topochemical reaction, which is correct on a pellet basis[8], but on a grain level, the reaction progression might not follow the same mechanisms. In the given reactions "R" can be replaced with the reducing agent ($H_{2(g)}$, $CO_{(g)}$, $C_{(s)}$), and "RO" will be the product gas ($H_2O_{(g)}$, $CO_{2(g)}$. $CO_{(g)}$).

Stage 1

Jones[58] mentions that the initial reaction occurring in ilmenite reduction is the transition from trivalent iron to divalent iron ($Fe^{3+} \rightarrow Fe^{2+}$). The step has an endpoint of ilmenite and depending on the oxidation degree will at most account for 33% of the conversion degree.
As mentioned previously pseudorutile can either occur naturally or during oxidation, under certain parameters. During heating, pseudorutile can break down to ferric pseudobrookite and rutile, as seen in Reaction 2.10. If it is still present when the reducing gas is introduced, it can be reduced directly to ilmenite and rutile, given in Reaction 2.11

$$\mathrm{Fe_2Ti_3O_9} = \mathrm{Fe_2TiO_5} + 2\,\mathrm{TiO_2} \tag{2.10}$$

$$\mathrm{Fe_2Ti_3O_9} + \mathrm{R} = 2\,\mathrm{FeTiO_3} + \mathrm{TiO_2} + \mathrm{RO} \tag{2.11}$$

Commonly a solid solution of ferric and ferro pseudobrookite can be formed, given the general chemical equation of ($Fe_3Ti_3O_{10}$) or ((Fe_2TiO_5-$FeTi_2O_5$)$_{ss}$). The solid solution reduces to ilmenite through the following reaction.

$$(\mathrm{Fe_2TiO_5}{-}\mathrm{FeTi_2O_5})_{\mathrm{ss}} + \mathrm{R} = 3\,\mathrm{FeTiO_3} + \mathrm{RO} \tag{2.12}$$

Hematite can be present either in a solid solution with ilmenite or by itself. It will follow the previously discussed reduction routes for iron oxides, which is temperature dependant. It has further been mentioned by Merk and Pickles[49] and Östberg[34] that hematite reduces either completely before ilmenite reduces or to magnetite inclusions. The reactions are shown in Section 2.3.1 given in Reactions 2.1-2.3.

Stage 2

The second stage of ilmenite reduction is the further progression of divalent iron to metallic iron. This stage will account for the remaining 77% conversion of ilmenite, where all the oxygen connected to the iron will be removed. The main reaction occurring is the reduction of ilmenite to rutile and metallic iron, as shown in Reaction 2.13.

$$\mathrm{FeTiO_3} + \mathrm{R} = \mathrm{Fe} + \mathrm{TiO_2} + \mathrm{RO} \tag{2.13}$$

Stage 3

As mentioned previously, for certain reducing agents lower titanium oxides can occur during pre-reduction of ilmenite. The conversion degree is calculated by the amount of oxygen connected to iron atoms. This means that if the conversion degree were to exceed 100%, there would be more oxygen being removed from the sample than what is connected to just iron. In most cases, this is due to the reduction of titanium oxides, like rutile. For stronger reducing agents, like hydrogen, this occurs more frequently[34][8][59]. For reduction with carbon, the rutile can reduce all the way to TiO or TiC[56]. It is further argued that this only occurs towards the end or after ilmenite reduction is complete. Zhao and Shadman argued that this was due to the creation of metallic iron[48] producing a higher partial pressure of H_2O, preventing the reduction of rutile. For ilmenites with high impurities, like ilmenite from the Panzhihua region that has high magnesium concentration, there was seen no reduction of titanium oxides. This was believed to be due to the impurities preventing complete ilmenite reduction[60]. When manganese was the main impurity lower titanium oxides were detected[33].

Both time and temperature can determine the stable end product for rutile reduction in ilmenite. Magnéli phases have been found as an intermediate product by both Lobo[8] and Kaam[36] as well as Canaguier[22]. From their results one can see that equilibrium was not obtained, which matches well with other theories suggesting that Ti_3O_5 is the stable end product of rutile in hydrogen reduction[61][62][63]. There seems to be a lower temperature limit to when the reduction can occur with the lowest found temperature of 900°C[63][48][61]. For very high temperatures, 1200°C, one could see the creation of ferro-pseudobrookite as an intermediate product before slowly converting to Ti_3O_5[33][56][61][62]. Since there is a high concentration of iron in ilmenite, the iron can create a solid solution of the M_3O_5 phase. The reaction for the creation of lower titanium oxides, including the Magnéli phases, is shown below.

$$nTiO_2 + H_2 = Ti_nO_{2n-1} + H_2O \tag{2.14}$$

2.6.2 Parameters dependency

Changing the reduction parameters, like temperature or reduction gas, changes the kinetics, reaction driving force as well as the phases present after reduction. In the following section, some of the effects these changes can have are discussed.

Temperature dependence

A change in reduction temperature can lead to changes in the reactions that can or can not occur and changes in mass transport, which in turn affects the kinetics of reduction. It can be seen from previous results that the reduction of ilmenite is very temperature dependant. Some examples were obtained by Chen and Xiao[64], where carbon was used for reduction. When they varied the temperature between 800°C and 950°C the reduction degree obtained after 100 minutes varied between 25 and 80%. They also mention that smaller particle size leads to an increase in kinetics due to a greater surface area[62][56]. For the use of hydrogen as a reductant the difference was seen to be less[61]. Another example of this can be seen in Si et. al.[62] results, where a Panzhihua ilmenite was reduced with hydrogen at different temperatures. In Figure 2.22 one can see the reduction curves that were found. As the temperature increases the total reduction achieved also increases. The difference becomes smaller above 900°C, and at very high temperatures complete reduction is not reached. They also mention that for lower reduction temperatures, approximately 700°C, ilmenite should not reduce, but there is still metallic iron present after reduction, which is attributed to the presence of hematite in the starting material.

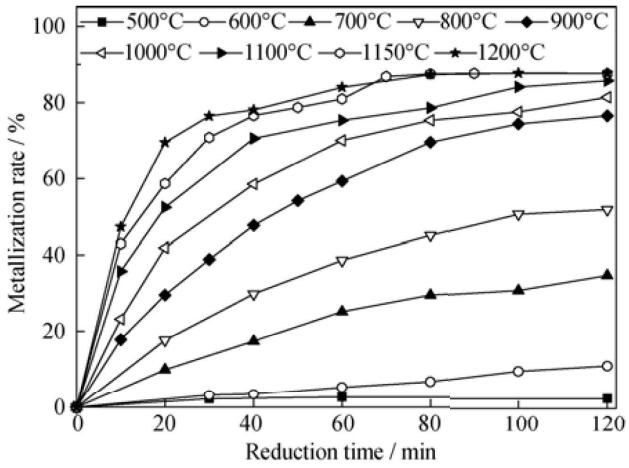

Figure 2.22: Reduction curves for Panzhihua ilmenite at different temperatures[62].

Reducing agent

Different reducing agents will change both the end products and the reaction kinetics. Most commonly today carbon monoxide is used for the reduction of ilmenite, while reduction using hydrogen is thought to be the more environmentally friendly alternative. The main difference between the two reducing agents is seen in the reduction kinetics. For hydrogen, the reduction kinetics are greater compared to carbon monoxide[8]. As well as previously mentioned the presence of a third stage can be seen for hydrogen reduction. The difference can be seen in Figure 2.23. In Lobo's[8] experiments ilmenite pellets were used in a thermogravimetric furnace to record the weight change over time.

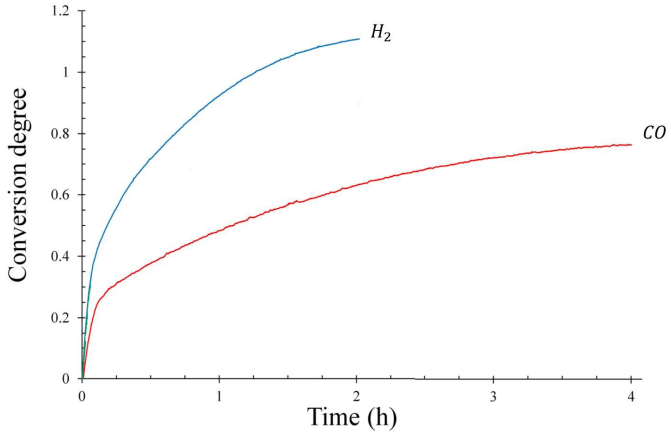

Figure 2.23: Reduction curves from Lobo[8] experiments, for pure hydrogen and pure carbon monoxide.

As well as the use of hydrogen as a reducing agent, experiments have been conducted for varying amounts of hydrogen content in the inlet gas. Wang et. al.[63] conducted a series of experiments on natural ilmenite concentrate with varying hydrogen content mixed with argon. The results can be seen in Figure 2.24. As can be seen from the figure, as the hydrogen content increases the reduction degree increases along with it. Also, there seems to be less change for 50 vol% hydrogen compared to pure hydrogen. Similar findings have been presented by other authors[48][60][63][60]. For pre-oxidized ilmenite reduction to ilmenite, the effect of varying hydrogen content seems to be small[24].

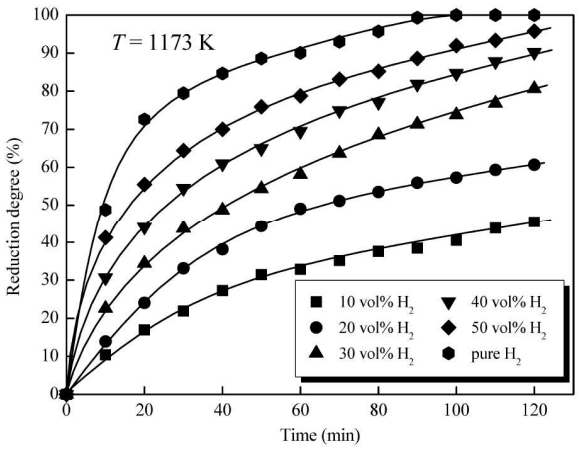

Figure 2.24: Reduction curves as found by Wang et. al.[63], showing varying hydrogen content for natural ilmenite concentrate.

2.6.3 Morphology

Before reduction with carbon monoxide, the ilmenite can be pelletized. Previous studies mention that on a pellet scale, the ilmenite reduction mechanism progresses topochemically, which is why Lobo[8] proposed a schematic for the different layers that occur during reduction, in accordance with Levenspiel's shrinking core model(SCM)[57]. In Figure 2.25 one can see the different steps that can occur during ilmenite reduction. The correctness of the SCM has been proven to work for ilmenite discs[65] as well as pellets[48].

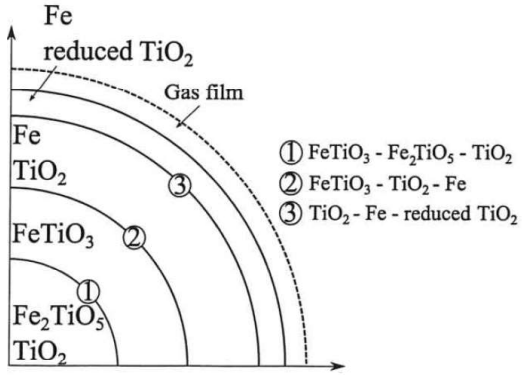

Figure 2.25: Schematic drawing of the shrinking core model applied to ilmenite reduction, as drawn by Lobo[8].

Even though the reaction occurs topochemically in a pellet, when considering each individual grain, the reaction does not follow the same progression[65]. The formation of cracks also occurs during reduction, which is thought to be because of the removal of oxygen from the oxide. That in turn leads to a shrinkage in volume[61]. The formation of the cracks was found to be temperature dependant. For high-temperature reduction, the pores were found to be round while for lower temperatures created finer veins of pores. The switch between these two types was found to be approximately 1000 K[65]. As the cracks form, the metallic iron nucleates along its border and where hematite or magnetite was present as well[34][62][48].

Iron distribution

As mentioned previously, iron can nucleate in different ways. When Dang et. al.[61] investigated the reduction of ilmenite powder with hydrogen they found that initially iron forms on the edge of the grain. As the reaction progresses inwards, the iron forms a lamellae structure, common for unoxidized ilmenite. Further reaction progresses, and the iron globules appeared to be unstable and therefore agglomerate. The driving force behind this is believed to be the minimization of surface area[63]. One author who contributed to the classification of iron nucleation in ilmenite reduction is Gustaf Östberg[34]. He investigated the solid state reduction of ilmenite with different gas mixtures in the temperature range 500°C to 1200°C. He found that initially the magnetite present in the ilmenite reduced to metallic iron. The magnetite served as a nucleation site for iron, even if it had been completely dissolved. In Figure 2.26 the initial stage of reduction is shown.

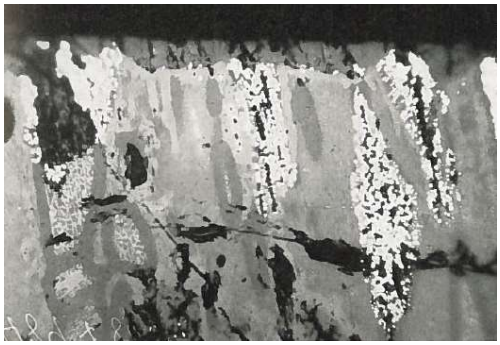

Figure 2.26: Ilmenite from Egersund, Norway, reduced at 1100°C in a CO atmosphere for 5 minutes. Precipitated iron (white), oxide (gray)[34].

When the temperature is increased, mass transport tends to increase with it. This in turn can lead to greater or lesser iron agglomeration. Jones[33] conducted an investigation into the changes occurring during ilmenite reduction with carbon monoxide. He found that for temperatures above 1000°C the iron already agglomerated into larger globules and started moving towards the edge of the particles while increasing the temperature even further to 1100°C led to the formation of an iron layer around the grains. This has in turn been found by other authors as well[49][56]. Östberg[34] conducted experiments with hydrogen at different temperatures, shown in Figure 2.27. From the figure, one can see that at low temperatures, 700°C, one can see that the iron does not agglomerate to the same extent as for 1200°C.

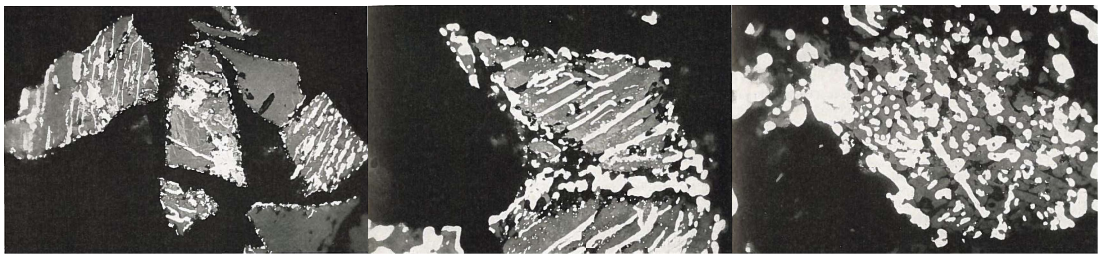

(a) Ilmenite reduced with hydrogen for 150 minutes at 700°C.

(b) Ilmenite reduced with hydrogen for 200 minutes at 900°C.

(c) Ilmenite reduced with hydrogen for 30 minutes at 1200°C.

Figure 2.27: Micrograph as found by Östberg[34], white is metallic iron, gray is oxide.

Similar changes for a change in temperature can be found when different reducing agents are used. When grading the reducing agents on a scale of reducing potential, hydrogen has a stronger reducing potential than carbon monoxide in the temperature range of 700°C to 1000°C. The reducing potential of a gas can be lowered by introducing product gas in the inlet. As the reduction potential decreases, the iron was found to become more coarse[34][63]. Si et. al[62] found that initially, hydrogen created fine pores during reduction which eventually got clogged up with metallic iron. The fine pores created from the hydrogen as well as the greater diffusivity of hydrogen lead to a greater extent of internal reduction, in similarity to the reduction of iron oxide[34]. For carbon monoxide reduction on the other hand the iron has a greater tendency to agglomerate along the grain boundaries rather than internal reduction[8][34][33].

As mentioned previously, oxidation of ilmenite breaks down the ilmenite crystals into a polycrystalline structure. It has been suggested that this will help with reduction. One of the reasons this might be the case was found by Jones[33]. He suggested that the original ilmenite crystal will be divided up into smaller fragments that experience a topochemical reduction. Since the iron no longer forms around the outside of the parent grain but rather along the edge of the smaller grains it will not hinder the reduction to the same extent and lead to the creation of smaller iron particles[34], similar to the effect of a higher reduction potential in the gas. Even if the ilmenite is oxidized prior to reduction, there can be a big difference in the changes occurring during reduction. Salehi et. al.[41] characterized 5 different grain types in the raw material and suggested routes for how they changed during oxidation and subsequent reduction. In Figure 2.28 one can see that even after oxidation at 1000°C for 60 minutes and with hydrogen as a reducing agent one still can see both iron distributions, coarse and fine distribution. This is believed to be due to the different starting phases in untreated ilmenite.

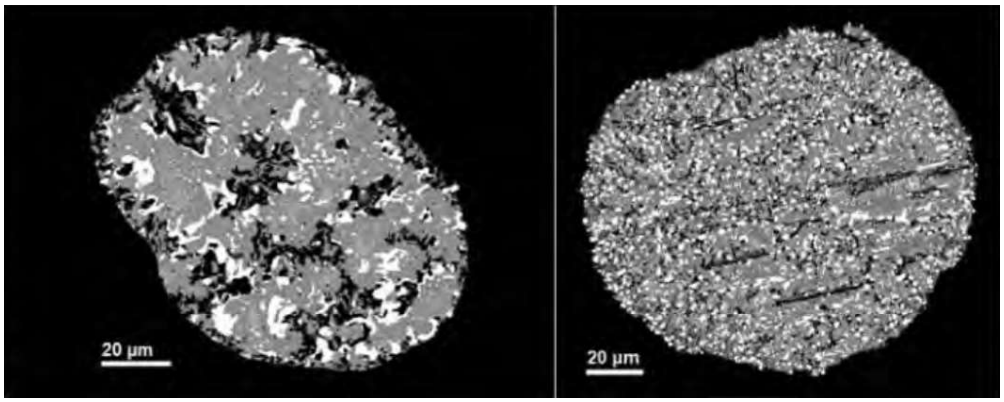

Figure 2.28: Two grains reduced at 1000°C in an hydrogen atmosphere[41].

2.7 Impurities

Common impurities in ilmenite are represented in Table 2.1. As one can see for certain regions or ilmenite types the impurities vary. A rule of thumb could be that rock-ilmenite usually contain greater amounts of magnesium- or silicon-oxide, while sand-ilmenite has lower concentrations due to effects like weathering. In this section how these impurities can impact the reduction mechanism is discussed.

2.7.1 Reduction

To investigate the effects different impurities have on ilmenite reduction with carbon monoxide Merk and Pickles[49] conducted a series of reduction runs with the addition of 1 wt% manganese, magnesium, and calcium oxide. The results are represented in Figure 2.29, as one can see the addition of other oxides lowers the overall reduction degree[63]. Furthermore, magnesium oxide seems to have the largest effect.

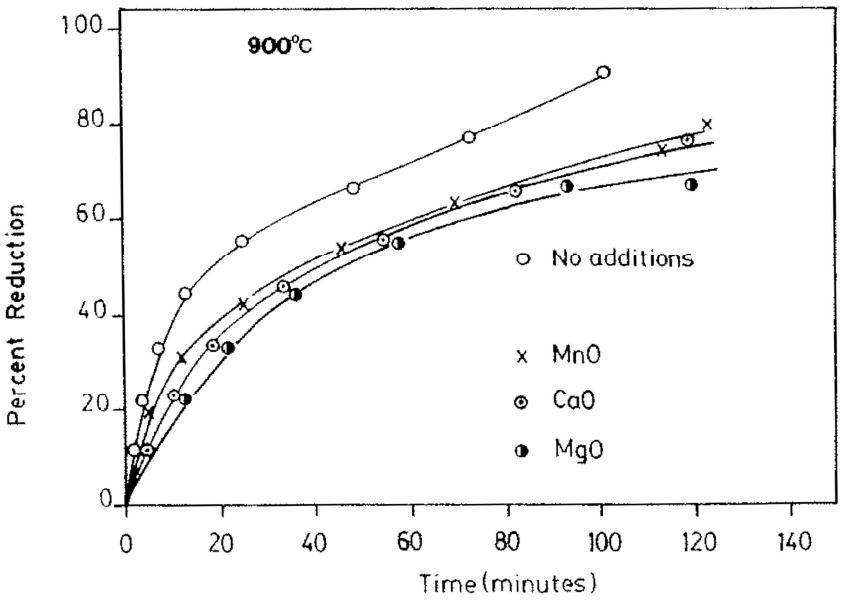

Figure 2.29: Effects of 1wt% of different impurities compared to the as received material[49]. Reduction at conducted at 900°C.

Magnesium is also one of the biggest impurities found in rock-ilmenite, like the ilmenite found in the Panzhihua province in China. This is why the effects of magnesium have been investigated[62][8][24][41]. It was found that the reason for magnesium lowering the reduction degree of ilmenite was due to its stabilizing effect on the M_3O_5-phase. This can lead to the M_3O_5 phase appearing at lower temperatures[33]. Salehi et. al.[41] mention that the presence of magnesium lowers the activity of Fe^{2+} ions, which eventually leads to the oxide phase being more stable than the metallic iron[49].

As well as stabilizing the oxide phase, impurities can also hinder further reduction through the barrier effect[45]. It has been found that the impurities of magnesium and manganese tend to move inwards ahead of the reduction interface[33][60]. As the impurities move towards the center of the grain, the concentration increases[64]. At a certain stage, the driving force for further reduction is not high enough to convert more ilmenite to metallic iron and the reaction stops. In a similar manner to the creation of a metallic iron layer around the grain, the barrier created by the presence of impurities can hamper the diffusion of hydrogen to the reaction interface, which in turn lowers the driving force for the reaction[60]. Since this is a mass transfer issue, the barrier effect weakens as the reduction temperature increases. Some authors have seen it completely disappear for temperatures as low as 1000°C[60][33], while others still see it present at 1200°C[33].

Another effect of impurities was the increased difficulty of analysis, mentioned by Salehi et. al.[26]. They argued that the impurities could strain the crystal structure, which in turn led to a shift in the d-spacing of the crystal lattice. Increasing the difficulty of XRD analysis. Dang et. al.[61] conducted a series of non-isothermal tests, where it was found that this could increase the overall reduction degree, overcome the barrier effect, and reduce titanium oxides to lower oxides. Shi-qing et. al.[52] mention that if the ilmenite contains a large amount of magnesium it can lead to an extra stage occurring during the reduction of ilmenite. As the oxidized samples were reduced the formation of $(Fe, Mg)TiO_3$ was seen from the decomposition of Fe_2MgTiO_{10} phase. The magnesium-heavy phase was seen to reduce before the reduction of ilmenite could start.

2.8 Sulfuric acid leaching and the sulfate process

One of the analytical methods chosen in this work was hot acid leaching with sulphuric acid. The method is similar to the end treatment of high titania slag and or ilmenite. An explanation of the process is therefore warranted. The following section is attributed to this.

The sulfate process was initially invented by P. Farup and G. Jebsen[66]. Reck and Richards described the commercial process in their life cycle analysis of rutile[66]. The starting material can be both ilmenite or high titania slag. The raw material is dissolved in sulfuric acid with a strength of approximately 90%. The solution is then agitated with superheated steam so that it maintains a temperature of 100°C. At this temperature, the ilmenite starts reacting with sulphuric acid to create iron and titanium sulfate. This in turn gets dissolved in water or dilute acid to reduce the iron. To remove the dissolved iron the solution is then cooled, which crystallizes the ferrous sulfate. Hydrolysis is then used to produce hydrous titanium dioxide which undergoes further steps before the end product of rutile is obtained.

Studies have also been conducted for using sulfuric acid to upgrade natural ilmenite in combination with oxidation to upgrade the rutile content of the ore by removing some of the iron present[67][68]. They mention that due to the different solubility of pseudobrookite and rutile, the pseudobrookite will dissolve to a certain extent while leaving the rutile in a solid state. It is further considered that rutile itself is considered inert in the dissolution reaction.

Dubenko et. al[69] investigated the effects of increasing the concentration of sulfuric acid on the leaching of titanium in ilmenite. Their results are shown in Figure 2.30. From the figure, one can see that as the sulfuric acid concentration increases the fraction of titanium that gets dissolved increases along with it. The same goes for longer leaching times. In this case, the starting material consisted mostly of pseudorutile and small amounts of ilmenite and rutile.

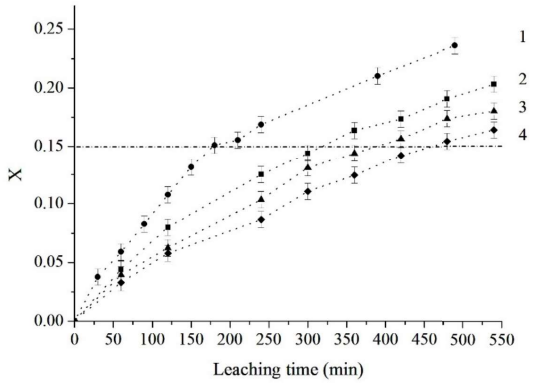

Figure 2.30: Total dissolution of titanium in fraction plotted against leaching time, leaching temperature of 100°C was used, varying concentrations (1) 85wt% (2) 80wt%, (3) 60wt%, (4) 50wt%[69].

Jia et. al.[70] investigated the leaching of Panzhihua ilmenite with sulphuric acid. When increasing the reaction temperature, they found that the dissolution of iron increased while the dissolution of titanium was found to increase, as seen in Figure 2.31. The decrease in titanium dissolution as temperature increases is thought to be because of the hydrolysis of titanium ions.

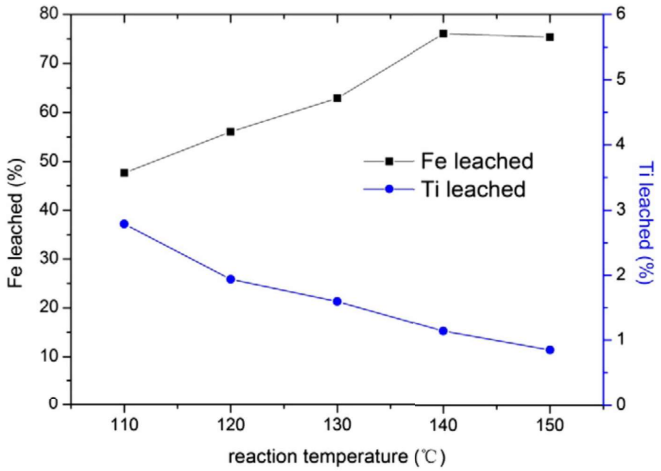

Figure 2.31: Effect of reaction temperature, $H2SO_4$ concentration of 20 wt%, with a reaction time of 3 hours[70].

Furthermore, they also found a decrease in iron dissolution when varying the acid concentration. It was found that there was a decrease in dissolution for iron when the acid concentration was increased from 40 wt% to 50 wt%. This was due to agglomeration that formed around the unreacted ilmenite particles, which prevented further reaction between ilmenite and sulphuric acid.

The size dependency for titanium and iron recovery was investigated by Baba et. al[71] and Han et. al.[72] respectively. Different ilmenites were used in Nigerian ilmenite for titanium extraction and ilmenite from Thailand for iron extraction. Both had approximately 30 wt% titanium and 28 wt% iron. The results from the analysis can be seen in Figure 2.32. From the figure, it becomes clear that for a decreasing particle size both the dissolution of iron and titanium increases.

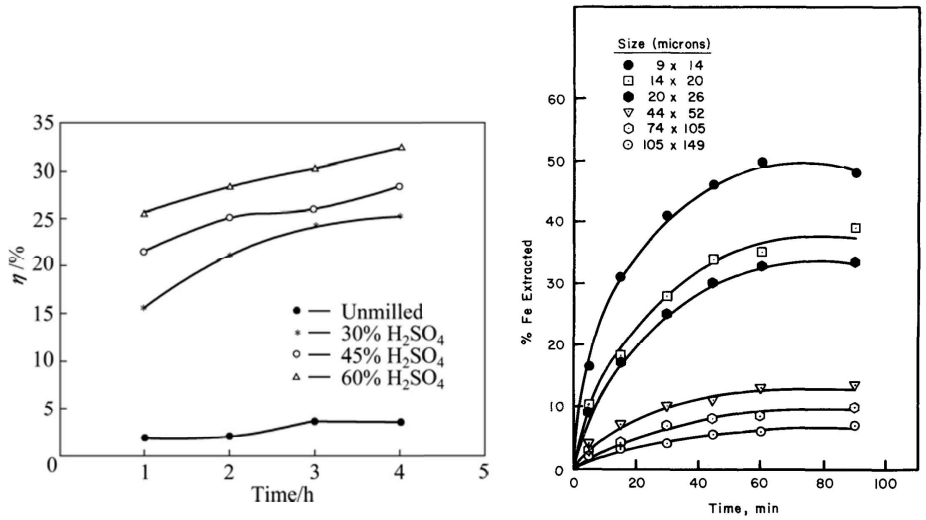

(a) Extracted titanium, with different H_2SO_4 concentration, milled particle size(d_{50}=3.89μm), un-milled(d_{50}=68μm)[71].

(b) Extracted iron, with H_2SO_4 concentration of 18.8M[72].

Figure 2.32: Extracted concentration plotted against leaching times.

2.9 Summary

In this chapter, a wide range of theory has been presented. An explanation of the iron system and how iron oxides act during oxidation and reduction has been presented. This has been done to be able to compare the changes occurring during ilmenite oxidation and reduction to that of iron. Since the iron system and the changes that occur have been well documented one can draw lines between the two systems and use it to explain some of the results presented later on. To be able to draw these conclusions, one also needs an understanding of the iron-titanium and iron system. The relevant theory for this has been presented and how ilmenite reduction progresses has been given. Special attention has been given to the morphology of iron during reduction. Finally, an overview of the sulfate process was presented. The reason for this is that it forms a good basis for discussion of the ICP results presented later.

3 Method and Materials

In the following chapter the different materials that were used during the experiments, ilmenite concentrate and crucibles are mentioned as well as the methodology and equipment used for oxidation and reduction. The different analysis methods are explained, and the parameters used for each are brought forth.

3.1 Materials

3.1.1 Ilmenite concentrate

Two ilmenite concentrates were used. One was sourced from Mintek, KwaZulu-Natal beach sand(KZN), and the other was obtained from Eramet Titanium and Iron AS and will be referred to as GCO. In the following section, the analysis of the different samples is given.

In Tables 3.1 and 3.2 the chemical analysis of GCO ilmenite and KZN ilmenite are given respectively. Since both are sand-ilmenite their composition is similar, where the main difference can be seen in Ti:Fe ratios, 1.2:1 and 0.9:1 respectively.

Table 3.1: XRF and wet chemical analysis performed on GCO ilmenite, by Eramet Titanium and Iron AS, given in wt%.

TiO_2	Fe_{tot}	FeO	Fe_2O_3	MgO	Al_2O_3	SiO_2
53.46	30.61	19.2	22.4	0.6	0.56	0.13
V_2O_5	Cr_2O_3	MnO	P_2O_5	Nb	Zn	ZrO_2
0.308	0.156	1.02	0.025	0.058	0.0139	0.158

Table 3.2: XRF and wet chemical analysis performed on KZN ilmenite, by Eramet Titanium and Iron AS, given in wt%.

TiO_2	Fe_{tot}	FeO	Fe_2O_3	MgO	Al_2O_3	SiO_2
47.4	36.2	31.9	16.3	0.4	0.3	0.3
V_2O_5	Cr_2O_3	MnO	P_2O_5	CaO		
0.3	0.08	1.1	0.01	0.03		

Laser diffraction was used to determine the particle size distribution of the ilmenite samples. A Malvern Mastersizer 3000 was used to obtain the results. During measurements, the samples were continuously stirred at 2400 rpm. In Figure 3.1 the distribution of the ilmenite samples is shown. (a) GCO, (b) KZN ilmenite. The d_{10}, d_{50} and d_{90} values are given in Table 3.3.

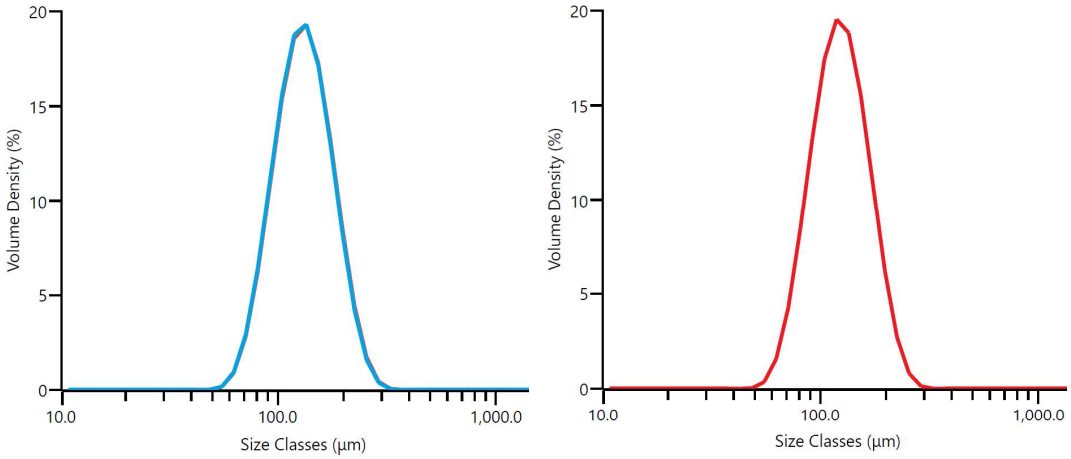

(a) GCO sample (b) KZN sample

Figure 3.1: Size distribution of ilmenite samples.

Table 3.3: d_{10}, d_{50} and d_{90} values given in μm.

	$d_{10}(\mu m)$	$d_{50}(\mu m)$	$d_{90}(\mu m)$
GCO	88.5	131	193
KZN	83.5	123	180

3.1.2 Crucibles

In experiments conducted at HySA alumina crucibles were used for both oxidation and reduction with the measurements of 14.9 cm x3.3 cm x1.5 cm.

3.2 Methodology

In the following section, the scientific approach is given for each experimental method and analytical techniques.

3.2.1 Oxidation

To get more insight into the oxidation progression micro thermogravimetric analysis(TGA) was used at different heating rates. An SDT Q 600 from TA instruments was used and approximately 20 mg of ilmenite sample was heated up to 1000°C under a synthetic air atmosphere with a flow rate of 50 ml/min. The heating rates that were chosen were 2.5, 5, 10, 20, and 30°C/min for the GCO sample and 2.5, 10, and 20°C for KZN ilmenite. Some of the oxidation runs included an extra step to remove any moisture or crystalline water. This was achieved by heating the ilmenite powder to 150°C for 4 hours before oxidizing at the set point temperature.

For oxidation, a Lenton Elite BRF 15/5 muffle furnace was used. The heating rate was set to 20°C per minute, and three different oxidation temperatures were chosen. The holding time after reaching the set point temperature was 1 hour. The three temperatures chosen were 700, 800, and 1000°C. An alumina crucible was filled with 30 grams of ilmenite sample. Weights before and after were recorded.

The oxidized ilmenite was sent to Eramet Titanium and Iron AS in Norway for wet chemical analysis. The sample was milled and then dissolved in acid. The FeO amount was found through titration, and the Fe_2O_3 amount was calculated from these results along with XRF data.

3.2.2 Reduction

For reduction, a Carbolite CTF 12/65/550 alumina tube furnace was used. A thermocouple inserted below the tube was used for temperature control, and the tube was sealed off to prevent air intrusion into the tube to prevent sample oxidation and H_2 ignition. The heating rate was given as 7 °C per minute. During heating, the reaction chamber was purged with nitrogen at 1.75 liters per minute until the set point temperature was reached. For the GCO sample, three different set points were used, 800, 900, and 1000°C, while for the KZN ilmenite, the set point of 800°C was used. The reason for not using higher reduction temperatures was due to time constraints. After the set point was reached, hydrogen gas was introduced into the furnace tube at 2.4 liters per minute. The holding time was varied between four times i.e., 5, 15, 35, and 60 minutes. The weight before and after reduction was then recorded using an Adam PGW 253e scale with an accuracy of 0.001 g.

Calculating conversion

The conversion degree was calculated by only considering the oxygen that was bound to iron. The irons valence state decides the amount of oxygen connected to it. The valence state, in turn, varies with the oxidation degree. Since the mass changes are recorded from each experiment, in combination with wet chemical analysis, one can indicate the theoretical conversion obtained through the following equations. Where m^O_{ox} would be the total mass of oxygen bonded to iron oxides, $m^O_{Fe^{2+}}$ and $m^O_{Fe^{3+}}$ is the mass of oxygen connected to ferrous and ferric iron respectively. The values for $wt\%FeO$ and $wt\%Fe_2O_3$ are obtained through chemical analysis, while the mass change Δm is measured before and after reduction. The conversion degree (Z) can then be calculated through Equation 3.5, shown below.

$$m^O_{ox} = m^O_{Fe^{2+}} + m^O_{Fe^{3+}} \tag{3.1}$$

$$m^O_{Fe^{2+}} = (wt\%FeO * m_{start}) * \frac{16}{16 + 55,85} \tag{3.2}$$

$$m^O_{Fe^{3+}} = (wt\%Fe_2O_3 * m_{start}) * \frac{3 * 16}{(3 * 16) + (2 * 55,85)} \tag{3.3}$$

$$\Delta m = m_{start} - m_{end} \tag{3.4}$$

$$Z = \frac{\Delta m}{m^O_{ox}} \tag{3.5}$$

Calculating oxygen to iron ratio(O:Fe)

Another comparison method used was the oxygen-to-iron ratio(O:Fe). During reduction, it has previously been assumed that the only oxygen removed is connected to iron, which is the case for lower temperatures. With this assumption, the weight loss is a direct indication of the amount of oxygen removed from the sample. When this information is used in combination with the wet chemical analysis, one can get an indication of the remaining oxygen in the sample. The ratio is then calculated based on the total iron present in the sample and the remaining oxygen.

Weight change

For the staring point for each oxidation temperature some assumptions were made. Since the different oxidation temperatures lead to different amounts of FeO and Fe_2O_3 some assumptions had to be made in regards to the starting points for the weight change. Since there was a noticeable change after removing the moisture from ilmenite, the weight change recorded for this oxidation at each temperature was used as a starting point in the %weight change vs. temperature graphs.

3.2.3 X-Ray diffraction

To conduct the XRD analysis a PANanlytical XPERT-PRO was used with a Cobalt source. A 2θ system was used with a starting point of 4°, and an endpoint of 100 was analyzed. The machine used a PW3064 spinner stage and had a step size of 0.0170. A Fixed slit was employed with a slit size of 0.4354. The databases used for the analyses were the Powder Diffraction File 4+(PDF-4+) and Crystallography Open Database 2020(COD2020).

3.2.4 Secondary electron microscopy

To obtain backscattered electron(BSE), secondary electron(SE) images, and EDS analysis a secondary electron microscope(SEM) was used. The model was a FEI FEG Quanta 250. Installed with an Oxford EDS detector working through the INCA platform. An accelerating voltage of 15 kV was used during the analysis. To coat the specimens an Emscope TB500 carbon coater was used. The samples were coated with carbon under vacuum.

To examine the cross-section of the grains, a selected set of samples where cast in epoxy resin and polished to a 1 μm finish. For topology analysis, the powder was mounted on an aluminum stub with carbon tape before carbon coating.

3.2.5 ICP-OES

To prepare for ICP-OES the following steps were taken. The as-received samples along with the different reduced samples were analyzed using an Agilent 5110 ICP-OES Instrument coupled with a VistaChip II CCD detector. Ultraspec aqueous-certified single-element reference standards, iron, and titanium, obtained from De Bruyn Spectroscopic Solutions, were used.

Alkaline fusion

Alkaline fusion was done on the as-received samples to determine the total iron and titanium content in each ilmenite. The ilmenite was milled for 4 minutes to reach a sufficient grain size for the fusion. 0.2 g of the milled sample was weighed, along with 2 g of Na_2O_2 and 0.5 g of Na_2CO_3. This was heated in a zirconium crucible. After cooling the fused material was solubilized using a 20% mixture of 1:1 water to HNO_3.

Hot acid leaching

To determine the extent of iron and titanium dissolution hot acid leaching was performed on the reduced samples as well as the as-received and oxidized samples. It was believed that this method could be a reliable way to determine iron metallization. A 50 vol% H_2SO_4 was prepared. 100 mL of the acid mixture was added along with 1 g of sample in a Pyrex beaker. To determine a baseline, as-received samples were leached for different times at 80°C. Any dissolved Fe and Ti were subtracted from proceeding leachings to account for the unintentional dissolution of the target elements, i.e., Fe and Ti. Based on these findings, the remaining samples were leached for 90 minutes. After which, the solution was filtered through a 40 μm filter. The leachate was dried, and the filtrate was diluted down in a 500 mL volumetric flask before being sent to ICP-OES.

4 Results

4.1 Starting material

Weathered ilmenite can be complex, leading to difficulty in determining the phases present and what amount of each phase can be found. For this reason, the first section of the results is dedicated to identifying the structure and phases of the two starting materials used for the experiments.

4.1.1 GCO ilmenite

The XRD results obtained atNWU were analyzed through two different databases, PDF-4+ and COD. A sample was also analyzed in Norway at NTNU for comparison. The analysis, as well as the Rietveld analysis, are shown in Table 4.1.

Table 4.1: Rietveld analysis based on XRD results presented in Appendix B for the GCO sample.

(wt%)	NTNU (PDF-4+)	NWU (PDF-4+)	COD-2020
Rutile	9.52	-	-
Pseudorutile	52.15	49.1	x
Ilmenite	38.33	32.1	x
Hematite	-	18.8	-
Pseudobrookite	-	-	-

Topology and cross-section of the grains were also analyzed. Some of the grains cross-sectioned are shown in Figure 4.1, with the accompanying EDS analysis shown in Table 4.2. From the figure, one can see that in some of the grains, a lighter gray phase is visible in a vein-like structure, while the outside of the grain has a darker shade. Other grains like shown in Figure 4.1c) indicate little difference in composition by having similar shades of gray.

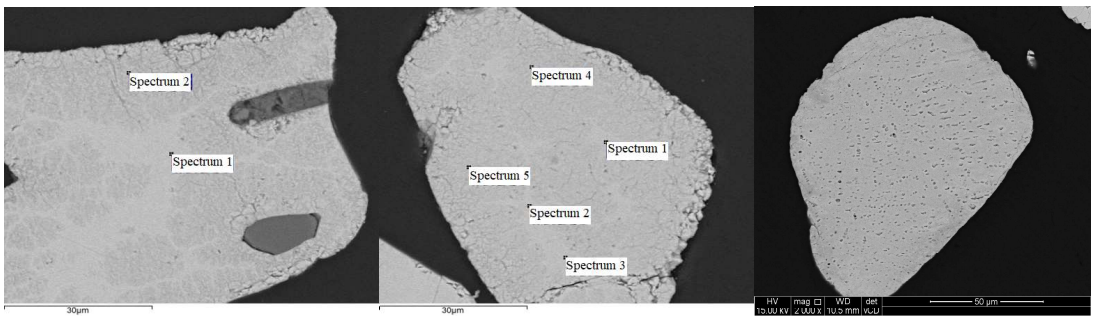

(a) (b) (c)

Figure 4.1: Grains in as-received GCO sample, cross-section, EDS values shown in Table 4.2.

Table 4.2: Values detected during EDS analysis shown in Figure 4.1a (left), and 4.1b (right).

At%	Ti	Fe	O
Spectrum 1	15.8	13.9	70.4
Spectrum 2	19.4	12.4	68.2

At%	Ti	Fe	Mn	Mg	O
Spectrum 1	15.6	15	0.8	0	68.7
Spectrum 2	15.5	15.1	0.5	0	68.84
Spectrum 3	15.2	15.7	0	0.6	68.6
Spectrum 4	15.7	12.3	0.4	0	71.6
Spectrum 5	16.2	12.1	0.5	0.6	70.7

In Figure 4.2 the secondary electron images are presented of the topology for different grains at 8500x and 30000x magnification. From the EDS analysis, it became clear that the outside of the grain had a Ti:Fe mol ratio of approximately 1.3-1.8. Furthermore, there were grains with a rougher surface than Figure 4.2b). For Figure 4.2a) the surface was found to be an average representation of the other grains at this magnification.

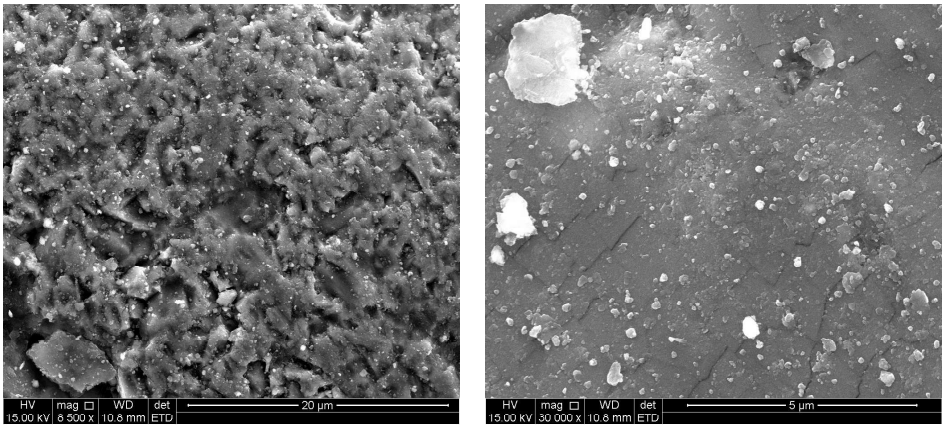

(a) (b)

Figure 4.2: Grains in as-received GCO sample, topology.

4.1.2 KZN ilmenite

Rietveld analysis was performed on the KZN ilmenite by the North-West University(NWU). The results are shown in Table 4.7. From the table, one can see a substantial ilmenite content, 84.6 wt%, with smaller amounts of hematite and rutile, 13.6 and 1.8 wt%, respectively.

EDS analysis was performed on the KZN ilmenite. Some of the grains are shown in Figure 4.3. The KZN ilmenite contained more impurities (i.e., non-Fe.and -Ti constituents than the GCO sample. During the analysis, one could see grains that were encompassed by oxides high in silicon, Figure 4.3a). One also found phases giving an indication of being pure iron oxides, while others were found to have a composition close to rutile. From the cross-sections, a complex inner structure was revealed for some of the grains, while others contained compositions close to ilmenite.

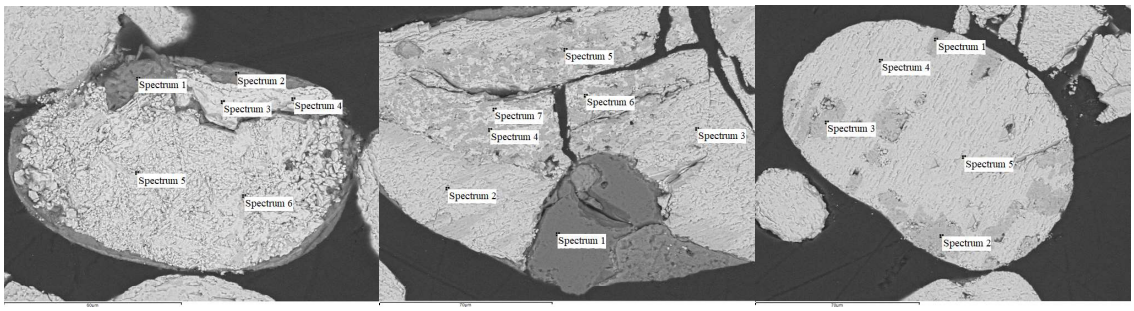

(a) EDS values shown in Table 4.3. (b) EDS values shown in Table 4.4. (c) EDS values shown in Table 4.5.

Figure 4.3: Observed dissimilar grains present in the cross-sectioned KZN ilmenite.

A substantial amount of EDS analyses was conducted on the different phases found during the cross-sectional analysis. The results are presented in Tables 4.3-4.5. Points of interest are the high concentrations of impurities in some phases compared to others. For instance, the particle analyzed in Figure 4.3a) had equal to or less than 0.4 at% Ti and had a Fe:O ranging between 0.3 and 1.1. Other particles shown in Figure 4.3 had phases comparing Ti:O ratios to stochiometric rutile, i.e., atomic ratio of 1:2.

Table 4.3: EDS analysis for grain shown in Figure 4.3a).

At%	Ti	Fe	Mg	Al	Si	Ca	P	Na	Cl	K	O
Spectrum 1	0.3	4.2	1.5	6	21.4	0.3	0	1.5	0	1.7	63.3
Spectrum 2	0	1.76	2.3	2.1	11.7	8.90	5.5	0	0.1	0.7	67.1
Spectrum 3	0.3	34.4	0	0	0	0	0	0	0	0	65.3
Spectrum 4	0.3	30.1	0	0	0	0	0	0	0	0	70
Spectrum 5	0.4	57.8	0	0	0.9	0	0	0	0	0	46
Spectrum 6	0	33.3		0	0	0	0	0	0	0	66.7

Table 4.4: EDS analysis for grain shown in Figure 4.3b).

At%	Ti	Fe	Si	Mn	O
Spectrum 1	0	0	31	0	69
Spectrum 2	16.4	13.8	0	1.9	67.9
Spectrum 3	15.9	13.8	0	2.1	68.2
Spectrum 4	21.7	6.4	0	0	71.9
Spectrum 5	20.2	12.7	2.5	0.3	64.3
Spectrum 6	7.1	26.1	0	0	66.8
Spectrum 7	6.5	26.2	0	0	67.3

Table 4.5: EDS analysis for grain shown in Figure 4.3c).

At%	Ti	Fe	Si	Al	Ca	Mn	O
Spectrum 1	23.4	3.2	0.2	0.3	0.1	0	72.8
Spectrum 2	22.6	7.1	0.4	0.4	0	0	69.4
Spectrum 3	18.1	7.8	0	0	0	0	74.1
Spectrum 4	17.5	17.4	0	0	0	1.9	63.2
Spectrum 5	16.5	16.2	0	0	0	1.8	65.5

The topology for the KZN ilmenite is shown in Figure 4.4. In a similar fashion as the GCO ilmenite, two secondary electron images are given with magnifications of 8500x and 30000x. EDS was performed on chosen grains, and a Ti/Fe ratio seemed to differ substantially from grain to grain, with mol ratios ranging from 0.2-1.4. For the grains with the lowest Ti/Fe ratios, Fe/O ratios were calculated to be 0.5, similar ratios of FeO.

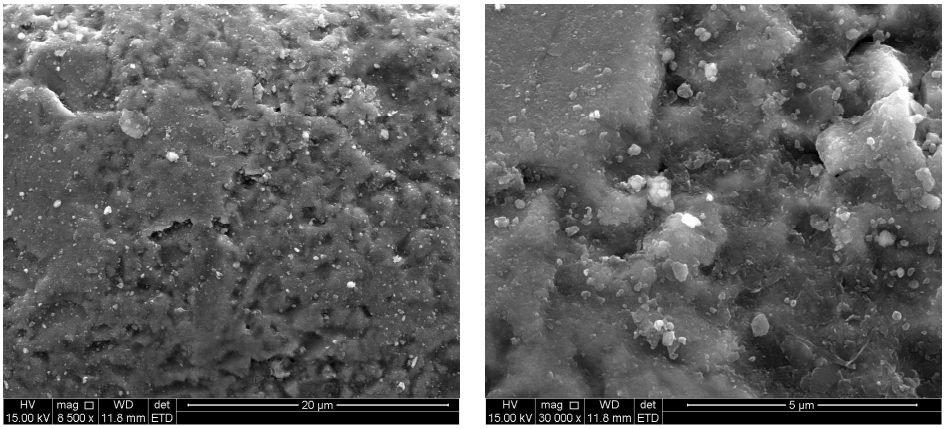

(a) (b)

Figure 4.4: Grains in as-received KZN sample, topology.

4.2 Understanding oxidation

To gain a better understanding of oxidation, TGA was performed. The results are presented below. The weight change in regards to temperature is shown in Figure 4.5. From the graph in Figure 4.5a) the GCO sample is presented. It can be seen that initially, the weight tends to decrease up to temperatures around 400°C. After which it increases with a linear rate up to temperatures of 700°C. Beyond this temperature, the rate first becomes greater before it slopes off. One can also notice that as the heating rate increases, the total weight change achieved decreases.

Similar findings were observed for the KZN ilmenite, Figure 4.5b), where the total weight achieved from oxidizing decreases with increasing heating rate. The weight change curves for the KZN sample show a more sigmoidal shape compared to the GCO sample, as well as reaching higher overall weight gain.

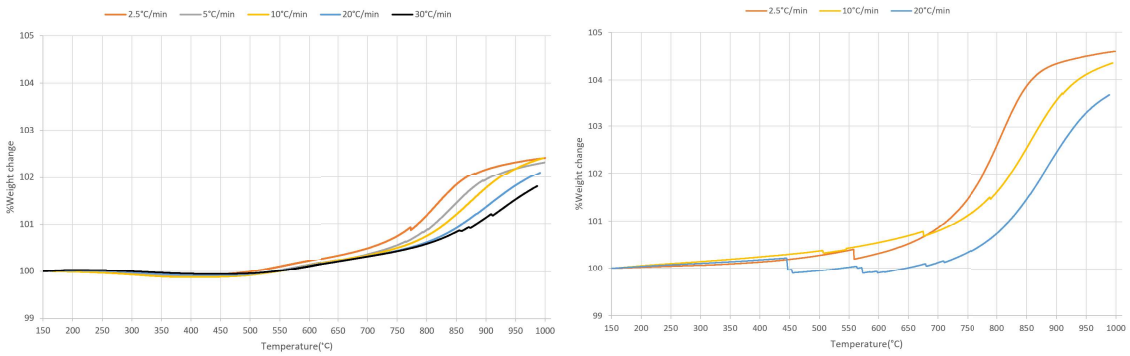

(a) GCO sample (b) KZN sample

Figure 4.5: The change in weight plotted against temperature for different heating rates.

In Figure 4.6, the change in %wt change per change in temperature is plotted against temperature. For the GCO sample, Figure 4.6a), one can see that the rate reaches a low point around 300°C. The graph shows a plateau between 530°C and 730°C, depending on the heating rate. After which there is seen a rate peak for all five heating rates, for 2.5°C/min it is around 820°C.

In Figure 4.6b), showing the KZN sample. The change in weight over the change in temperature shows a low rate up to 600°C before a sharp increase and peak at approximately 820°C for a heating rate of 2.5°C/min. For lower heating rates, the peak shifts towards higher temperatures.

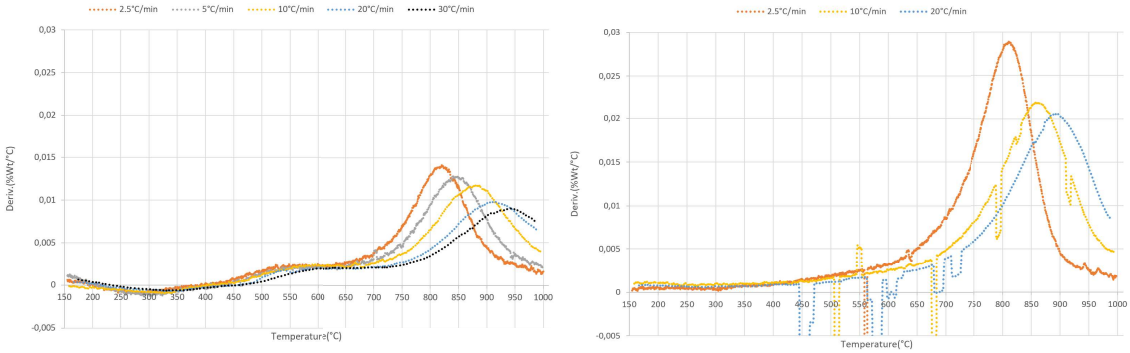

(a) GCO sample (b) KZN sample

Figure 4.6: The 1. derivative of %weight change as a function of temperature.

In Figure 4.7a), the first derivative of %weight change as a function of time for the GCO sample is given. As the heating rate increases, the peaks sharpness increases. The initial negative rate becomes more clear, while the plateau duration shortens at higher heating rates. The results for the KZN beach sample are shown in Figure 4.7b). One can see that the change in %weight change over the change in time shows an increasing trend with increasing heating rate, with the highest value given for the 20°C/min.

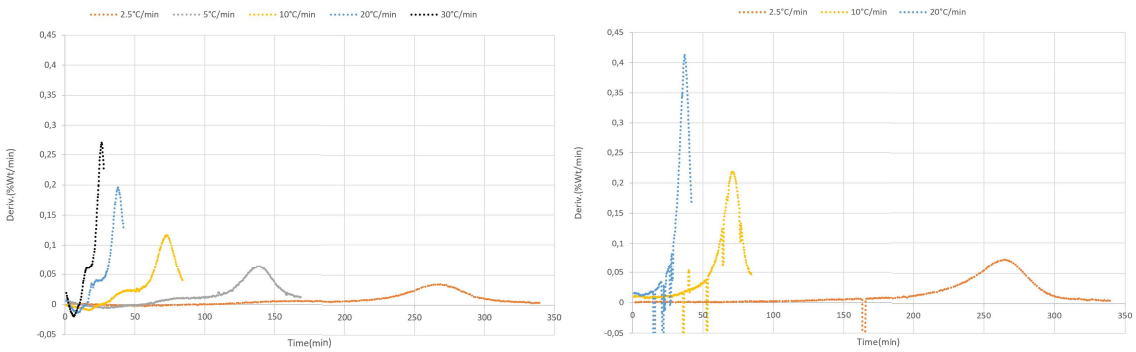

(a) GCO sample (b) KZN sample

Figure 4.7: The first derivative of %weight change as a function of time is plotted.

In Figure 4.8 one can see the measured heat flow as a function of temperature. The data from the GCO sample is plotted in Figure 4.8a) and the KZN ilmenite is plotted in Figure 4.8b). In the GCO sample, initially, there is a negative heat flow for the lower heating rates. For the highest heating rate of 30°C/min, it stays positive. Furthermore, a rate change can be seen around 550°C, before the peak is reached at approximately 850°C. For the KZN sample, the measured heat flow stays negative for all heating rates except the 20°C. The most distinguishable peak is found at approximately 520°C after which the slope switches from decreasing to increasing.

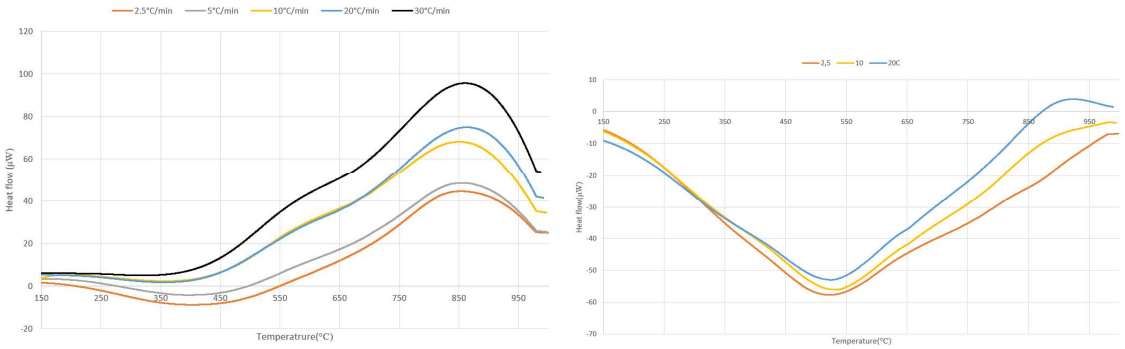

(a) GCO sample (b) KZN sample

Figure 4.8: Measured heat flow as a function of time for GCO and KZN ilmenite.

In the graph displayed in Figure 4.9, one can see the change in heat flow measured by the equipment per change in temperature. The measured heat flow can indicate the enthalpy of a possible reaction that occurs. For the GCO sample, shown in graph (a), it is clear that there are four different areas of change. Initially, the rate of change is negative before two positive peaks occur. After which, a sharp negative down turn towards the end of the experiment. In graph (b), for the KZN sample, two main areas are seen. Initially, a negative value is given before an increase to a positive value at approximately 530°C, after which it stays at the same value up until the end of the oxidation run.

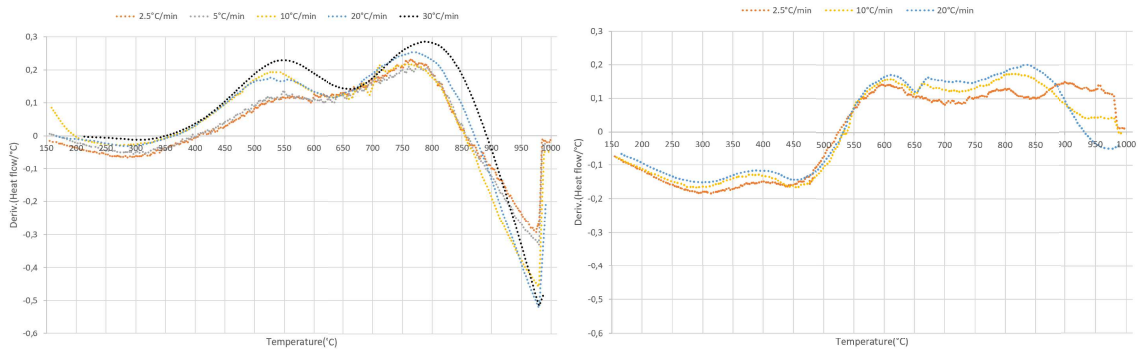

(a) GCO sample (b) KZN sample

Figure 4.9: The change in heat flow over the change in temperature is plotted against temperature.

Oxidation was performed for three set point temperatures, 700, 800, and 1000°C, in a muffle furnace. The weight change was noted down and is shown in Figure 4.10. For the GCO sample (a), it is important to note that for 700°C, the weight decreases. The greatest weight change recorded for each temperature was pre-heated to 150°C to remove moisture. The weight decrease accounted for 0.2%. Samples from KZN (b) showed positive values for all oxidation temperatures, and a max weight increase at 1000°C was seen to reach 3.5% weight gain.

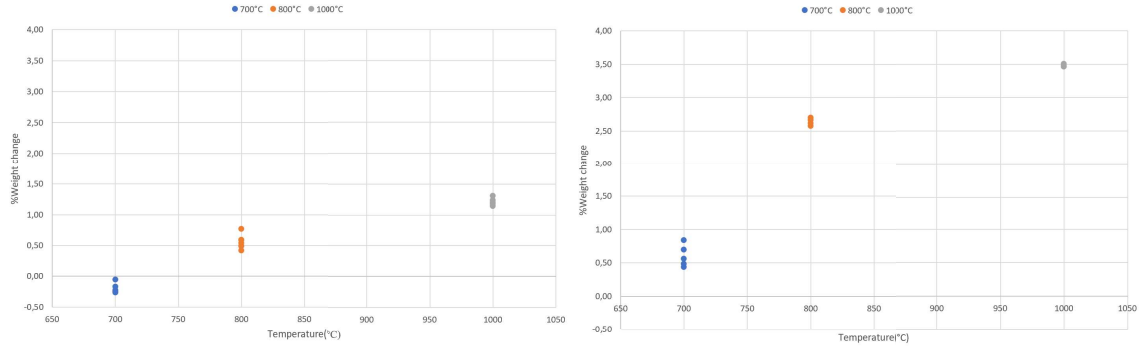

(a) GCO sample (b) KZN sample

Figure 4.10: Recorded weight change after oxidation for 1 hour at different temperatures.

As well as the weight change data shown above some of the oxidized samples were sent to GCO Titanium and Iron AS for analysis. This would give an accurate overview of the iron species distribution. In Figure 4.11a) one can see the distribution of Fe^{2+} and Fe^{3+} for the GCO sample. From the figure, one can see that samples oxidized at 700°C show a difference in the Fe_2O_3 found compared to the starting material. Furthermore, as the oxidation temperature increases the amount of Fe_2O_3 increases along with it. For all samples except the one oxidized at 1000°C and 1400°C for 7 hours, two parallels were conducted.

In Figure 4.11b) the same distribution is given but for the KZN ilmenite. For the starting material, more FeO is found than compared to the GCO ilmenite. The amount of Fe_2O_3 detected increases with increasing oxidation temperature. For the highest oxidation temperature recorded, 1000°C, the maximum amount of Fe_2O_3 was detected, 51.8 wt%.

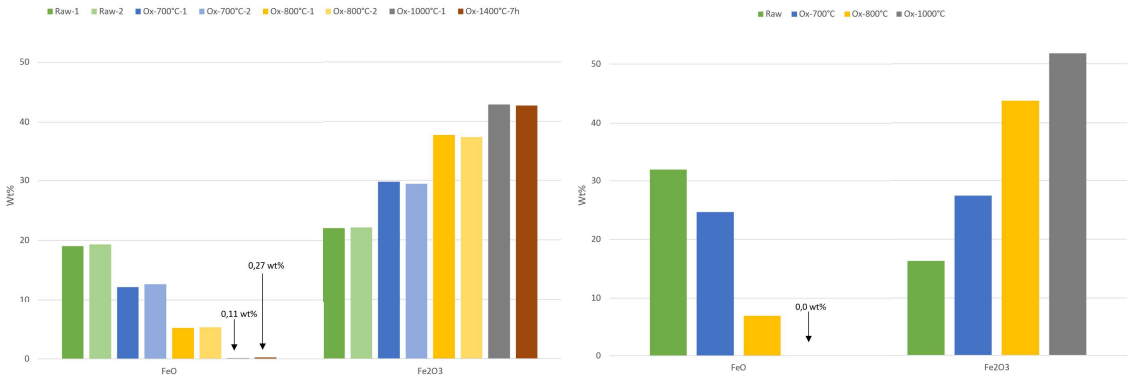

(a) GCO sample (b) KZN sample

Figure 4.11: Overview of iron species, given in weight percent.

4.2.1 XRD and Rietveld analysis

XRD analysis was performed on both the GCO sample and the KZN ilmenite. In Table 4.6, the Rietveld results for the GCO ilmenite are presented. The results can be used to give an indication of which reactions occur during oxidation. Findings to note are that at 700°C, pseudorutile is the main phase present, which is also present in the starting material. For higher oxidation temperatures, 800°C and 1000°C, the phase is no longer found. Instead, one found varying amounts of ilmenite, hematite, and rutile at 800°C and at 1000°C, pseudobrookite and rutile were the main remaining phases.

Table 4.6: Rietveld analysis based on NWU XRD results, normalized for phases found in the XRD analysis, GCO sample.

wt%	As-received	Ox-700	Ox-800	Ox-1000
Rutile	0	14	31.5	22.8
Pseudorutile	49.1	82.2	0	0
Ilmenite	32.1	3.8	51.4	0
Hematite	18.8	0	17.1	8.2
Pseudobrookite	0	0	0	69

In Tabel 4.7, the Rietveld analysis for the KZN ilmenite is presented. From the table, one can see that for the as-received material, the main phases found were ilmenite and hematite, while a small amount of rutile was detected. For the higher oxidation temperatures, the amount of rutile increases, while ilmenite and hematite make up the rest of the material. One thing to note in the analysis for the sample oxidized at 700°C is the high content of hematite detected, 55.5 wt%. For oxidation at 1000°C, one sees the presence of the pseudobrookite phase.

Table 4.7: Rietveld analysis of the KZN oxidized ilmenite.

Wt%/	As-received	Ox-700	Ox-800	Ox-1000
Rutile	1.8	12.8	32.2	15.8
Ilmenite	84.6	31.7	45.7	2.6
Hematite	13.6	55.5	22.2	20.5
Pseudobrookite	0	0	0	61.1

4.2.2 SEM and EDS analysis: Cross-section and topology

To retain clarity as to which sample was subjected to analysis, the GCO and KZN samples were presented separately. First, the cross-section for the GCO ilmenite is presented. Then the cross-section for the KZN ilmenite is presented. Finally, the differences in the topology for both ilmenites are mentioned.

GCO ilmenite

In Figure 4.12 an overview of different grains is shown from each oxidation temperature along with the as-received sample. EDS analysis was conducted on the different phases present in the grain for each oxidation temperature. For the sample oxidized at 700°C in Table 4.10 and Table 4.11, while for sample oxidized at 800°C are given in Table 4.8 and for the sample oxidized at 1000°C, the values are shown in Table 4.9.

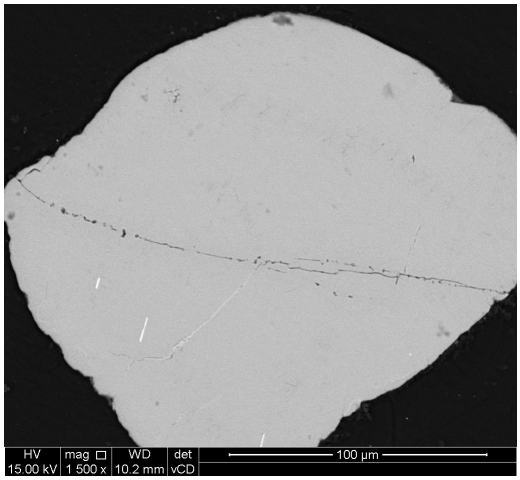

(a) Grain in sample oxidised at 700°C

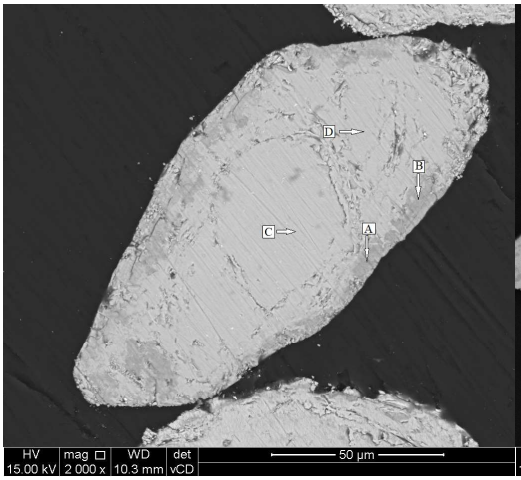

(b) Grain in sample oxidised at 800°C

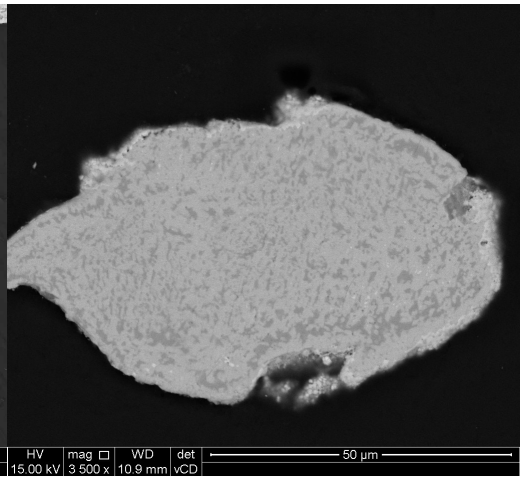

(c) Grain in sample oxidised at 1000°C

Figure 4.12: BSE images showing grains from samples oxidized at different temperatures.

The EDS analysis for the samples oxidized at 800°C are given in Table 4.8. Points of interest are that the darker phases towards the edge of the grain have a higher Ti:Fe ratio than the lighter gray phases towards the center of the grain.

Table 4.8: EDS analysis for GCO sample oxidised at 800°C, shown in Figure 4.12b).

At%	Ti	Fe	Mn	Mg	O
A	17.0	12.6	0	0.4	70.0
B	23.2	9.8	0	0.7	66.2
C	16.5	13.4	0	0.8	69.3
D	14.6	16.1	0.2	0.9	68.2

For the sample oxidized at 1000°C, the EDS values are given in Table 4.9. Two main phases were seen in the grains, dark gray and gray. The dark gray phase had a higher concentration of titanium while the gray phase was found to be a more even distribution.

Table 4.9: EDS analysis for GCO sample oxidised at 1000°C, shown in Figure 4.12c).

At%	Ti	Fe	O
Spectrum 1 (dark gray)	24.6	1.2	74.3
Spectrum 2 (dark gray)	19.2	7.76	73.1
Spectrum 3 (gray)	13.3	14.4	72.4
Spectrum 4 (gray)	14.7	11.7	73.5

GCO ilmenite oxidation for 700°C

Special attention is given to the sample oxidized at 700°C due to the obtained XRD results. From the images shown in Figure 4.13, it can be seen that the grains are largely homogeneous. The bright spot seen in Figure 4.13c were found to be phases high in Zirconium.

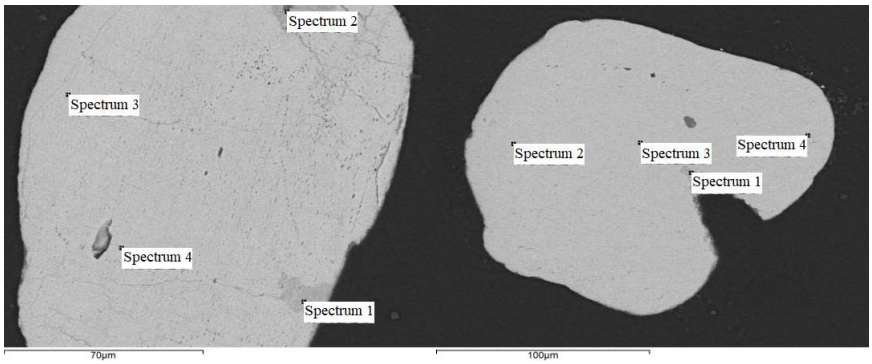

(a) (b)

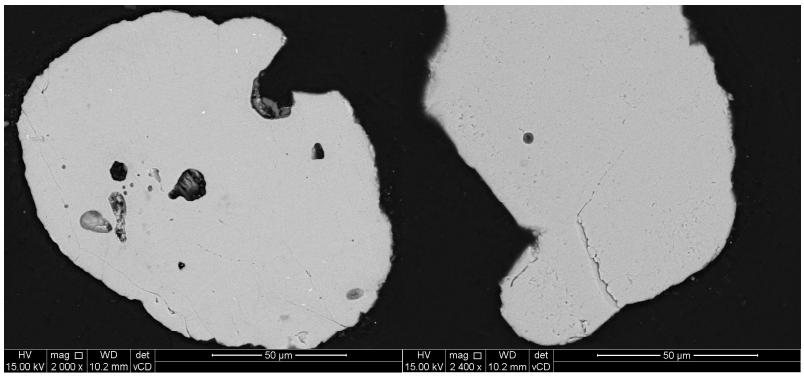

(c) (d)

Figure 4.13: Different grains from samples oxidized at 700°C.

EDS analysis was performed on grains shown in Figure 4.13a and 4.13b. The values are given in Table 4.10 and Table 4.11. From the tables, one can see that the darker phases tend to be higher in titanium along with other impurities like aluminum or silicon. While the brighter phases have a lower iron content than titanium and little to non impurities are present.

Table 4.10: EDS analysis of the grain displayed in Figure 4.13a.

At%	Ti	Fe	O	Al	Si	Mn
Spectrum 1	23.0	3.6	70.7	1.9	0.7	0
Spectrum 2	17.0	1.6	72.9	5.2	3.3	0
Spectrum 3	19.9	12.5	67.9	0	0	0.4
Spectrum 4	19.4	12.0	68.1	0.6	0	0

Table 4.11: EDS analysis of the grain displayed in Figure 4.13b.

At%	Ti	Fe	O	Al	Si	P
Spectrum 1	16.6	1.1	74.2	4.6	2.4	1.1
Spectrum 2	18.36	12.6	69.0	0	0	0
Spectrum 3	17.4	12.4	70.3	0	0	0
Spectrum 4	17.2	11.9	70.5	0.5	0	0

Oxidised KZN ilmenite

Due to the complexity of the grain in the KZN ilmenite, greater analysis was necessary. Considering the 700°C oxidation first, presented in Figure 4.14. A wide variety of grains were seen, and a selection was analyzed. In Figure 4.14a), the internal of the grain is free of impurities and has a Ti:Fe ratio close to 1. The darker phases along the edge of the grain were high in titanium and have a Ti:Fe ratio of 5-6. The grain in Figure 4.14b) was seen to have a central phase of high titanium content, separating phases that were high in iron with a Ti:Fe ratio of 0.1-0.3. In the last grain represented, a more natural structure was seen containing a titanium oxide center encompassed by a brighter phase with a higher iron content and an exterior phase with a Ti:Fe ratio of 1.3.

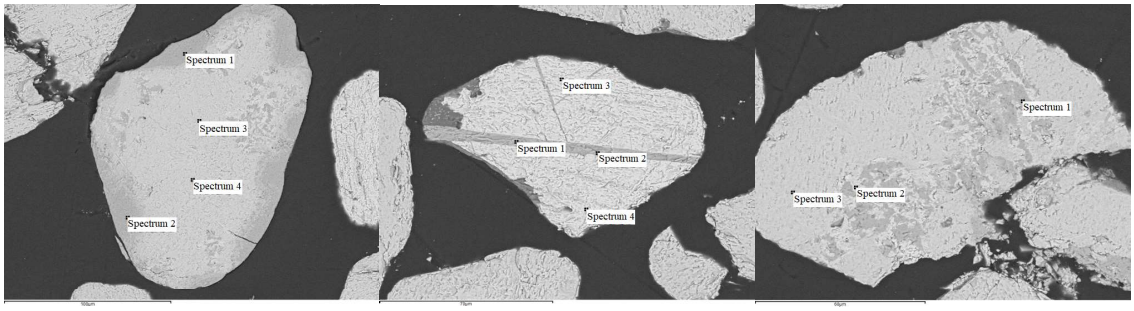

(a) EDS values shown in Table 4.12 (b) EDS values shown in Table 4.13 (c) EDS values shown in Table 4.14

Figure 4.14: Different grains from KZN samples oxidized at 700°C.

Table 4.12: EDS analysis of Figure 4.14a).

At%	Ti	Fe	Si	Al	K	P	Ca	Mn	V	Mg	O
Spectrum 1	21.8	3.4	2.6	0.4	0.3	0.2	0.3	0	0	0.4	70.8
Spectrum 2	22.2	4.1	2.4	0.4	0.2	0.2	0.2	0	0.4	0.4	69.5
Spectrum 3	20.4	20	0	0	0	0	0	0.3	0	0	59.43
Spectrum 4	16.2	16.5	0	0	0	0	0	0	0	0	67.3

Table 4.13: EDS analysis of Figure 4.14b).

At%	Ti	Fe	Mn	Nb	O
Spectrum 1	31.5	0.9	0	0.4	67.2
Spectrum 2	26.6	0.8	0	0	72.6
Spectrum 3	7.7	22.8	0	0	69.6
Spectrum 4	3.5	33.1	0.3	0	63.1

Table 4.14: EDS analysis of Figure 4.14c).

At%	Ti	Fe	Mn	O
Spectrum 1	26.1	0.7	0	72.2
Spectrum 2	10.7	23.5	0.7	65.2
Spectrum 3	18	14.4	2.7	65

The samples oxidized at 800°C showed signs of a more homogeneous internal structure. Two grains are presented in Figure 4.15. In Figure 4.15a), an outer shell was seen with a varying Ti:Fe ratio of 3.4-6, while the interior of the grain had a ratio of 1.3. For the grain shown in Figure 4.15b) an internal phase with a high iron content was seen, while the bulk of the grain was made up of a phase with a Ti:Fe ratio close to 1.

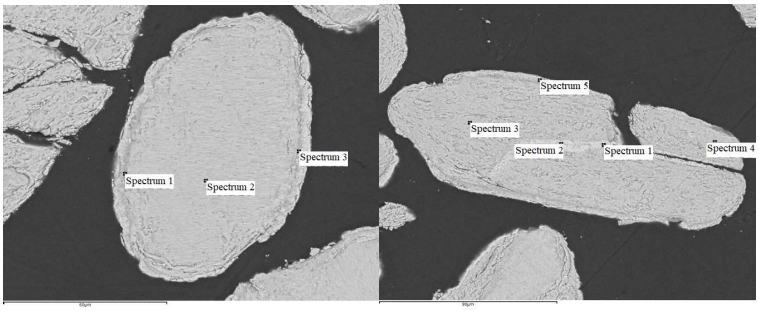

(a) EDS values shown in Table 4.15 (b) EDS values shown in Table 4.16

Figure 4.15: Different grains from KZN samples oxidized at 800°C.

Table 4.15: EDS analysis of Figure 4.15a).

At%	Ti	Fe	Si	O
Spectrum 1	24.4	7.4	0	68.2
Spectrum 2	17.6	13.4	0	69
Spectrum 3	24.4	3.9	0.2	71.5

Table 4.16: EDS analysis of Figure 4.15b).

At%	Ti	Fe	Mg	Mn	O
Spectrum 1	3.7	28.9	0.4	0.3	66.7
Spectrum 2	3	29.9	0.6	0.3	66.2
Spectrum 3	16.8	14.3	0	0.2	68.7
Spectrum 4	16.3	14	0	0.5	69.2
Spectrum 5	14	14.7	0	0	71.4

For the highest oxidation temperature 1000°C, shown in Figure 4.16. From the figures, one can see that different phases are present depending on the grain. For Figure 4.16a), the interior has a Ti:Fe ratio ranging from 1.2 to 1.5 while the exterior ranges from 2.4 to 4.5. In figure b) the phases present seem to be more intermixed. From the two points analyzed one has a very high Ti:Fe ratio, while the other is closer to equimolar ratios.

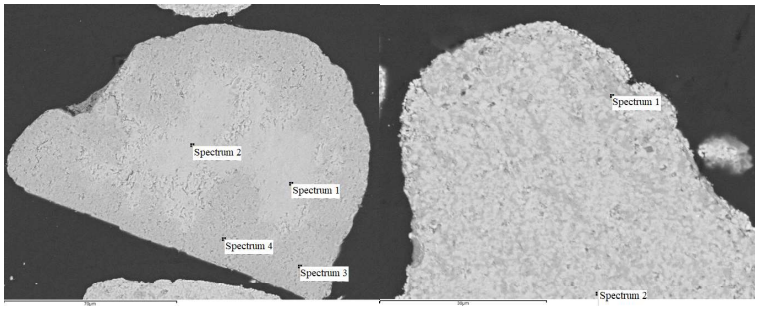

(a) EDS values shown in Table 4.17 (b) EDS values shown in Table 4.18

Figure 4.16: Different grains from KZN samples oxidized at 1000°C.

Table 4.17: EDS analysis of Figure 4.16a).

At%	Ti	Fe	Si	Al	Mn	O
Spectrum 1	18.5	12.1	0	0	1.1	68.4
Spectrum 2	17	13.7	0	0	1.7	67.6
Spectrum 3	21	8.6	0.4	1.1	0	68.9
Spectrum 4	22.4	5	0.4	0.8	0	71.4

Table 4.18: EDS analysis of Figure 4.16b).

At%	Ti	Fe	Mg	Mn	V	O
Spectrum 1	27.1	1.2	0	0	0.9	70.9
Spectrum 2	16.8	15	0.5	0.3	0.6	66.8

Topology of GCO and KZN ilmenite

Looking at how the topology changes during oxidation can give insight into how it will affect the proceeding reduction. In Figure 4.17, the topology of GCO and KZN samples are given for oxidation temperatures of 700 and 1000°C. Things to note when comparing the differences between the two temperatures are as follows. For the GCO sample, the surface is uneven at 700°C, while at 1000°C there seems to be more growth on the surface as well as clearer grains at larger magnifications. While for the KZN sample, the surface is still intact at 700°C and again at 1000°C one can see the formation of small grains on the surface of the grain. Comparing the two ilmenite samples with each other, it seems like the GCO sample has undergone larger changes at lower temperatures compared to the KZN ilmenite. At higher temperatures, it seems that they are similar. More examples of topology changes occurring can be found in Appendix C.

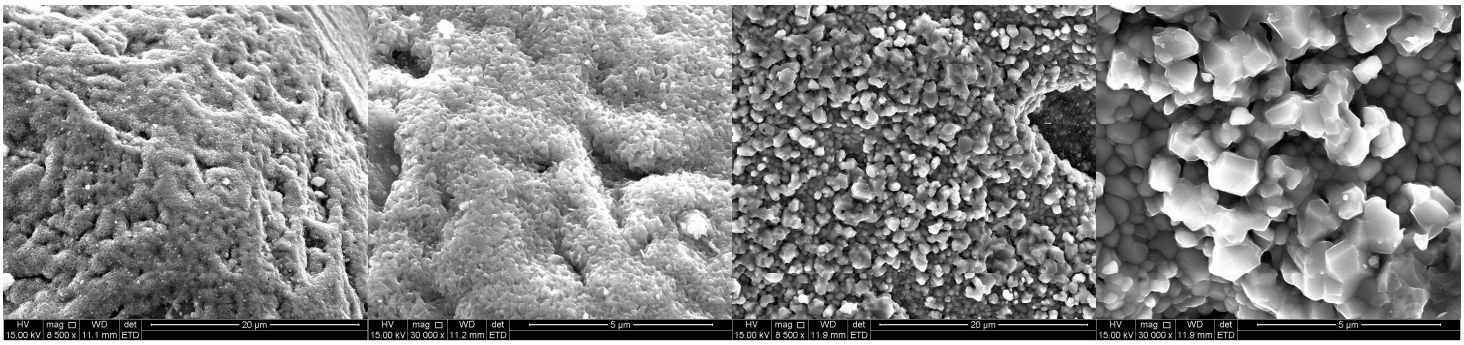

(a) GCO, 700°C, 8500x (b) 700°C, 30000x (c) 1000°C, 8500x (d) 1000°C, 30000x

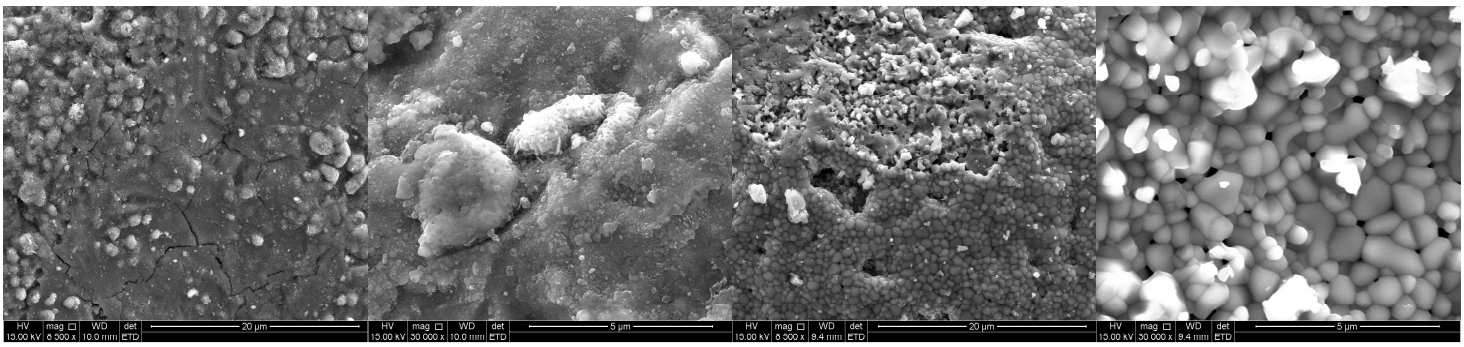

(e) KZN, 700°C, 8500x (f) 700°C, 30000x (g) 1000°C, 8500x (h) 1000°C, 30000x

Figure 4.17: Topology of from both GCO(a-d) and KZN(e-h) sample for oxidation temperatures of 700 and 1000°C.

4.3 Results from reduction

In the following section, the data collected during reduction experiments are presented. The mass loss data are presented in two formats, based on reduction temperature and based on oxidation temperature, giving a good overview for the discussion. After which selected XRD and SEM findings are shown, and points of interest are given. Finally, the results from sulphuric acid leaching are presented. The dissolution rates of iron and titanium are of interest, and how the grains change prior to and after, leaching are given through XRD and SEM results. The experimental data collected from the KZN ilmenite are given separately.

4.3.1 Effect of oxidation temperature

In the following section, the results relating to the oxidation temperature will be presented. In Figure 4.18 one can see both the %weight change curves(a) for the GCO sample reduced at 800°C as well as the oxygen to iron ratio(O:Fe)(b). Due to the different oxidation degrees, the starting point for each sample was different. Common in both curves was that the higher the oxidation degree, the higher the starting point was. The positioning of the weight change curves was calculated based on the mass gain during oxidation, while the O:Fe ratio was from chemical analysis. Furthermore, from the curves themselves, one can see that higher oxidation degrees will reach complete theoretical metallization (O:Fe=0) faster than lower oxidation degrees. While the sample oxidized at 700°C did not reach this value. For the sample oxidized at 1000°C, one can see a reduction run of 28 minutes instead of 35 due to an alarm going off.

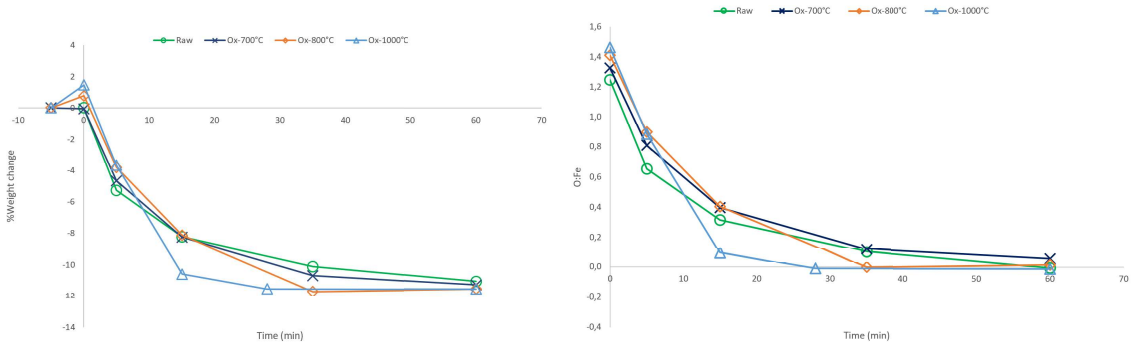

(a) %Weight change curves

(b) O:Fe ratio

Figure 4.18: Weight change(a) and O:Fe(b) curves for GCO sample reduced at 800°C.

The %weight change curves and oxygen-to-iron ratios for samples reduced at 900°C are shown in Figure 4.19. From the weight change curves, one can see that the curves for the oxidized samples are grouped together, while the as-received(Raw) sample indicates a slower reaction rate and final reduction degree. In comparison, the oxygen-to-iron ratio for all the curves indicates the same rate, while the as-received samples show an increased reduction degree compared to the other three.

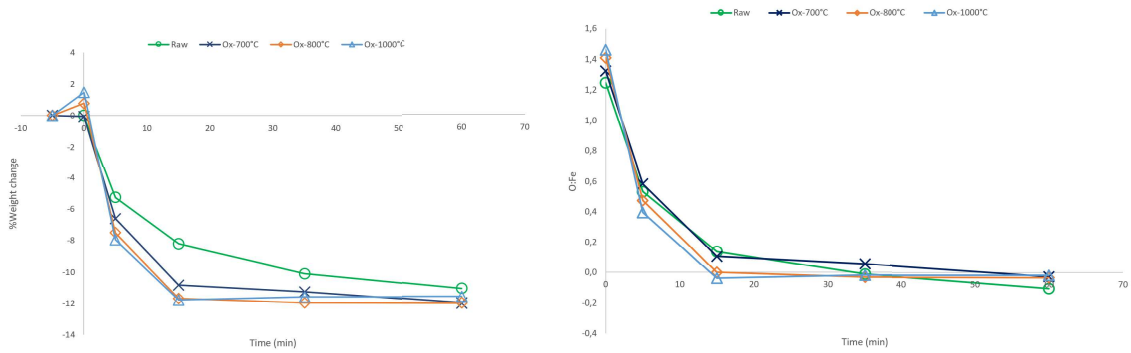

(a) %Weight change curves (b) O:Fe ratio

Figure 4.19: Weight change(a) and O:Fe(b) curves for GCO sample reduced at 900°C.

In Figure 4.20 the weight change and O:Fe ratio curves for samples reduced at 1000°C are represented. From the graph, it can be seen that initially, the highly oxidized sample reaches greater weight changes, while after 15 minutes, the weight change curves plateau around the same level for all samples. For the O:Fe ratio, the values are negative after 15 minutes of reduction.

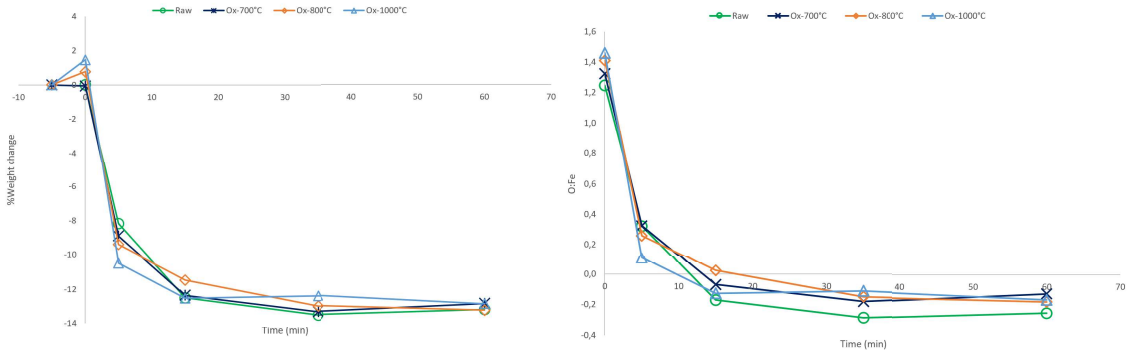

(a) %Weight change curves (b) O:Fe ratio

Figure 4.20: Weight change(a) and O:Fe(b) curves for GCO sample reduced at 1000°C.

4.3.2 Effect of reduction temperature

The following section displays the weight change and conversion obtained from the reduction reaction but separated by the oxidation temperatures. The curves obtained for the as-received sample are shown in Figure 4.21, while for the samples oxidized at 700°C are shown in Figure 4.22, for oxidation at 800°C is shown in Figure 4.23 and for 1000°C in Figure 4.24. The lines labeled as Fe^{3+} and Fe^{2+} show the final points where the pseudobrookite and ilmenite are used up, respectively.

Comparing Figures 4.21-4.24, it becomes evident that increasing the reduction temperature will lead to higher weight changes or conversion degrees. For samples oxidized at 1000°C, the difference is less. Weight change curves for both reduction temperatures of 800°C and 900°C end in similar areas, while an increase of reduction temperature to 1000°C lead to a higher mass loss.

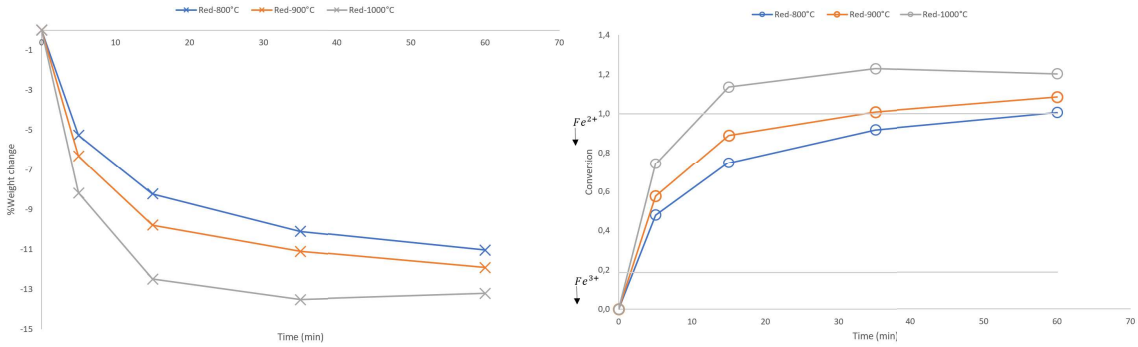

(a) Weight change curves (b) Conversion curves

Figure 4.21: Weight change(a) and conversion(b) curves for as-received GCO sample.

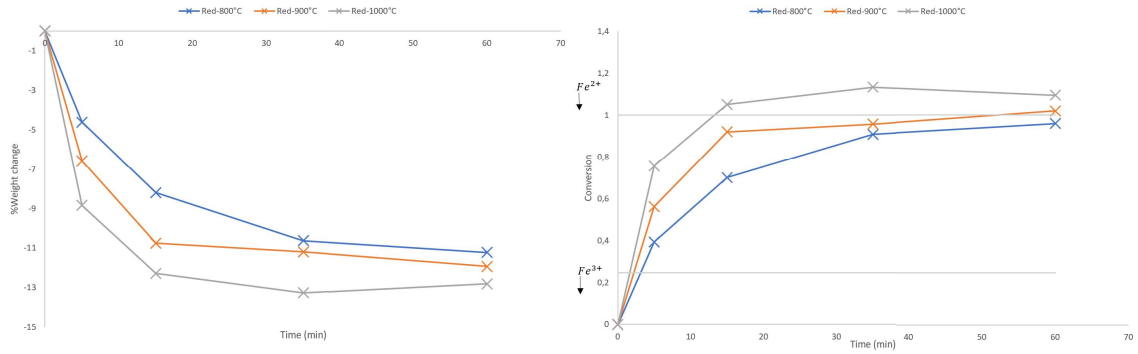

(a) Weight change curves (b) Conversion curves

Figure 4.22: Weight change(a) and conversion(b) curves for GCO sample oxidised at 700°C.

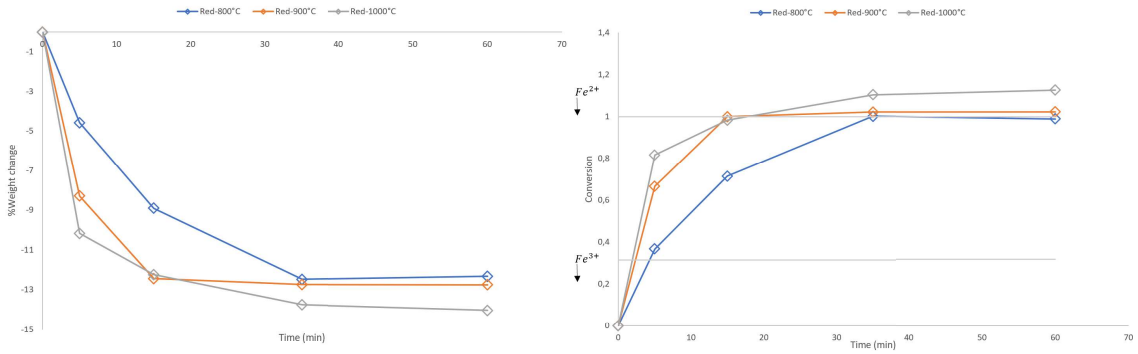

(a) Weight change curves (b) Conversion curves

Figure 4.23: Weight change(a) and conversion(b) curves for GCO sample oxidised at 800°C.

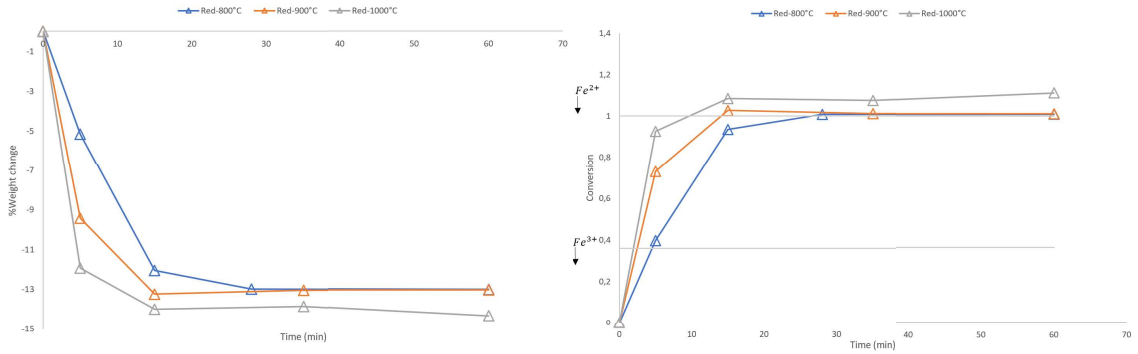

(a) Weight change curves (b) Conversion curves

Figure 4.24: Weight change(a) and conversion(b) curves for GCO sample oxidised at 1000°C.

4.3.3 XRD and Rietveld analysis

In the following tables an overview of the phases found during XRD analysis and amounts determined by Rietveld analysis. By looking at the trends of the amounts of different phases, one can see that the amount of iron and rutile increases and plateaus around the same level. There are no other major impurity phases found or present at the end of reduction. The iron that is present in Fe^{3+} state like hematite and pseudobrookite, has disappeared after 5 minutes of reduction, while pseudorutile only disappears after 15 minutes of reduction. Ilmenite tends to disappear faster for higher oxidation degrees and is still present after 35 minutes of reduction in the as-received sample.

Table 4.19: Rietveld analysis of the XRD results obtained from analyzing the reduction path of as-received ilmenite, reduced at 800°C.

Wt%/Reduction time	0 min	5 min	15 min	35 min	60 min
Metallic Fe	0	2.8	30.1	30.5	41.6
Rutile	9.5	27.5	49.0	49.4	58.4
Ilmenite	38.3	60.4	20.9	15.1	0
Hematite	0	0	0	0	0
Pseudorutile	52.2	9.3	0	0	0

Table 4.20: Rietveld analysis of the XRD results obtained from analyzing the reduction path of ilmenite oxidized at 700°C, reduced at 800°C.

Wt%/Reduction time	0 min	5 min	15 min	35 min	60 min
Metallic Fe	0	9.9	26.4	38.9	42.2
Rutile	14	24.8	44.9	58.2	57.8
Ilmenite	3.8	55.5	28.7	2.9	0
Hematite	0	0	0	0	0
Pseudorutile	82.2	9.8	0	0	0

Table 4.21: Rietveld analysis of the XRD results obtained from analyzing the reduction path of ilmenite oxidized at 800°C, reduced at 800°C.

Wt%/Reduction time	0 min	5 min	15 min	35 min	60 min
Metallic Fe	0	2.4	26.1	40.6	41.1
Rutile	31.5	21.6	48.5	59.4	58.6
Ilmenite	51.4	75.9	25.4	0	0
Hematite	17.1	0	0	0	0
Pseudorutile	0	0	0	0	0

Table 4.22: Rietveld analysis of the XRD results obtained from analyzing the reduction path of ilmenite oxidized at 1000°C, reduced at 800°C.

Wt%/Reduction time	0 min	5 min	15 min	35 min	60 min
Metallic Fe	0	3.3	37.3	45.1	46.6
Rutile	22.8	28.8	49.3	54.9	53.4
Ilmenite	0	67.9	13.3	0	0
Hematite	8.2	0	0	0	0
Pseudorutile	0	0	0	0	0
Pseudobrookite	69	0	0	0	0

The as-received GCO samples that had undergone reduction at 1000°C were analyzed with XRD analysis. The values from the Rietveld analysis are shown in Table 4.23. From the table, one can see that the lower titanium oxides make up an increasing portion of the composition with increasing reduction time. The ilmenite content seems to be decreasing for all reduction times.

Table 4.23: Rietveld analysis of the XRD results obtained from analyzing the reduction path of as-received ilmenite, reduced at 1000°C.

Wt%/Reduction time(min)	0 min	5 min	15 min	35 min	60 min
Metallic Fe	0	29.6	46.4	72.8	65.4
Rutile	9.5	47.4	35.8	1.4	2
Ilmenite	38.3	22.8	0	0	0
Pseudorutile	52.2	0	0	0	0
Lower titanium oxides	0	0.2	17.7	25.8	32.6

4.3.4 SEM and EDS

In this section, an overview of the backscattered electron images and EDS analysis for the GCO sample are presented. The morphological changes occurring during reduction are highlighted as well as topology changes.

The BSE images of the different samples showed a wide range of morphology changes during reduction. Mostly the nucleation of iron changed from one grain to the next. In Figure 4.25 one can see the different stages of reduction for an as-received sample. One can see from the images that reduction starts either along pores within the grain or along the outside of the grain before it works its way toward the center of the grain.

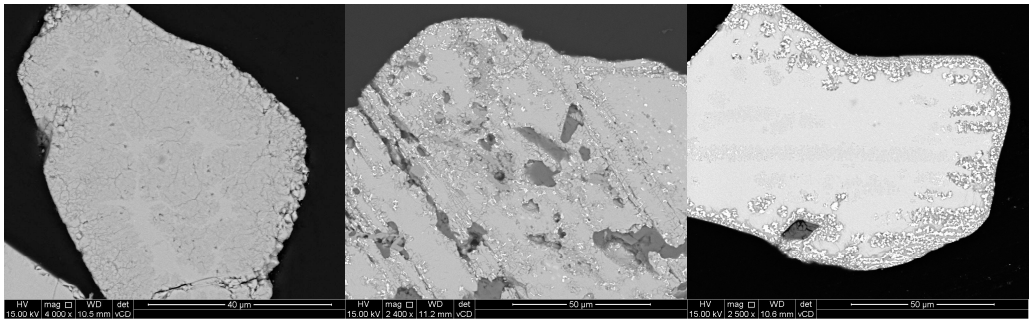

(a) Grain in as-received sample (b) Reduced for 5 minutes. (c) Reduced for 15 minutes.

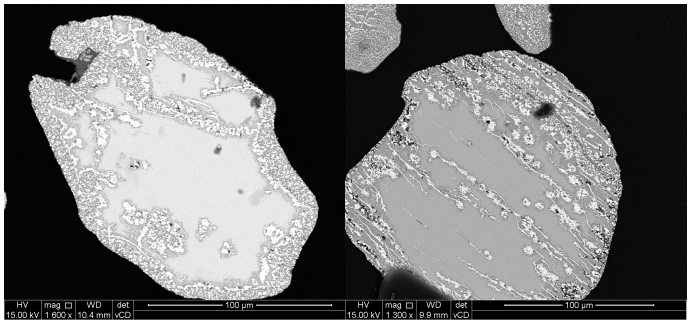

(d) Reduced for 35 minutes. (e) Reduced for 60 minutes.

Figure 4.25: BSE images of grains from the as-received GCO sample, for different reduction times, the bright phase is metallic iron.

The samples oxidized at 700°C and then reduced are shown in Figure 4.26. From the figures presented one can see that a darker gray matrix encompasses the metallic iron(white), while the internal structure of the grain is presented in light gray. EDS analysis was conducted on the different phases found during the progression of reduction and are presented in Tables 4.24, 4.25, and 4.26.

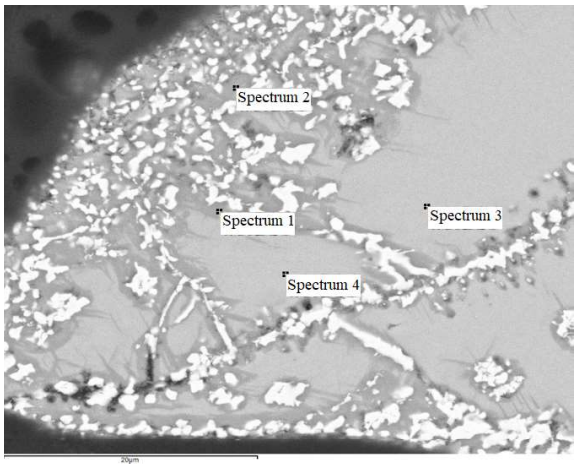

(a) Reduced for 15 minutes.

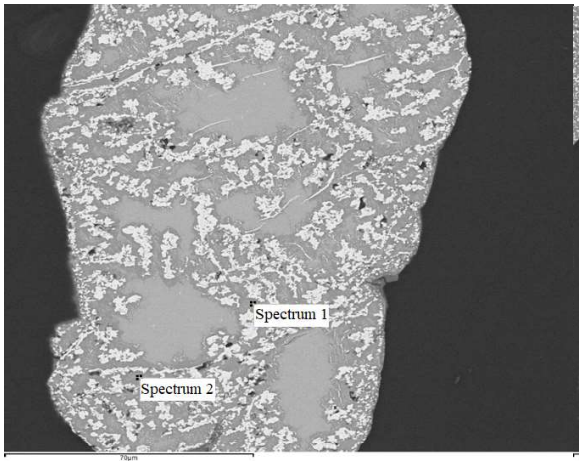

(b) Reduced for 35 minutes.

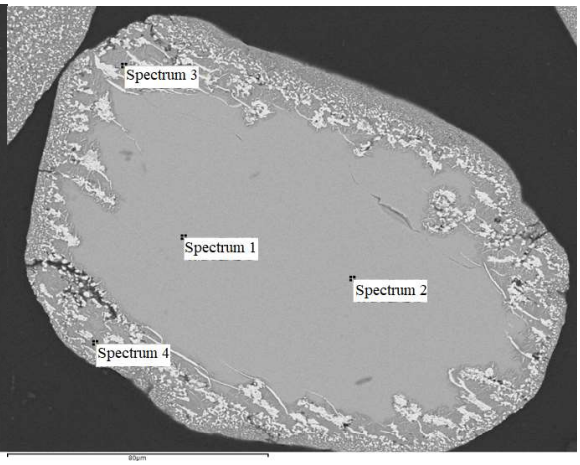

(c) Reduced for 60 minutes.

Figure 4.26: BSE images of grains from 700°C oxidized sample, for different reduction times, the bright phase is metallic iron.

From the tables shown below one can see that the darker gray matrix surrounding the metallic iron has a high Ti:Fe molar ratio, while the central, lighter gray phases have a molar Ti:Fe ratio close to 1. Furthermore, the samples with a high reduction time, 60 minutes, presented in Table 4.26, show two distinct phases, one equimolar phase of Ti:Fe and one with a high Ti:Fe ratio.

Table 4.24: EDS analysis conducted on the grain shown in Figure 4.26a).

At%	Ti	Fe	Mn	Mg	O
Spectrum 1	28.9	3.7	0	0	67.4
Spectrum 2	25.8	4.8	0.5	0.4	68.5
Spectrum 3	16.9	17.9	0.2	0	65
Spectrum 4	16.8	17.4	0.3	0	65.5

Table 4.25: EDS analysis conducted on the grain shown in Figure 4.26b).

At%	Ti	Fe	Mn	Mg	O
Spectrum 1	26	5.5	0.9	0.4	67.2
Spectrum 2	24.5	3.9	2.8	1	67.9

Table 4.26: EDS analysis conducted on the grain shown in Figure 4.26c).

At%	Ti	Fe	Mn	Mg	O
Spectrum 1	16.1	16.7	0	0	67.2
Spectrum 2	16.1	17.3	0	0	66.6
Spectrum 3	22.8	6.7	1.2	1.5	67.8
Spectrum 4	26.7	5.8	0.6	0.3	66.7

For the samples oxidized at 1000°C, there was seen different iron morphologies initially. In Figure 4.27 some examples are given for grains reduced at 800°C for 5 minutes. From the images, one can see two different reductions, one with internal reduction, where iron nucleates throughout the entire grain, Figure 4.27a), and one where the iron nucleation is confined to a darker gray phase, Figure 4.27b) and c). The bright spots in the images are metallic iron.

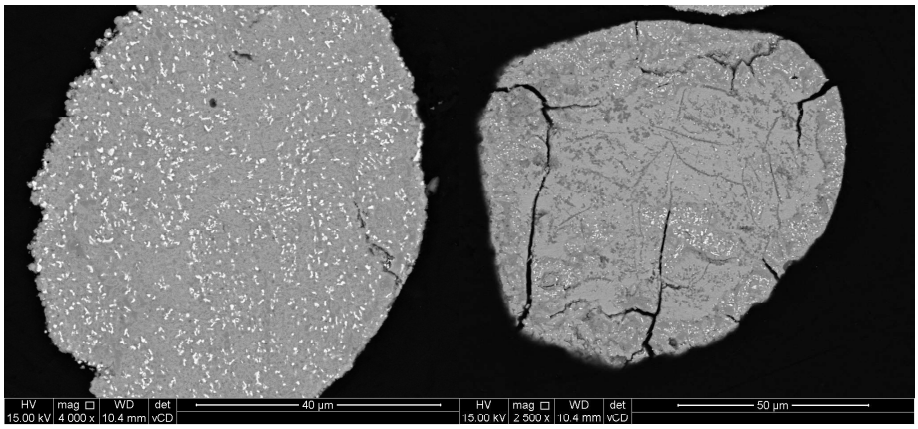

(a) (b)

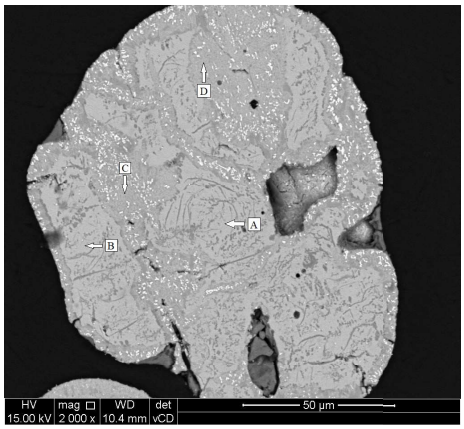

(c) EDS analyses are given in Table 4.27

Figure 4.27: BSE images of samples oxidised at 1000°C, reduced at 800°C for 5 minutes.

In Table 4.27, one can see an overview of the points analyzed in Figure 4.27c. From the table, it becomes clear that the two phases are difficult to separate. The gray phase had a Ti:Fe ratio of 1.2, and the darker phase had a ratio of 1.3.

Table 4.27: Point analysis for grain shown in Figure 4.27c.

At%	Ti	Fe	Mn	O
A	17.5	17.5	0	65.1
B	20	13.2	0	66.9
C	18	16.2	0.5	65.4
D	19.1	12.8	0	68.1

In Figure 4.28 a comparison of the reduction of the as-received sample and the 1000°C oxidized sample is seen. From the figures, one can see that the distribution of iron is much finer for the oxidized sample compared to the as-received sample.

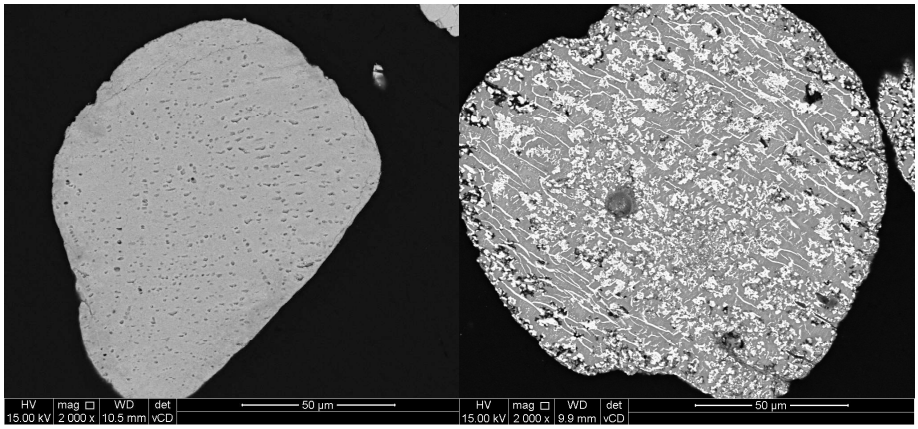

(a) Grain in as-received °C

(b) Grain in as-received samples, reduced for 60 minutes.

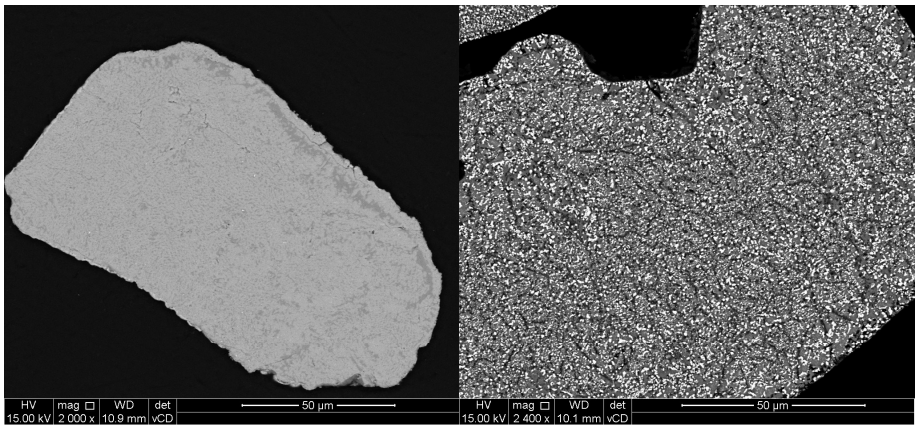

(c) Grain in sample oxidised at 1000°C.

(d) Grain in sample oxidised at 1000°C, reduced for 60 minutes.

Figure 4.28: BSE images of grains from the as-received sample and different reduction times. The white phases are assumed to be metallic iron.

A topology analysis was performed on some of the as-received reduced GCO samples. In Figure 4.29 the reduction progression on a topological level is shown. There was seen little difference in the surface of each grain from one step to the other. There was however seen a scale of roughness when it came to different grains in each experiment. The rougher grains were found to have a higher iron content compared to the smoother grains, which were higher in titanium. The Ti:Fe ratios ranged from 0.3 to 0.6 for the rougher grains, while the smoother grains had a Ti:Fe ratio ranging from 3 to 8.3.

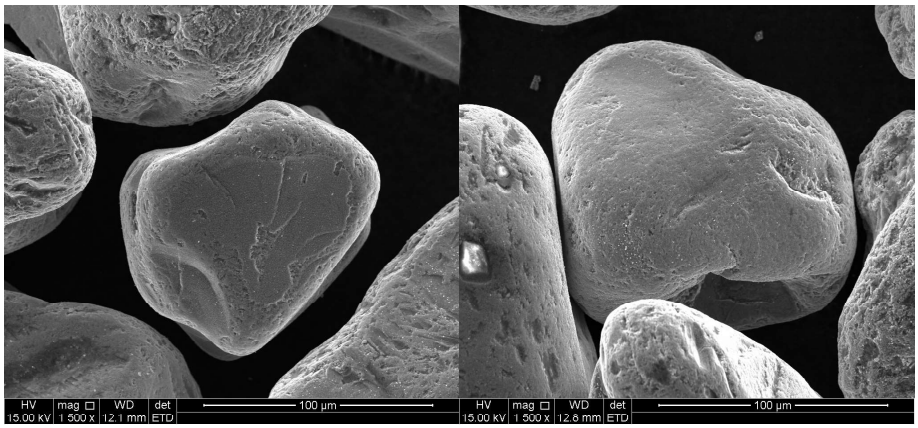

(a) As-received sample, reduced for 5 minutes.

(b) As-received sample, reduced for 15 minutes.

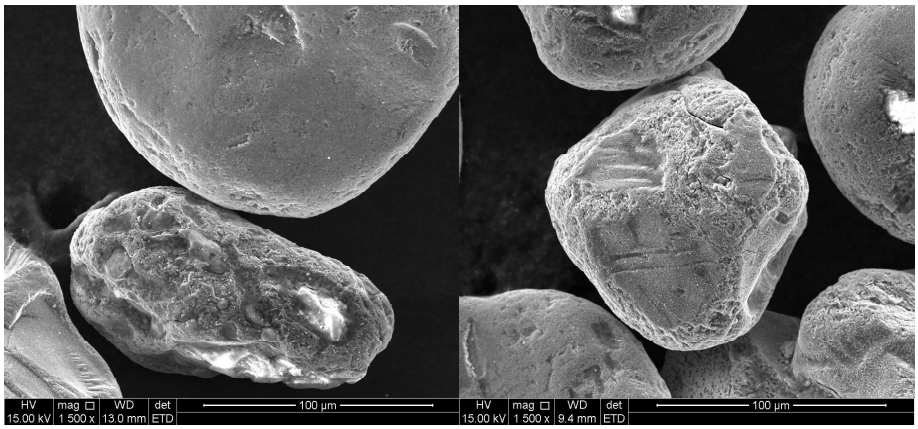

(c) As-received sample, reduced for 35 minutes.

(d) As-received sample, reduced for 60 minutes.

Figure 4.29: SE images of as-received GCO sample reduced at 800°C.

4.3.5 Iron and titanium dissolution

In the following section, the ICP-OES results are presented for the GCO samples. The compounds of interest were titanium and iron, which are both represented in percentages and in ppm levels. The KZN sample was not fully characterized, and so the majority of the results focus on the GCO analysis.

Oxidised samples

Hot acid leaching was conducted on the oxidized material. The results are presented in Figure A.2. In the figure, the dissolution (ppm) of titanium and iron is presented as a function of oxidation temperature. From the figure, one can see that initially, the dissolution decreases from the starting material, where it reaches a low point for the 800°C oxidized sample. After which, one can see an increase, with a maximum found in the sample oxidized at 1168°C.

Reduction at 800°C

In Figure 4.30 one can see the results from ICP analysis for GCO ilmenite reduced at 800°C. The percentage is based on the total amount of iron and titanium present, found through alkaline fusion. From Figure 4.30a), one can see that dissolution of iron increases with increasing reduction time for all samples except for ones oxidized at 1000°C, where it is decreasing. Along with this, the other three samples end up around the same concentration of iron after 60 minutes of reduction.

Figure 4.30b shows the titanium concentration for samples reduced at 800°C. The same goes for the graph showing iron concentration. The concentration for samples oxidized at 1000°C follows the opposite trend as the other samples. For the other three, as-received, 700 and 800°C end up in the same concentration range after 60 minutes of reduction.

One other way to illustrate the results is by representing the concentrations on ppm levels. This in turn gives better grounds for comparisons. In Figure 4.30c and 4.30d the ppm levels are given. One can see the same trends here as for previous figures.

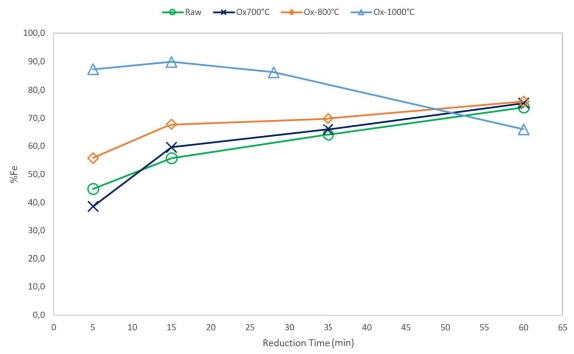

(a) Iron dissolution in %

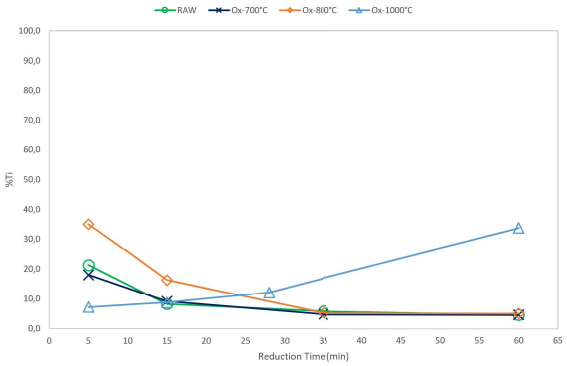

(b) Titanium dissolution in %

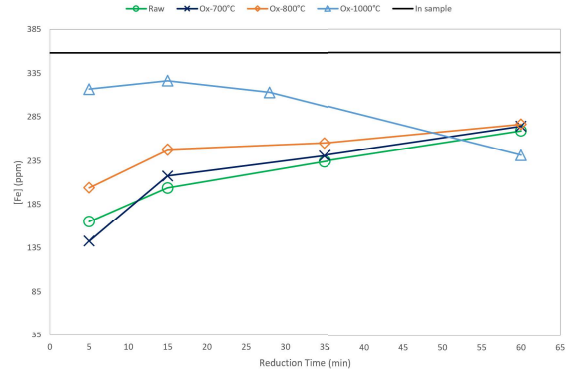

(c) Iron dissolution given in ppm

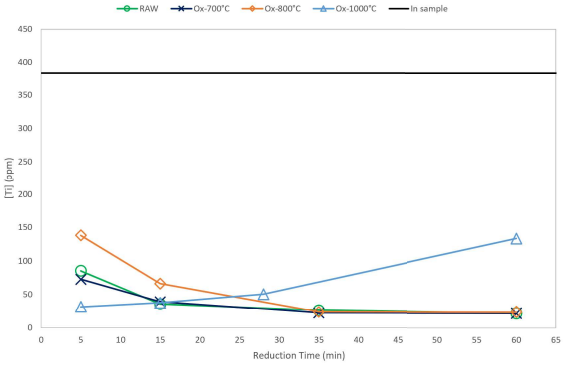

(d) Titanium dissolution given in ppm

Figure 4.30: Iron and titanium dissolution given in % (a, b) and ppm values(c, d), reduced at 800°C.

Reduction at 1000°C

For the samples reduced at 1000°C, the ICP results are shown in Figure 4.31. From Figure 4.31a), one can see that the iron concentration is lowest for both the as-received sample and the 700°C oxidized sample after 5 minutes of reduction. The samples oxidized at 800°C and 1000°C show a higher concentration. Furthermore, for the oxidized samples, one can see a high point at a reduction time of 35 minutes before a decrease in iron dissolution is seen. The as-received sample has an increasing trend for the entire reduction path.

In Figure 4.31b one can see the %titanium that was dissolved. For the sample oxidized at 1000°C, the concentration stays around the same level. The other samples see a concentration increase over the reduction time. Common for all the oxidized samples was that at 15 minutes of reduction, there was a titanium concentration decrease before it rose again. The as-received sample reaches the highest titanium concentration by the end of the reduction.

To gain a better overview when comparing the reduction temperatures the ppm levels for the samples reduced at 1000°C are given in Figure 4.31c and 4.31d. From the figure, one can see that the total titanium concentration stays around the same level for the duration of reduction.

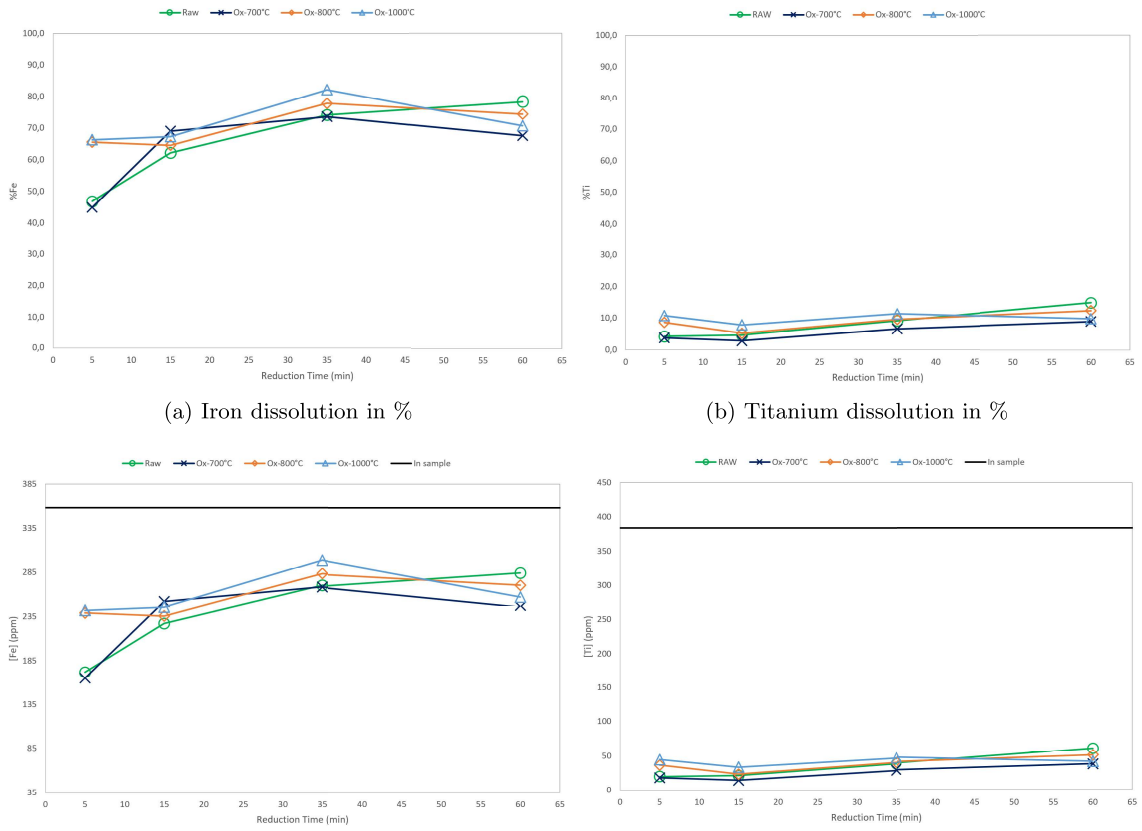

(a) Iron dissolution in %

(b) Titanium dissolution in %

(c) Iron dissolution given in ppm

(d) Titanium dissolution given in ppm

Figure 4.31: Iron and titanium dissolution given in % (a, b) and ppm values(c, d), reduced at 1000°C.

XRD results from leached samples

XRD analysis was performed on the leachate. A zero background was used due to the small sample size. From the results, one can see that after the leaching of samples for 120 minutes, there was no iron detected for any of the analyzed samples, 20-30 μm of the sample surface. The phases of rutile and ilmenite, where it was present in the starting material, were left. One point of interest is the broad peaks identified as ilmenite peaks.

A Rietveld analysis was also performed on some of the leached samples. The results are given in Table 4.28. Some points of interest that can be taken away are that pseudorutile is detected in all of the analyses, as well as pseudobrookite in the sample oxidized at 800°C. The amount of rutile increases as the reduction times increase as well.

Table 4.28: Rietveld analysis performed on some of the leachates, leached for 120 minutes. The sample identification is given in the following order, oxidation temperature - reduction temperature -reduction time.

(wt%)	Rutile	Ilmenite	Hematite	Pseudorutile	Pseudobrookite
800-800-15-120	62.5	0	0.9	34.2	2
1000-800-05-120	55.5	27.4	0	16.7	0
1000-800-15-120	89.9	0.7	0	7.6	1.1
1000-800-60-120	87.3	0	0	12	0.2

SEM and EDS analysis of leached GCO samples

In Figure 4.32 one can see the cross-section of grains oxidized at 800°C and 1000°C, reduced at 800°C for 15 minutes, then leached for 120 minutes. From the images, one can see that there is still metallic iron remaining in some of the grains. Along with a brighter circle around the center of the grain for both oxidation temperatures.

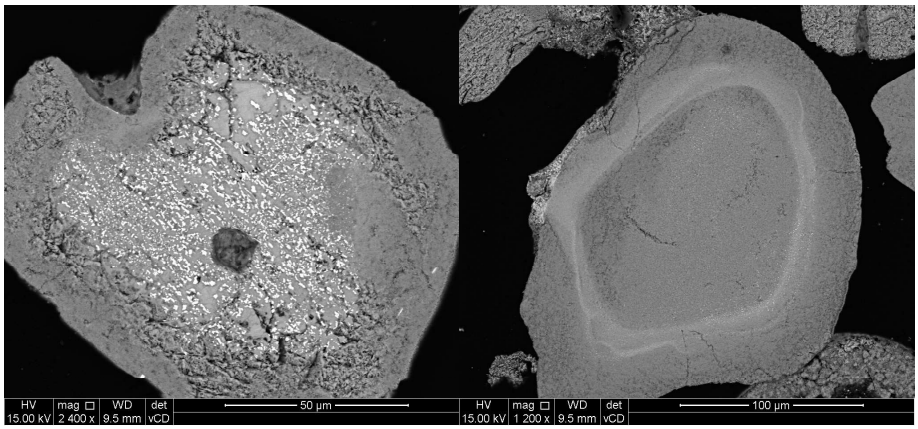

(a) Sample oxidised at 800°C, reduced at 800°C for 15 minutes.

(b) Sample oxidised at 800°C, reduced at 800°C for 15 minutes.

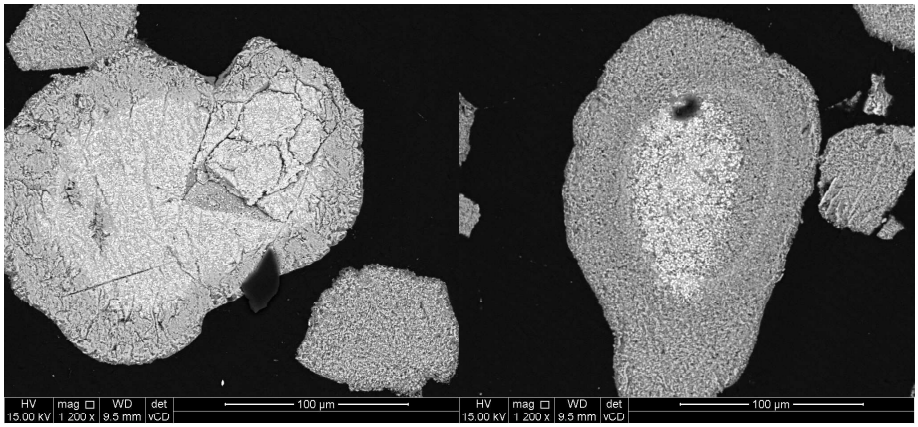

(c) Sample oxidised at 1000°C, reduced at 800°C for 15 minutes.

(d) Sample oxidised at 1000°C, reduced at 800°C for 15 minutes.

Figure 4.32: BSE images of grains from samples oxidized at 800°C and 1000°C reduced at 800 degrees for 15 minutes and leached for 120 minutes.

A closer look was given to the inner circle found in the leached samples. In Figure 4.33 some of the findings are represented. From the mapping of the circle, one can see that the iron concentration increases towards the inner edge of the circle before it decreases.

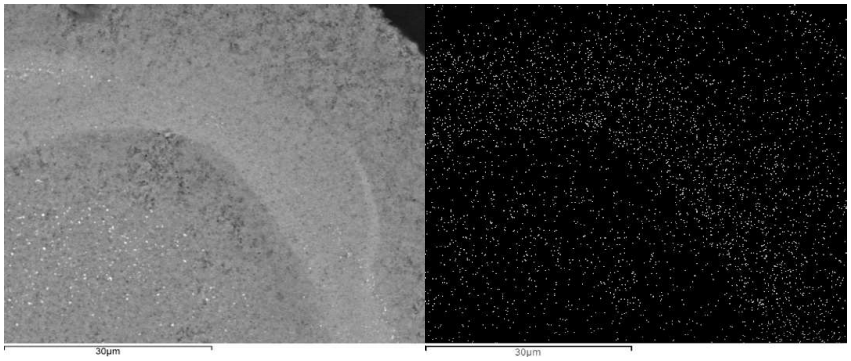

(a) Sample oxidised at 800°C, reduced for 15 minutes at 800°C

(b) Mapping of oxidised at 800°C, reduced for 15 minutes at 800°C

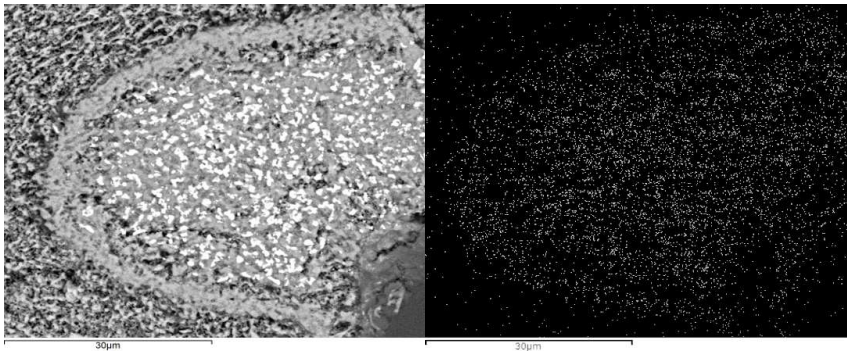

(c) Sample oxidised at 1000°C, reduced at 800°C for 15 minutes

(d) Mapping showing iron concentration of sample oxidised at 1000°C, reduced at 800°C for 15 minutes

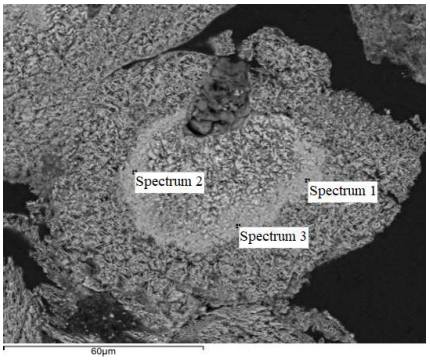

(e) Sample oxidised at 800°C, reduced for 15 minutes at 800°C, EDS analysis given in Table 4.29

Figure 4.33: BSE, mapping, and point analysis of samples that have been leached for 120 minutes.

Point analysis was conducted on one of the circles. These are shown in Figure 4.32e, along with the values shown in Table 4.29. From the analysis one can see that they are high in titanium and low in iron. Some magnesium was also found in one of the points.

Table 4.29: Value for point analysis shown in Figure 4.33e.

(At%)	Ti	Fe	O	Mg
Spectrum 1	19.7	4.5	75	0.6
Spectrum 2	19.2	7.8	73	0
Spectrum 3	16.5	9.6	73.9	0

The topology of the leached samples was analyzed. In Figure 4.34 two examples are presented. The analysis showed a wide variety of grain types. Some are more affected by the acid than others. From Figure 4.34a) one can see very smooth grains as well as grains with a rougher surface. From EDS analysis grains with ilmenite ratios of Ti/Fe were found as well as grains mostly consisting of rutile.

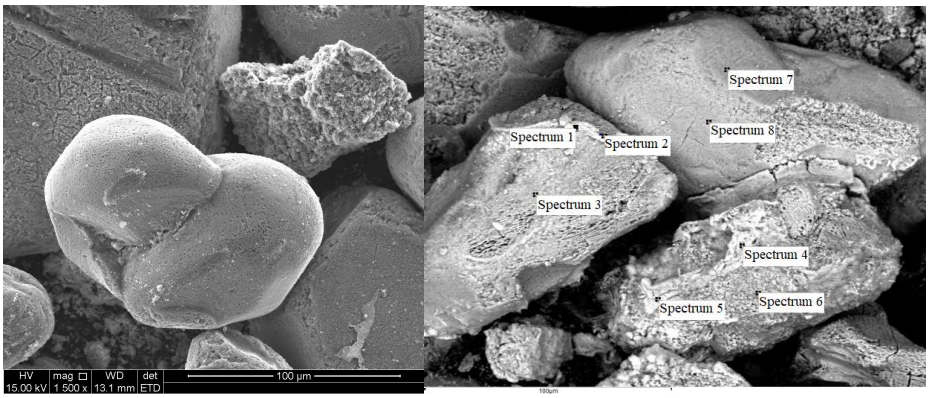

(a) SE image of as-received samples reduced at 800°C for 15 minutes.

(b) BSE image of as-received sample reduced at 800°C for 35 minutes.

Figure 4.34: Topology image and EDS analysis of leached grain surface from reduced samples. Values from EDS are shown in Table 4.30.

In Figure 4.34 multiple different grains were found to be in close proximity to each other. As well as different compositions on each area of each grain. One example of high iron contents on the surface is shown in Spectrum 5, with an At% of 74, Table 4.30.

Table 4.30: Values from EDS analysis for leached grains found in Figure 4.34b).

(At%)	Ti	Fe	S	Si	O
Spectrum 1	2.4	19.2	1.3	0	77.1
Spectrum 2	3.2	17.4	0.9	0.6	77.9
Spectrum 3	13.6	6.1	0.5	0.4	79.4
Spectrum 4	2.2	22.2	1.1	0	74.6
Spectrum 5	6.0	74.3	0	0	18.8
Spectrum 6	35.4	7.9	0	0	56.7
Spectrum 7	14.5	3.7	0	0	81.8
Spectrum 8	39.3	3.2	0	0	57.6

4.3.6 KZN ilmenite: Experimental data and analyses

The KZN ilmenite was reduced at 800°C with different oxidation degrees. The weight change data for the four different samples are shown in Figure 4.35a). The starting point for each oxidation degree was calculated based on the weight change of four oxidation experiments per temperature. The moisture was measured in the sample by the same method as the GCO sample and was found to be less than 0.1% and hence could be neglected. From the figure, one can see a difference between the samples oxidized at 800°C and 1000°C compared to as-received and 700°C oxidation. The maximum weight change reached was 11.59% and 8.3%, respectively. Furthermore, the sample oxidized at 1000°C already crosses the as-received line after approximately 4 minutes.

The O:Fe ratio of the KZN ilmenite is given in Figure 4.35b). From the figure, one can see that as the ilmenite oxidizes the O:Fe ratio increases, with a maximum value of 1.49. Furthermore, there is seen a difference between samples oxidized at a 1000°C and 800°C compared to 700°C and as-received samples. The two higher oxidation temperatures reach values close to 0 for O:Fe ratio after 60 minutes of reduction. The 700°C and as-received sample reach values of 0.46 and 0.39 respectively.

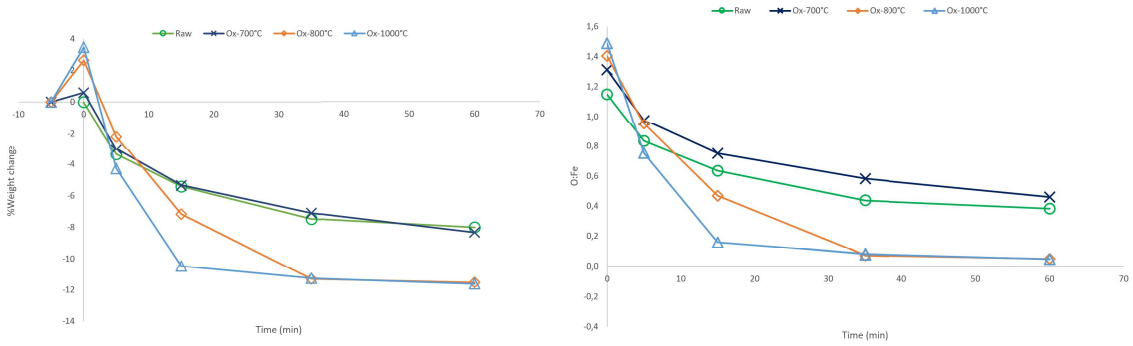

(a) %weight change as a function of reduction time

(b) O:Fe ratio as a function of reduction time

Figure 4.35: %Weight change curves(a) and O:Fe ratio(b) for the KZN ilmenite, reduced at 800°C.

In Tables 4.31-4.34 the Rietveld analysis from of the KZN reduced ilmenite is presented. For the as-received material, shown in Table 4.31, one can see that the ilmenite and hematite content decreases with increasing reduction time. The values of ilmenite after 60 minutes of reduction was 14.2 wt%. The values of rutile and iron can be seen to increase with increasing reduction time. For the sample oxidized at 700°C, shown in Table 4.32, similar findings can be seen, where the ilmenite content was found to be 22.2 wt% after 60 minutes of reduction.

Table 4.31: Rietveld analysis of the XRD results obtained from analyzing the reduction path of as received KZN ilmenite, reduced at 800°C.

Wt%/Reduction time	0 min	5 min	15 min	35 min	60 min
Metallic Fe	0	17.6	31.6	37.3	43.7
Ilmenite	84.4	70.6	39	27.7	17.2
Rutile	1.8	11.7	29.4	35	39.1
Hematite	13.6	0	0	0	0

Table 4.32: Rietveld analysis of the XRD results obtained from analyzing the reduction path of the KZN ilmenite oxidized at 700°C, reduced at 800°C.

Wt%/Reduction time	0 min	5 min	15 min	35 min	60 min
Metallic Fe	0	17	30.4	38.7	41.3
Ilmenite	31.7	72	30.4	24.7	22.2
Rutile	12.8	10.9	26.2	30.3	36.5
Dolomite	0	0	0	6.3	0
Hematite	55.5	0	0	0	0

When the oxidation temperature was increased further, 800 to 1000°C shown in Tables 4.33 and 4.34 the weight % of ilmenite after 60 minutes of reduction decreased to 2.3 and 0, respectively. The remaining phases after 60 minutes were iron and rutile in both cases. For all oxidation temperatures that had gone through 5 minutes of reduction, the ilmenite content was seen to increase from the starting concentration.

Table 4.33: Rietveld analysis of the XRD results obtained from analyzing the reduction path of the KZN ilmenite oxidized at 800°C, reduced at 800°C.

Wt%/Reduction time	0 min	5 min	15 min	35 min	60 min
Metallic Fe	0	11.2	36	51.5	49.7
Ilmenite	45.7	74.7	29.6	2.3	2.3
Rutile	32.2	14.4	35.4	46.3	47.9
Hematite	22.2	0	0	0	0

Table 4.34: Rietveld analysis of the XRD results obtained from analyzing the reduction path of the KZN ilmenite oxidized at 1000°C, reduced at 800°C.

Wt%/Reduction time	0 min	5 min	15 min	35 min	60 min
Metallic Fe	0	23.5	45	52.9	60
Ilmenite	2.6	61.1	16.5	0	0
Rutile	15.8	15.4	38.5	47.1	40
Hematite	20.5	0	0	0	0
Pseudobrookite	61.1	0	0	0	0

SEM analysis and EDS were performed on the cross-sections of as-received and oxidized at 1000°C that had been reduced for 5 and 60 minutes to understand the initial and final points of reduction. In Figure 4.36 the cross-sections of the samples reduced for 5 minutes are presented. In both the as-received and oxidized samples grains were found that showed signs of complete reduction already after 5 minutes, Figure 4.36b) and d). From the analysis, one can see that the metalization of iron is limited to certain phases. Other phases have not started reducing yet or show minimal signs of reduction. The phases without metallic iron were found to have a Ti:Fe ratio close to 1. There were also phases found with little to no iron present in the oxide, mostly containing titanium and oxygen. The values for the EDS analysis are presented in Table 4.35 and Table 4.36.

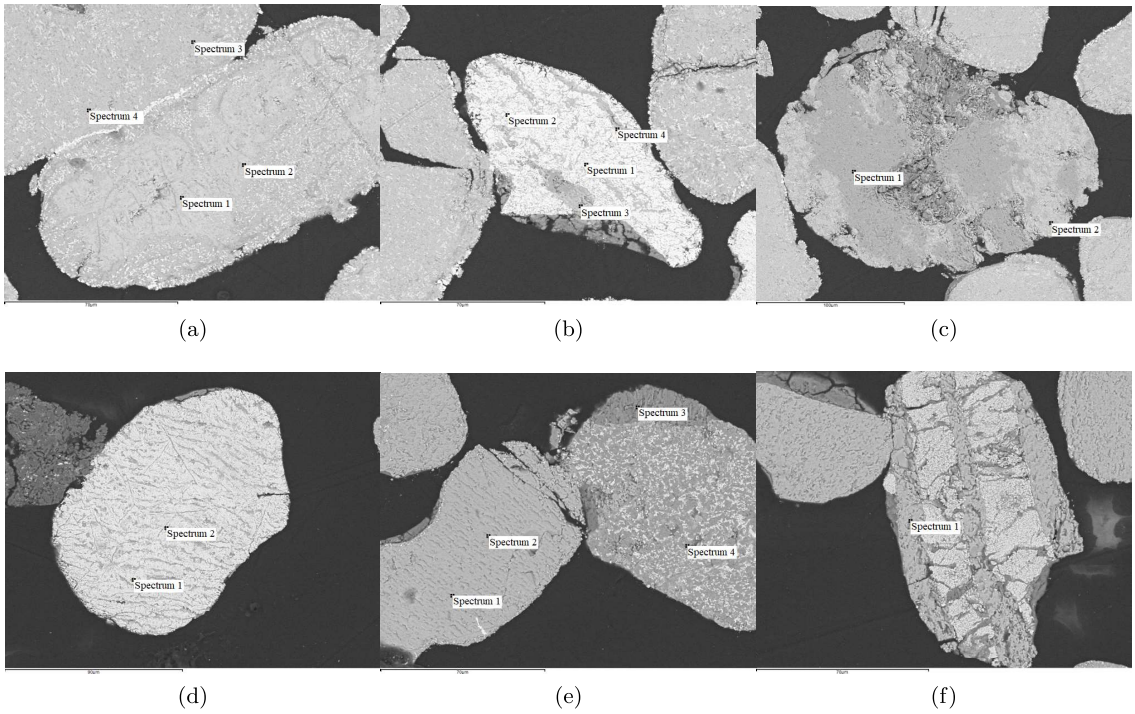

(a) (b) (c)

(d) (e) (f)

Figure 4.36: Cross-section of KZN ilmenite reduced for 5 minutes, a)-c) are as-received, d)-f) are oxidised at 1000°C. EDS values given in Tables 4.35 and 4.36 respectively.

Table 4.35: EDS analysis for the grains shown in Figures 4.36a)-c).

At%	Ti	Fe	Mg	Mn	Si	Al	K	Ca	O
a) Spectrum 1	17.1	15.5	0	0	0	0	0	0	65.3
a) Spectrum 2	18.4	18.1	0	0.3	0	0	0	0	63.3
a) Spectrum 3	20.3	13.5	0.4	0.4	0	0	0	0	65.4
a) Spectrum 4	18.4	15.6	0.7	0.4	0	0	0	0	64.9
b) Spectrum 1	4.2	68	0	0.5	0	0	0	0	27.4
b) Spectrum 2	6.6	55.3	0	0.7	0	0	0	0	47.4
b) Spectrum 3	19	10.5	0	0	1.7	0.8	0.2	0	67.8
b) Spectrum 4	17.2	5.6	0	0.2	1.5	0.6	0.1	0	74.9
c) Spectrum 1	28.8	0.7	0	0	0	0	0	0	70.6
c) Spectrum 2	14.4	8.7	0	1.3	5	1.2	0	3.9	65.5

Table 4.36: EDS analysis for the grains shown in Figures 4.36d)-f).

At%	Ti	Fe	Mg	Mn	Si	Al	Na	Ca	O
d) Spectrum 1	7.4	64.1	0	0	0	0	0	0	28.5
d) Spectrum 2	9.5	49.6	0	0.5	0	0	0	0	40.4
e) Spectrum 1	17.1	18	0.7	0	0	0	0.5	0	63.6
e) Spectrum 2	15.4	16.1	0.8	0.2	0	0	0	0	67.5
e) Spectrum 3	9.4	0.9	0.2	0	10.6	0.8	0	8.2	69.8
e) Spectrum 4	26	1.7	0	0	0.2	0	0	0	72.1
f) Spectrum 1	16.7	17	0	0.8	0	0	0	0	65.3

In Figure 4.37 one can see the cross-sections of the as-received and 1000°C oxidized samples reduced for 60 minutes. The concentrations found during the EDS analysis are shown in Tables 4.37 and 4.38. From the figures, one can see different iron distributions. Some grains in the as-received sample had a large degree of internal reduction while others had a more connected iron structure. In the samples oxidized at 1000°C one saw a more uniform distribution of iron throughout the grain. In Figure 4.37d) one can see an iron and titanium oxide encompassed by a gangue material consisting of mostly calcium and phosphor oxide.

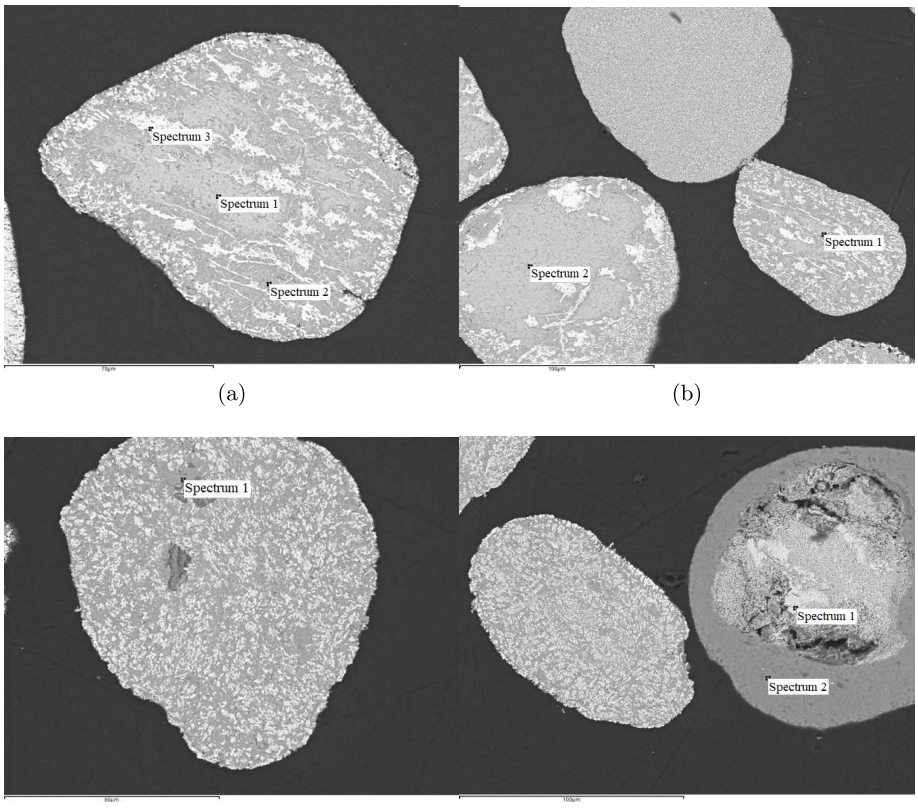

(a) (b)

(c) (d)

Figure 4.37: Cross-section of KZN ilmenite reduced for 60 minutes, a) and b) as-received, c) and d) oxidized at 1000°C. EDS values given in Tables 4.37 and 4.38 respectively.

Table 4.37: EDS analysis for the grains shown in Figures 4.37a) and b).

At%	Ti	Fe	Mg	Mn	O
a) Spectrum 1	16.9	17.8	0	0.4	64.9
a) Spectrum 2	27.2	6.6	0	0.3	65.9
a) Spectrum 3	3.6	85.2	0	0	11.2
b) Spectrum 1	17.4	17.1	0	0.2	65.4
b) Spectrum 2	17.5	17.3	0.5	0	64.8

Table 4.38: EDS analysis for the grains shown in Figures 4.37c) and d).

At%	Ti	Fe	Mg	Mn	Si	Al	Ca	Na	P	S	F	O
c) Spectrum 1	28.2	0.2	0	0	0	0	0	0	0	0	0	71.6
d) Spectrum 1	9.4	59.1	0.6	0.4	0.8	0.5	0.4	0	0	0	0	28.8
d) Spectrum 2	0.2	0.7	0.5	0	2.1	0.9	17.2	0.3	11.2	0.3	3.3	63.4

The KZN samples reduced at 800°C are presented in Figure 4.38, given in % (a, b) and ppm (c, d). From Figure 4.38a), one can see that the dissolution of iron increases with increasing reduction time as well as increasing oxidation temperature. The highest iron dissolution reached is found in the leaching of the 1000°C oxidized sample, 93.6%. The as-received sample and 700°C oxidized sample reach an iron dissolution of 55.5% after 60 minutes of reduction. In Figure 4.38b) the titanium dissolution is given. As the reduction time is increasing the titanium dissolution was seen to decrease. After 5 minutes of reduction, the found titanium dissolution was seen to increase with increasing oxidation temperature. Where the highest dissolution was found for the sample oxidized at 1000°C, 65.1%. In Figure 4.38c) and d) the ppm measurements for iron and titanium are presented, showing similar trends as the % values.

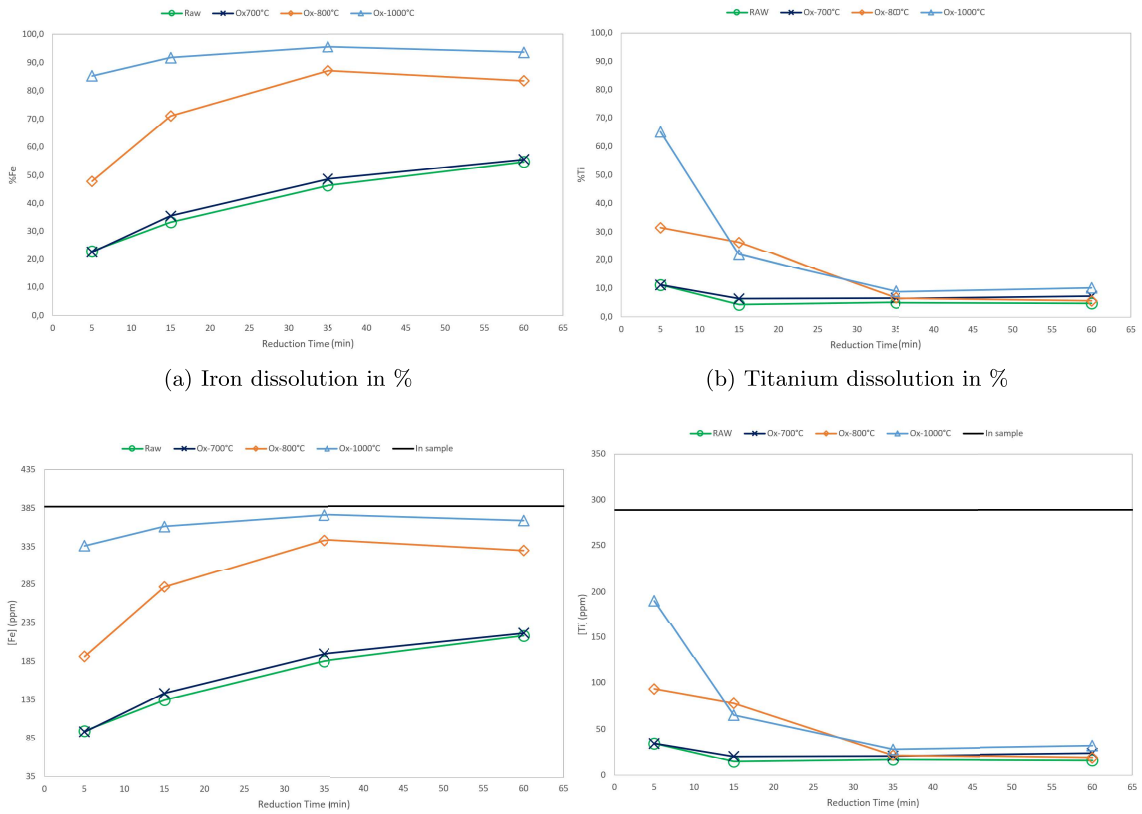

(a) Iron dissolution in %

(b) Titanium dissolution in %

(c) Iron dissolution given in ppm

(d) Titanium dissolution given in ppm

Figure 4.38: Iron and titanium dissolution of the KZN ilmenite given in % (a, b) and ppm values(c, d), reduced at 800°C.

5 Discussion

In this section, the results will be discussed. First, the differences in the two starting materials will be discussed before the TGA is brought forth. How they differ and how these differences can affect oxidation is summarised and will be carried on into the discussion regarding oxidation. First, the oxidation progression and analysis for the GCO ilmenite will be discussed before the results of reduction are mentioned. After this, the analysis of the GCO sample is discussed. The XRD, SEM, and ICP results for this ilmenite are given in this section. Finally, the KZN ilmenite data will be discussed and how these differ from the GCO sample is mentioned, along with possible reasons for these differences. The analytical results obtained from the KZN reduced samples are presented in this discussion as well.

5.1 Differences in starting material

Multiple XRD analyses were conducted on the GCO ilmenite to try and determine the phases present and the amount of each phase. From Table 4.1, it becomes clear that there is a difference depending on how the results are interpreted. One of the reasons for this is that the phases present in natural ilmenite have overlapping peaks. From the XRD analyses given in the appendix, phases like ilmenite, rutile, and pseudorutile are seen to have overlapping peaks. Two analyses were conducted with the PDF-4+ database and one with the COD database. In the analysis conducted at NTNU, rutile was found, and no hematite. In the NWU analysis, hematite was found, and no rutile. For the analysis with the COD database, ilmenite was distinguishable with a few other unused peaks. If manganese was included in the search, a pseudorutile phase was detected with the chemical formula $Fe_{4.728}Mn_{0.272}Ti_{9.67}O_{27}$. From the EDS analysis for the GCO ilmenite, one can see indications of a pseudorutile phase as a darker gray phase. As for which analysis gives the most accurate compositing can be found by including the chemical analysis of the starting material. We know that the Ti:Fe mol ratio for GCO ilmenite is 1.2:1. This leads one to believe there should be an excess of rutile instead of hematite. When including the wet chemical analysis for the as-received material. The amount of FeO and Fe_2O_3 found was 19.1 and 22 wt%, respectively. Using the phase amounts found during the NTNU XRD analysis, we can calculate the theoretical amount of FeO and Fe_2O_3 connected to ilmenite and pseudorutile, where the iron in pseudorutile is Fe^{3+}. The theoretical value from the given composition gives FeO and Fe_2O_3 amount to 18 and 20.9 wt% respectively. With this information, we can conclude that the Rietveld analysis from NTNU gives the closest values, considering all known factors. For all other analyses the NWU data was used to present phase transformations the ilmenite underwent during oxidation and reduction.

The XRD Rietveld analysis of the as-received KZN material shows some differences from the GCO ilmenite. There are similar phases, ilmenite, and hematite, but the KZN sample contains no pseudorutile. As mentioned, the pseudorutile is challenging to detect since the peaks overlap with ilmenite, rutile, and pseudorutile. Since pseudorutile is a meta-stable phase[43], it could indicate a lower degree of weathering in the KZN sample. The overlapping peaks also make it difficult to determine the exact amounts of present phases. Rietveld refined XRD is a quantitative approach to analyze crystalline materials, accurate analysis remains an obstacle due to the presence of the number of phases, and chemical and structural variability. From Table 4.7, one can see a large amount of ilmenite in the starting material. This corresponds well to the chemical analysis showing iron speciation, where the FeO content and Fe_2O_3 were given as 31.9

and 16.3, respectively. Comparing this to the GCO sample, where the FeO and Fe_2O_3 were 19.1 and 22 wt%, one can expect a greater ilmenite concentration in the KZN sample.

The SEM of cross-section of the as-received materials made it clear that the two ilmenites differ. The GCO ilmenite showed an internal structure consisting of mainly two phases. One had a Ti:Fe ratio close to 1. Since stoichiometric ilmenite has a Ti:Fe ratio of 1, it is believed that this phase is ilmenite. There is a large area of solid solution in the M_2O_3 system, as shown by Rosenqvist[30], but that is more towards the iron-rich side of the phase diagram. For the titanium side, the M_2O_3 phase can be found alongside metallic iron and rutile, which puts further arguments towards the NTNU XRD. The outer phase had a Ti:Fe ratio higher than 1. This was considered to be pseudorutile. This also makes sense when considering weathering since the weathering works its way toward the center of the grain, washing away the iron and leaving a phase with a Ti:Fe ratio larger than 1. The non-weathered core was made up of ilmenite. In the cross-section of the KZN ilmenite, a complex inner structure was discovered. Some grains mainly contain iron oxides, while others have phases close to stoichiometric ilmenite. Other parts of the grain have a Ti:Fe ratio of >2.3. These phases could be rutile, and the iron detected in the phase could be from what is beneath the surface of the grain. A larger amount of impurities were also found, sometimes encapsulating the grain or making up a large amount of the grain's mass. The grains consisting of iron oxide were found to be porous, while the other grains appeared denser. As mentioned, it is believed that this morphology is a product of the KZN ilmenite being less weathered. The differences found during the SEM analysis could also be the reason for the different reduction paths discussed later.

5.2 GCO ilmenite: Discussion

Now that an overview of the starting material has been given, the results from the oxidation experiments are given. First, the micro-TGA is discussed for a better understanding of what occurs during oxidation before the analysis of oxidized GCO ilmenite is presented. An overview of the phases present after oxidation is also given. From this point on the GCO and KZN results are discussed separately.

5.2.1 Micro-TGA results

From Figure 4.5, showing the weight change as a function of temperature, one can see three distinct areas of weight change. Initially, there is a mass loss with a low point around 400°C, before a linear increase in weight gain to around 700°C, after which the curve follows a sigmoidal shape. The reason for reaching different weight changes for different rates is believed to be attributed to the increased inaccuracy of the machine as the heating rate increases, along with shorter times to reach the set point temperature of 1000°C and shorter time to reach the set point. This could indicate that the chemical reaction is not fast enough to keep up with the heating rate.

The weight decrease at the start of the heating curve occurring from 150°C to 400°C was initially believed to be because of moisture evaporation. When the GCO sample was heated to 150°C and held there for 4 hours, the mass loss recorded was 0.2%. Further arguments that the initial mass loss is from moisture evaporation can be found when the weight change was plotted against the change in time. The curve representing the heating rate of 2.5 °C/min sees very little change up to 120 minutes, corresponding to 300°C, meaning that little is occurring in the sample. As the heating rate increases, the low point shifts towards lower temperatures and greater negative values. Further arguments that no reaction is occurring and that this mass loss was due to water evaporation can be found in the literature, with multiple authors mentioning that in the temperature range of 500 to 600°C, little change occurs in the ilmenite[25][43][44].

After the temperature reaches 400°C, the rate switches from negative to positive, as seen in Figure 4.6. This indicates that even though the change is small, a reaction occurs within the ilmenite after 400°C. The reaction rate continues to increase to approximately 520°C, after which one sees a plateau. When the first derivative of weight change as a function of temperature is considered the plateau shows up as linear. One explanation of this plateau could be a reaction involving pseudorutile. Since pseudorutile is considered a meta-stable product of ilmenite oxidation and is not well defined, there is a lot of discussion about how it is created during oxidation. Most authors agree that for temperatures below 900°C, the phase can occur as an intermediate product of oxidation. It was observed that at temperatures between 600°C, the pseudorutile undergoes a breakdown process and transforms into hematite and rutile. However, at higher temperatures of 800°C, the oxidation product pseudorutile is visible as an intermediate product. If it were the creation of a pseudorutile phase, it would explain the homogeneous grains found for oxidation temperatures of 700°C as well as the Rietveld analysis that is shown in Table 4.20. These results will be discussed in a later section. A further indication of a reaction occurring can be seen in Figure 4.9. The two peaks shown signify a change in heat flow which in turn signifies two different reactions occurring. Another explanation of the linear part of the curve could be a change in the rate-determining step(RDS) or reaction mechanism.

To summarize the TGA results, the oxidation rate stays low until around 700°C to 800°C after which the rate reaches its high point at 820°. There seem to be two separate mechanisms playing a role in different temperature ranges of oxidation. Either the creation of hematite and rutile or the creation of pseudorutile could occur at the lower temperature range, while for the higher temperature range, the oxidation of ilmenite to pseudobrookite is considered the main reaction.

5.2.2 GCO Ilmenite oxidation

With the summary in mind, one can start to discuss the oxidized GCO samples used for reduction. From Figure 4.10 the trends highlighted during TGA become clear. For oxidation at 700°C, one can see a negative weight change even after 1 hour of oxidation. When the oxidized samples were analyzed with wet chemical analysis, it became clear that some of the Fe^{2+} was oxidized to Fe^{3+}, which would lead to an overall mass gain. As the oxidation temperatures increase, the amount of Fe^{3+} was seen to increase. For the highest oxidation temperature of 1000°C, the maximum amount of hematite was found, accounting for 42 wt%. To make sure that this was the highest obtainable oxidation degree another sample was prepared with a set point of 1400°C and a run time of 7 hours. The analysis showed that around the same amount of ferric iron was present in the sample, meaning the highest obtainable oxidation was reached. The phases found after oxidation show that the oxidation reaction was not at equilibrium for 700 or 800°C. Considering pseudorutile an intermediate compound at 700°C, with end products of hematite and rutile, as proposed by Gupta et. al[27]. One would assume that by leaving the reaction for long enough, these compounds would become more prevalent. For 800°C we end

up in the transition area for which different compounds are stable, hematite and rutile on one side, while pseudobrookite and rutile on the other. From the XRD results it becomes clear that ilmenite, hematite, and rutile are all present, while pseudobrookite is not. For higher oxidation temperatures of 1000°C, we no longer saw the presence of ilmenite but rather a combination of rutile, hematite, and pseudobrookite. From literature[25][43][44] and the TGA results one can see that the reaction rate peaks around 820°C for this type of ilmenite but the oxidation time of 1 hour is not sufficient for completing the transition to pseudobrookite. With that being said there are examples of longer oxidation times still having both hematite and rutile present[24], which in turn might also be because of impurities present in the sample.

Ilmenite oxidation: XRD

XRD analysis was performed on the as-received and oxidized GCO ilmenite. From Table 4.6, one can see that in the as-received material, there are three main phases of pseudorutile, ilmenite, and hematite. After the lowest oxidation temperature of 700°C, the remaining phases seem to be pseudorutile, rutile, and small amounts of ilmenite. There is currently a lack of understanding and agreement regarding whether pseudorutile is an intermediate product of oxidation or not. The process by which it occurs during oxidation is not well understood. What happens to the naturally created pseudorutile phase during oxidation is also disputed. According to Salehi et al.[41], pseudorutile still exists after being oxidized at 1000°C for one hour. However, Gao et al.'s XRD data[40] indicates that the natural pseudorutile phase disappears at 600°C, and the oxidation product H239 becomes an intermediate compound at 800°C, before eventually reacting to produce pseudobrookite and rutile after 60 minutes of oxidation. From the TGA conducted on the GCO ilmenite, it becomes clear that a separate reaction is occurring up until 650°C after which a larger reaction takes place, believed to be the oxidation of ilmenite to pseudobrookite. The TGA data can indicate that for this type of ilmenite, pseudorutile is the main phase present after 1 hour of oxidation. It might not be the stable end product for this temperature, but due to the slow kinetics of the separation reaction, it appears to be the largest phase present. It is also worth mentioning that the iron speciation found through chemical analysis indicates a different distribution of the phases, showing that the amount of pseudorutile given from the Rietveld analysis may be over-estimated.

Increasing the oxidation temperature to 800°C one sees that pseudorutile is no longer present. According to Reaction 2.10 it can break down to ferric pseudobrookite and rutile. Since there was no pseudobrookite detected in the sample, it can be assumed that this reaction is not followed since the pseudobrookite phase can be stable at 800°C given enough time[55]. Instead, the main phases found during analysis were ilmenite, rutile, and hematite. Indicating that the reverse of Reaction 2.7 could occur alongside the creation of ilmenite. The same goes for this sample as for the sample oxidized at 700°C. From the chemical analysis for iron speciation, the FeO content is too low to account for the amount of ilmenite detected from the Rietveld analysis. Since no pseudobrookite peaks were detected during analysis, it is fair to assume that more hematite should be present after oxidation. This also coincides well with the findings of Cheng et. al.[40] who found that ilmenite similar in composition to the GCO ilmenite had mostly rutile and hematite after 60 minutes of oxidation. When the results were filtered through the COD database, one can also see that some of the peaks for ilmenite, θ 62.5 and θ 41.5, have either shifted or are hidden from the analysis due to the broadness of other peaks. This in turn can also be explained by the large solid solution possible between the Ti_2O_3 and Fe_2O_3. It might be for this reason that the phase amounts are not accurate.

The highest oxidation temperature of 1000°C equilibrium is still not reached since rutile and hematite are present. Given the Ti/Fe mol ratio of 1.2, it is reasonable to assume that the hematite will be consumed before rutile, leaving it in equilibrium with pseudobrookite, which has been found to be the stable end phases at this temperature[27]. When comparing the Rietveld analysis to the chemical analysis, the results coincide better than the other oxidation temperatures. Almost all of the iron is found in a ferric state, while only 0.11 wt% is found in a ferrous state.

Ilmenite oxidation: SEM

Cross-sectional SEM analysis was performed on the oxidized sample to gain a greater understanding of the morphological changes occurring during oxidation. There are noticeable differences between the grains oxidized at different temperatures. The samples oxidized at 700°C a homogeneous grain was observed. EDS analysis was performed on the main gray phase, and it was found that the Ti:Fe molar ratios were between 1.6-1.4, which is close to the molar ratios of the pseudorutile. The darker gray phases found were high in titanium and oxygen, giving the impression that it could be rutile. This coincides well with the Rietveld analysis performed for this oxidation degree, with the main phases detected being pseudorutile and rutile. Increasing the oxidation temperature to 800°C led to a more porous structure in the grain. There was also found a greater difference in Ti:Fe ratio at this oxidation temperature with values ranging from 2.4 to 0.9. From the literature, one can find that at this temperature, the phase combination of hematite and rutile is meta-stable before oxidizing further to pseudobrookite, given enough time[55]. There was found similar a structure to what is shown in Figure 2.20, where rutile appears as whiskers in a hematite matrix, but from our analysis, no hematite was found. This could be due to the high solubility found in the M_2O_3 phase, as well as elements beneath the surface being picked up by the detector. Comparing the SEM to the XRD results the Ti:Fe molar ratios for both ilmenite and rutile were detected, while no hematite was found. It has been mentioned that hematite forms on the surface of the grains[41], which could explain the difficulty of finding it in a cross-sectional analysis. The highest oxidation temperature examined with SEM for the GCO ilmenite was 1000°C. One saw two distinct phases of gray and dark gray, with Ti:Fe molar ratios between 20.5 to 0.7. The high molar ratio may be due to a relatively high purity rutile phase, while the lower ratio possibly is a pseudobrookite phase. This coincides well with the XRD results for this temperature. The porous structure found at 800°C was no longer present at this temperature. Rutile and pseudobrookite are the stable end phases at this temperature, which coincides well with our results, the rutile being found in a pseudobrookite matrix.

The topological changes were also examined for the GCO ilmenite, oxidized at different temperatures. From the findings, it becomes clear that the grains undergo noticeable changes during oxidation. Initially, the surface was found to be flat, which changes to a more dynamic surface with micropores and multiple folds at an oxidation temperature of 700°C. For this oxidation temperature, two distinct areas could be detected, one smooth with a higher Ti:Fe molar ratio, while the more porous faces had a lower Ti:Fe ratio containing more iron. Comparing this to the surface of the 1000°C oxidized sample one can see more growth on the surface of some of the grains as well as spheres making up the majority of the grain. It should be mentioned that not all grains have the same growth on the surface. Grains found with a high Ti:Fe ratio, 1.3, were found to be smooth. Salehi et.al.[41] have mentioned that the pseudorutile phase remains unaffected by oxidation, which our results could indicate as well. When taking the XRD results into account, there were found no peaks for pseudorutile. This could mean that the surface of the grain has similar ratios to pseudorutile, but the actual amount of the phase is not enough to show up in the XRD results. The more porous grains were found to have a molar ratio closer

to 0.5 to 0.6. This in turn is possibly due to the creation of pseudobrookite, with a stoichiometric Ti:Fe ratio of 0.5. The literature mentions that the larger ilmenite crystals break down to multiple smaller crystals of rutile and pseudobrookite as the oxidation progresses[45], which is clear when comparing the topology of the as-received samples to that of the 1000°C oxidized samples.

Based on these findings, one may assume that different oxidation degrees were reached and different phase combinations were present prior to reduction, as well as different morphologies. For oxidation at 700°C, the main phases, based on the detected at%, likely correspond to pseudorutile, rutile, and ilmenite. At 800°C, ilmenite, rutile, and hematite were the likely phases. At 1000°C, ferric pseudobrookite, rutile, and ilmenite were found. The exact amounts of each phase could not be determined with certainty using SEM-EDS.

With the oxidation summary presented, one can start discussing the experimental results for the GCO ilmenite. The results are separated in two ways highlighting the effects of changing different parameters. First, the effect of oxidation temperature is discussed before the effects of changing reduction temperature are presented.

5.2.3 Effect of oxidation temperature on reduction

The idea of oxidizing ilmenite prior to reduction stems from the iron industry, where naturally occurring magnetite ores have a denser outer shell when compared to hematite[10][17]. This can create a dense outer iron layer that hampers further reduction of the ore. As well as preventing the formation of an outer iron layer, it was also found that during oxidation, pores were created in the oxide[16][19], which could lead to better gas transport. During the reduction of oxidized magnetite or natural hematite, pores were also formed from removing the extra oxygen, further enhancing the gas transport.

For the GCO sample, three reduction degrees were used, 800, 900, and 1000°C. Each of these will be discussed individually, and the focus will be given to how the oxidation temperature affected the reduction curve at the given reduction temperature. Since the starting point differs from each oxidation temperature, the weight change curves and the oxygen-to-iron ratios are the most convenient representation of results.

Considering the GCO samples reduced at 800°C first. The different oxidation degrees become clear in the starting points of the weight change curves and O:Fe ratios. Complete oxidation gives an oxygen-to-iron ratio close to 1.5, which can be seen for an oxidation temperature of 1000°C with the value of 1.46. Indicating that not all the ferrous iron has been oxidized, similar to the findings of Lobo[8]. It has been shown that impurities can stabilize the iron titanium oxides. One example of this is the Panzhihua ilmenite containing a high concentration of magnesium oxide[24]. Given the different starting points of the oxide, the improvement oxidation could have on reduction kinetics at 800°C can be seen at the point where the curves cross the as-received line. Mainly focusing on the O:Fe ratio, given these are the most accurate starting points, oxidation at 800 and 1000°C showed an improvement in reduction kinetics, crossing the as-received line at 25 and 10 minutes respectively. While oxidation at 700°C shows worse kinetics and lower overall reduction degrees. The reason for this could be the starting phases that are present in the sample. As mentioned, XRD results show that the main phases present before reduction are pseudorutile and rutile, with the pseudorutile not being present at oxidation at 800°C. The pseudorutile phase could then be considered to hamper the reduction kinetics at a reduction temperature of 800°C.

Increasing the reduction temperature to 900°C one can see a greater difference in the %weight change curves compared to the O:Fe ratios. In the weight change curve, the as-received sample reaches higher mass loss values as well as a slower reduction when taking the weight gain from oxidation into account. The O:Fe ratio shows the opposite. The as-received material is similar in reduction kinetics to the 700°C sample, while towards the end of reduction, it reaches lower values for O:Fe ratios, indicating that lower titanium oxides were created. The samples that underwent oxidation seem to all reach the same endpoint, just below 0 showing complete conversion to metallic iron. Similar to the lower reduction temperature of 800°C, ilmenite oxidized at 1000°C reaches this value first at approximately 15 minutes, while the sample oxidized at 800°C reaches the plateau around 26 minutes. The 700°C oxidized sample shows the slowest kinetics but still ends up in a similar ratio as the others.

For the highest reduction temperature used, 1000°C, an inverse trend was seen compared to the other two temperatures. Initially, the oxidized samples reduced the fastest, but after 15 minutes of reduction, the as-received material showed the lowest O:Fe ratios. Indicating that more titanium oxides got reduced compared to the other samples. The as-received samples reached a ratio of -0.25, while the oxidized samples were in the range of -0.13 to -0.18. Furthermore, the sample oxidized at 700°C seemed to show faster kinetics compared to the sample oxidized at 800°C, closely following the initial reduction path of the as-received sample. This could indicate that at higher temperatures the pseudorutile phase is capable of faster reduction kinetics compared to hematite and rutile for 800°C oxidation or pseudobrookite and rutile at 1000°C oxidation. Since the main phases found in both the as-received and the 700°C oxidized material was pseudorutile. This could be due to the increased mass transport accompanied by the increased reduction in temperature.

To summarise the findings so far. At lower reduction temperatures, 800°C, oxidation of 800°C and 1000°C showed an increase in reduction kinetics, while the sample oxidized at 700°C showed a decrease in reduction kinetics. This is initially believed to be due to the pseudorutile phase present in the starting material. Increasing the reduction temperature to 900°C showed similar signs as the 800°C reduction series, however the as-received material reached greater reduction degrees in the final stages of reduction. Furthermore, based on the O:Fe data there was created very small amounts of lower titanium oxides. At the highest reduction temperature of 1000°C, the oxidation seemed to lower the reduction kinetics after 15 minutes of reduction as well as reaching lower final conversion values.

5.2.4 Effect of reduction temperature

A second way of looking at the results is by separating them into oxidation temperatures. This gives the samples the same starting point, removing the uncertainties created by averaging weight changes and oxidation degrees. This also gives a clearer indication of the effects of reduction temperatures.

Starting with the as-received reduction curves for the GCO sample. The conversion degree is used for comparison in this case since the starting points of each sample are the same, making it easier to compare. Based on the results, it is apparent that the higher the reduction temperature, the greater the kinetics and overall reduction achieved. Furthermore, for reduction at 800°C and 900°C, it does not seem that equilibrium is reached, while at the highest reduction temperature of 1000°C, a plateau is reached around 1.2 (120%) conversion. When comparing the results obtained in this thesis with literature[62], we can see similarities in the reduction kinetics increasing with increasing temperatures. In S et. al.'s results, one can see that the biggest jump in overall reduction degree is between 800 and 900°C, while for our results one sees

the largest jump in reduction degree between 900 and 1000°C. One of the main reasons for the difference could be that the Panzihuan ilmenite used in Si et. al.'s[62] case is high in magnesium oxide, leading to the presence of the barrier effect. Since the barrier effect can be overcome if the mass transfer rate is high enough an increase in reduction temperature can lead to it being neglected[60][33].

Looking at the oxidized samples the same trend is seen, but the differences between the different reduction temperatures become less clear with increasing oxidation temperature. One still sees an increase in reduction kinetics as the reduction temperature increases, but in the later stages of reduction, a plateau is reached for oxidation temperatures of 800 and 1000°C. The time it takes to reach this perceived equilibrium becomes less for higher oxidation temperatures. In other words, oxidation promotes reduction. This becomes most apparent by comparing the conversion degree at 15 minutes reduction with a reduction temperature of 800°C for each oxidation temperature. For 700°C at 15 minutes the conversion reached was 0.70. For 800°C it was 0.72, and at 1000°C the conversion was 0.93. When comparing this to the as-received material at 15 minutes and 800°C reduction, the conversion was 0.75. The total conversion degree at 15 minutes and 800°C reduction seems to initially go down for lower oxidation degrees before reaching higher overall conversion for higher oxidation degrees. When making the same comparison for reduction at 900°C, we see that the as-received sample at 15 minutes reduction has a conversion of 0.89, the 700°C oxidized sample reached 0.92, for 800°C oxidation 1.0 and 1000°C reached values of 1.03 conversion. This shows that the possible improvement of oxidation on preceding reduction is dependent on the reduction temperature. For reduction at 800°C one needs a stronger oxidation degree before there is a noticeable difference in reduction kinetics, while for reduction at 900°C an improvement in reduction kinetics can already be seen at 700°C oxidation. This effect is more clearly seen in Table 5.1. Where reduction at 1000°C shows little effect of oxidation and reduction at lower temperatures indicates greater effects. Further oxidation shows less of a benefit in regard to conversion and kinetics. So far this is only considering the GCO ilmenite, which naturally has a high degree of oxidation.

Table 5.1: Conversion degrees found after 15 minutes of reduction for different oxidation and reduction temperatures for GCO ilmenite.

Reduction (°C)→ Oxidation (°C)↓	800°C	900°C	1000°C
As-received	0.75	0.89	1.1
700°C	0.70	0.92	1.05
800°C	0.72	1.0	0.98
1000°C	0.93	1.03	1.09

5.3 Analytical results for the GCO ilmenite

With the data collected from reduction experiments discussed one can investigate the analytical results for the GCO ilmenite and try to explain some of the observations made. The XRD and Riedveldt analysis are mentioned first. Before the SEM analysis is discussed, both the cross-section and topology are mentioned. Finally, the ICP results and the analysis of the leachate are discussed.

5.3.1 XRD analysis

The XRD results were analyzed through Rietveld refined analysis and are presented in Tables 4.19-4.22. The reason for the short reduction time of 5 minutes was to get an insight into how the first step, Fe^{3+} to Fe^{2+}, progressed. But it became clear from the O:Fe ratios that already after 5 minutes the initial step was mostly complete, which was also reflected in the XRD analysis, where small amounts of pseudorutile were detected for the as-received and 700°C oxidized samples. While for the samples oxidized at 800°C and 1000°C no Fe^{3+} was found after 5 minutes of reduction. From further analysis of the XRD results it was proved difficult to ascertain the amount of pseudorutile present since the peaks for this phase overlap with ilmenite, hematite, and rutile. From the reduction curves presented by Lobo[8], one can see that for pellets the first step finishes after which a change in kinetics occurs. Showing a clear distinction between the first and second steps. It is also thought that little reduction of ilmenite occurs prior to the end of the first step, which one also can see in the presented analysis. There were low amounts of metallic iron detected. For all oxidation temperatures, the amount of ilmenite increased from the starting material after a reduction of 5 minutes. How pseudorutile breaks down during reduction is disputed, but based on these results it seems that the reaction found by Jones[58], Reaction 2.11 may be correct. In the presented results, one sees an increase in both ilmenite and rutile for the starting points high in pseudorutile, as-received, and 700°C oxidation. For further reaction progression past 5 minutes, the amount of ilmenite decreases and is replaced with metallic iron and rutile. For higher oxidation temperatures, the main difference was how fast the amount of ilmenite decreased and when it was no longer present. For the as-received material, the amount of ilmenite detected was 15.1 wt% after 35 minutes, while for 700°C oxidation, the amount detected at 35 minutes was 2.9 wt%. For the 800 and 1000°C oxidized samples, the ilmenite content at 15 minutes of reduction was 25.4 wt% to 13.3%, respectively, and was no longer present past this point. Confirming that oxidation past 800°C does enhance the reduction kinetics.

To gain a better understanding of what is occurring at higher reduction temperatures, the as-received GCO samples reduced at 1000°C were analyzed with XRD. It can be seen that as the reduction time increases the rutile phase reduces to create lower titanium oxides. Since the Magnéli phases exist as a wide range of titanium oxides, they have all been classified as lower titanium oxides. Quantifying the exact amounts of these lower titanium phases present has been proven difficult since they are hard to identify and the peaks from the XRD analysis are both wide and have a low intensity. Furthermore, from the Rietveld analysis, one can see that the initial increase in the wt% of ilmenite is no longer present, compared to the reduction at 800°C. Showing that the kinetics increased with increasing reduction temperature, which was also seen from the weight change graphs.

5.3.2 SEM analysis

The GCO samples reduced at 800°C were analyzed with SEM to help determine the morphological changes occurring during the progression of reduction. Common for all oxidation temperatures was that one could see a wide variety of iron morphology's, making it difficult to draw conclusions. Starting with the as-received material. From the grains presented one can see that the iron mainly metallized at the surface of the grain or at pore walls. There were however also found grains with a larger amount of internal reduction than what is shown in the figure. Salehi et. al.[41] tried to investigate how the morphology changes during the reduction of ilmenite, and according to the evidence presented by the author the gains starting out as pseudorutile or in combination with rutile showed the largest degree of internal reduction, where small iron globules were seen. The phase combination found in our starting material was found to be pseudorutile along the edge of the grain, with ilmenite at the center. How the iron agglomerates for

this combination of phases match well with that was found by Salehi et. al.[41]. Furthermore, one can see that towards the end of the reduction, iron has agglomerated in the pores of the grain. Leaving areas with no metallic iron present at the core of the grains. Based on the XRD results, these areas could be rutile, but the EDS analysis suggests that they still contain some iron in combination with titanium and oxygen. This could also be due to interference from phases beneath the surface, but it is difficult to say for certain.

The samples oxidized at 700°C saw similar iron nucleation as the as-received sample. The main difference is that during the reduction progression, one could see a clearer creation of the rutile matrix surrounding the metallic iron. From the results depicted in Figure 4.26 with the accompanying EDS analysis one can see that the darker gray phase surrounding the lighter gray center of the grains has a high Ti:Fe molar ratio, ranging from 3.4 to 7.8. The phase at the center seems to remain as ilmenite throughout the reduction process. Taking the O:Fe ratio and XRD analysis into account most of the grains found in the sample with a reduction time of 60 minutes should not contain any ilmenite, but most of the grains examined during the SEM analysis seemed to have the same build-up, with iron along the edge encompassed in a rutile matrix and an ilmenite grain core. There was however found a varying size of the ilmenite core.

The reduction path for the highest oxidized samples showed larger differences than what has been mentioned so far. As mentioned previously the oxidation of 1000°C led to a breakdown of the larger ilmenite grains to smaller pseudobrookite and rutile phases. This could be one of the reasons for the internal reduction being higher for higher oxidation degrees. The second reason for a larger degree of iron nucleation could be due to it being favored differently depending on the phase that undergoes reduction. Building further on this hypothesis can be done by examining the cross-section of samples oxidized at 1000°C and then reduced at 800°C for 5 minutes. One can see grains with a larger degree of internal reduction, Figure 4.27a), and others where iron nucleation is limited to certain phases, Figure 4.27b) and 4.27c). The internal reduction has been mentioned to occur for both iron oxides[14] and ilmenite[62] being reduced with hydrogen. In the case of ilmenite reduction with hydrogen, as mentioned by Si et. al.[62]. The hydrogen creates micropores as it diffuses into the grain and as the reduction progresses further the micro-pores created during this stage eventually fill up with metallic iron. In our case, it seems that some phases, pseudorutile or pseudobrookite, are initially more prone to this behavior than others. The large variance in iron distribution disappears as the reduction progresses, as can be seen in Appendix C. In the later stages of reduction, one can see a clear separation of iron from the pseudobrookite phase. The matrix surrounding the metallic iron is mostly made up of rutile. From the graphs showing weight change and O:Fe ratios, there are indications of reduction being complete after 28 minutes, with little to no weight change difference when reduced further. This in turn can be seen in the cross sections, where no meaningful difference is seen between the two. Furthermore, even though the reduction time at 800°C was doubled, there is little indication that the iron agglomerates in larger globules. The reason for this could be that the metallic iron is distributed in such a way that it does not connect to each other, so it does not allow for iron agglomeration.

Making a side-by-side comparison of the ilmenite prior to reduction and after 60 minutes of the as-received and 1000°C oxidation can be useful when highlighting the main changes occurring with increasing oxidation degree. From Figure 4.28 the differences become quite clear. The main one is how iron nucleates and agglomerates. For the as-received sample, the metallic iron seems mostly connected and appears in larger grain. While for the 1000°C oxidized sample, the iron is dispersed in small globules throughout the grain, with little connectivity between them and being encompassed by a rutile matrix. It has also become clear by doing this analysis that the changes each grain undergoes during reduction are dependent on the phases present

prior to reduction. A topology analysis was also conducted on the as-received grains reduced at different times, but little to no noticeable changes were found on the surface of the grain during the progression of reduction.

5.3.3 Acid digestion

Sulphuric acid leaching was conducted on the GCO samples reduced at 800 and 1000°C. Considering the discovered concentrations of iron and titanium for samples reduced at 800°C first. The change in iron concentration seems to follow three different paths as the reduction progresses. The as-received sample and the 700°C oxidized sample have a similar starting concentration after 5 minutes of reduction. After this, the concentration increases with increasing reduction time, where the final dissolution after 60 minutes of reduction was 73.8 and 75.3%, respectively. The sample oxidized at 800°C started at a higher concentration of iron before reaching around the same level as the previously mentioned reduction runs 75.9% of the total iron has been dissolved. The third concentration profile is seen for the sample oxidized at 1000°C, which shows complete opposite concentration curves. The detected iron concentration starts out at approximately 87.3% before increasing slightly and ending up with a final concentration of 66.1%.

The answer to the initial concentration difference can be found by delving deeper into the XRD results. After 5 minutes of reduction, the amount of detected ilmenite increases. Specifically, for the as-received sample, the percentage increases from 32.1 wt% to 60.4 wt%. For the 700°C oxidized sample, the percentage increases from 3.8 to 55.5%. For the 800°C oxidized sample, the percentage increases from 51.4 to 75.9%. Finally, for the 1000°C oxidized sample, the percentage increases from 0 to 67.9 wt%. From the literature, we know that the sulfate process uses similar conditions as acid leaching to dissolve ilmenite. Meaning that the increase in iron dissolution from zero to five minutes of reduction could in part be due to the creation of ilmenite during reduction. As the reduction time increases, the further increase of iron concentration is attributed to the metallization of iron. Furthermore, the lower concentration detected in the sample was reduced for 5 minutes and oxidized at 700°C, compared to the as-received sample can be due to the lower amounts of ilmenite detected. How pseudorutile acts in sulphuric acid is not well known. Based on the XRD results of the leachate, pseudorutile was found in all samples that were analyzed and when looking at some of the EDS results a wide range of Ti:Fe can be found with values ranging from 1.7 to 4.3 for the cross-sectioned samples and 2.3 to 4.5 for the topology analysis. This gives an indication that iron is found not only in a metallic state at the center of the grain but also in a compound together with titanium. It should be mentioned that the Rietveld analysis presented in Table 4.28 should be taken with a grain of salt since phases that were detected after leaching was not always present before leaching. Examples of this are pseudorutile for the 800°C and 1000°C oxidized sample. Literature for this occurrence was not found.

For the titanium concentrations, we see similar trends as for iron, but in reverse. Initially, it starts out high after 5 minutes of reduction. The 800°C oxidation reached the highest concentration of 35.1 wt% of total titanium being dissolved. This coincides well with the Rietveld analysis given since it has the highest amount of ilmenite present after 5 minutes of reduction. Again we also see the reverse trend for the sample oxidized at 1000°C. For the other samples as the reduction progresses further, the titanium concentration decreases, ending in a similar concentration for all samples at 5.2 wt%. During the leaching of ilmenite in the sulfate process rutile is considered to be inert[67][68], which explains the low concentration of titanium by the end of reduction. Keeping this in mind it can also be an indication that for these experimental parameters, the reduction can be considered close to complete after 35 minutes of reduction.

Samples that were reduced at 1000°C also underwent hot acid leaching. By inspecting the graphs, one can see some similarities in regards to the 800°C reduction discussed previously. Again the as-received and 700°C oxidized samples have the lowest initial concentration of both iron and titanium, 44.9 and 46.8 wt% respectively while the 800°C oxidized sample reached 65.5 wt%. In contrast to the 800°C reduction series, the 1000°C oxidized sample ends up with a similar iron concentration as the 800°C oxidized sample, 66.3 wt%. This can give an indication as to if the 1000°C oxidized, reduced at 800°C curve, might be wrong. Another interesting observation from the results is that as the reduction time reaches 60 minutes we can see a drop in iron concentration for all oxidized samples but not for the as-received sample. The exact reason for this is unclear since SEM and XRD results have not been performed on the series. Looking closer at the titanium concentration, the graph showing percentages can be misleading, which is why the ppm values are given as well. Here we see the titanium concentration stays relatively low for all of the reduction times. Since we know that lower titanium oxides are created after 15 minutes, one can conclude that the Magnéli phases or the Ti_3O_5 phase do not dissolve in sulphuric acid.

Considering the SEM images of the analyzed leached samples. As mentioned, one can see metallic iron in the core of some grains. This explains why the total iron dissolution detected from leaching does not reach higher than 89 wt%. There was little to no difference detected in the amount of iron left in the core of the grain between the different oxidation degrees. If oxidation of ilmenite leads to a porosity increase or not is somewhat discussed, but most authors agree to an increase in specific surface area[47][44][53]. This could explain the higher iron concentrations detected during the leaching of the samples oxidized at 1000°C and reduced at 800°C. But the findings in this thesis are not sufficient for any conclusion on the subject. Another interesting finding from the cross-sectional analysis was what looked like a ring surrounding the core of the particle. Mapping was conducted on the rings, and from the results presented, one can see the concentration of iron is higher in the ring before decreasing slightly. In the center of the rings, one could find metallic iron. Point analysis was done on some of the rings with inconclusive results on why the rings were present. Based on literature different arguments can be made to explain this. If the reaction proceeds topochemically, then the ring could be explained by something that occurs during reduction. It is well documented that in pellets the reaction proceeds in a topochemical fashion[8]. When it comes to grains, the same knowledge as to how ilmenite reduction progresses has not reached a satisfactory level. De Vries et. al.[65] argue that the reaction does not follow a topochemical progression in grains, which disproves in part the argument. Furthermore, the barrier effect was also considered to be a reason for the rings. As the reaction move towards the center of the grain, impurities like manganese moves ahead of the reaction interface[33][60] stabilizing phases like M_3O_5. This could explain the shape of the ring, in some sense mimicking the exterior of the grain. But from the point analysis conducted on some of the rings, manganese was not discovered while others found amounts of magnesium. If the reaction does not follow a topochemical progression and the barrier effect is disregarded, the remaining options could be that it is a result of oxidation or leaching of the sample.

The topology analysis of the leached samples revealed a wide range of different grains. The grains with a rough surface were found to contain larger amounts of titanium, while the smoothed-surfaced grains still had iron present alongside the titanium. One of the reasons for this could be that grains with a higher initial iron content reduced faster than grains with a lower iron-to-titanium ratio. There were of course exceptions to this with findings of high iron content in some points on the rough grains. The values detected during EDS analysis of the topology should not be taken at face value. Since the signals being reflected back up to the detector varies with a varying slope of the grain. If the grain is positioned correctly like in the cross-sectioned samples, the signals from the detector are closer to reality than if the surface is analyzed at a slope.

To summarize the ICP results. Acid digestion could not be used as a reliable method to determine the conversion degree of ilmenite reduction. The acid could not penetrate deep enough into the sample to dissolve all the metallic iron. Oxidation showed to increase the iron and titanium dissolution after 5 minutes of reduction. As the reduction progressed an increase in iron dissolution was seen while a decrease in titanium dissolution was found.

5.4 Discussion of KZN sample and comparison to GCO ilmenite

The second ilmenite sample from Mintek, KZN ilmenite, is discussed in the following section. Both the oxidation data collected from the TGA and the data from reduction at 800°C are discussed and compared to the GCO ilmenite.

5.4.1 Oxidation

The micro-TGA results for the KZN ilmenite showed that even though the chemical composition is similar, how the concentrates act during oxidation is very different. When the weight change was plotted against temperature, one saw that the overall mass gain from oxidation reached 4.6%. The mass gain was seen to decrease with increasing heating rates, in much the same way as the GCO ilmenite. The higher overall weight change can again be attributed to the fact of higher iron content in the as-received material and the lower degree of weathering, which is known to oxidize ferrous iron to ferric iron. When the first derivative of the weight change as a function of temperature was considered, one saw a slow initial rate increase up to approximately 600°C, after which a sharp increase followed with a peak at 820°C. When comparing this to the GCO ilmenite, one did not see the same variance in rates. Since no pseudorutile was found for the KZN ilmenite, it further builds upon the fact that the plateau seen in the GCO ilmenite can be due to the formation of pseudorutile. A further indication of one dominating reaction occurring can be seen in the heat flow charts where the measured heat flow was seen to be negative for most of the micro-TGA, which is indicative of an endothermic reaction. There is seen a shift in the first derivative of heat flow as a function of temperature, where the rates switch from negative to positive at approximately 450°C. Since there is such a difference in these similar ores, further analysis was needed to say something about what was going on.

The mass change occurring during the oxidation of KZN ilmenite was noted down, and some of the oxidized samples were sent for wet chemical analysis at Eramet Titanium and Iron AS. It was observed that the weight change increased for all oxidation temperatures. Since one did not see the initial mass loss in the micro-TGA as was observed in the GCO ilmenite, it further builds on the hypothesis that different reactions are occurring in the two concentrates at 700°C oxidation. The greatest mass gain in the KZN ilmenite was recorded to be 3.5 wt% which is more than twice the amount of what was recorded in the GCO ilmenite at 1000°C oxidation. There is also seen a non-linear relation to the mass gain from the different oxidation temperatures. The mass

gain achieved at 800°C was close to three times that of what was achieved at 700°C oxidation. Again the reason for this greater difference can be seen in the first derivative of weight change as a function of temperature. At 800°C the rate is close to the highest point recorded. When the wet chemical analysis is taken into account the difference in starting material becomes clearer. In the as-received material, the calculated weight% for FeO and Fe_2O_3 was 31 and 16 wt%. Comparing this to the GCO ilmenite, where the as-received material was found to have 19 and 22 wt% of FeO and Fe_2O_3, respectively. The same trends were seen in the GCO ilmenite. The content of FeO decreases, and the amount of Fe_2O_3 increases with increasing oxidation temperature. Where the highest theoretical value for Fe_2O_3 was found at 1000°C oxidation, 52 wt%. The higher content of Fe_2O_3 was believed to be due to the lower Ti:Fe ratio found in the KZN ilmenite. Again one can conclude that by oxidizing at different temperatures different oxidation degrees were reached.

The main difference between the GCO sample and the KZN ilmenite is that for the as-received and the sample oxidized at 700°C, no pseudorutile was detected. This could be due to a lower degree of weathering in the as-received sample. Where weathering is assumed to oxidize the ilmenite and remove iron. The reason for it not being present at the 700°C oxidation sample is not clear. From the chemical analysis, one can see that the Ti:Fe ratio of the KZN ilmenite is lower than the GCO sample, 0.9 compared to 1.2. This could lead to it not being a stable phase or an in-between step in oxidation. The pseudorutile phase requires more titanium present, which could push the oxidation path out of the stability area of the pseudorutile. Since the pseudorutile phase does not show up in a phase diagram, it is difficult to say this for certain. The phase not being an intermittent step in oxidation can also explain the difference in the TGA results. As for the GCO sample, a linear mass gain rate was seen between the temperatures of 530 to 700°C, while in the TGA for the KZN oxidation, this linear rate was not seen. As the oxidation temperature increases the phase composition of the two samples becomes more similar. At 800°C the main phases detected were ilmenite, rutile, and hematite, which both coincide well with literature and what was found for the GCO ilmenite. At the highest oxidation temperature, as for the GCO ilmenite, signs that equilibrium was not reached are there. Theoretically, rutile and hematite should combine to pseudobrookite at this temperature. The similarity between the two temperatures for both samples is also highlighted in the topology analysis.

Since the starting points of the as-received material are different, the phases present after oxidation also vary. The chemical composition was found to be similar between the two types of ilmenite, but the micro-structure varied. This means that the effect oxidation has on the morphology also varies. For 700°C oxidation, some grains mainly consisted of iron oxides but with a higher O:Fe ratio. Indicating that the iron oxides that were present initially had undergone oxidation to hematite, with some titanium dissolved in the structure. From the TGA and the wet chemical analysis, one can see some oxidation has occurred at 700°C. However, due to the slow reaction rates, the observed morphology is similar to the as-received material. As the oxidation temperature increases, so does the oxidation degree, seen by a lower FeO to Fe_2O_3 wt%-ratio. This in turn is reflected in the morphology of the grain examined, where one can see a more uniform structure. Where phases with a high Ti:Fe ratio are found, i.e., close to rutile compositions, as well as phases with equimolar ratio. Interestingly for most grains at this temperature, a small layer of rutile could be found along the edge of the grains, with low concentrations of iron present. In comparison to the GCO ilmenite, it was clearly visible that iron oxides were present in phases with little to no titanium. The Fe:O ratio for these phases was found to be between 0.37 to 0.47. Since oxygen is a difficult element to detect accurately due to it being a light element, these findings could indicate the presence of different iron oxides. This in turn fits well with the literature and that the overall Ti:Fe ratio is <1. For the highest oxidation temperature, both the topology and the cross-section of the KZN ilmenite are similar to the

GCO ilmenite. Where two phases are present, rutile is distributed in an iron titanium oxide matrix. Since the distribution is fine, it is difficult to get an accurate reading of concentrations present in the phases.

5.4.2 Reduction

From the TGA and oxidation data one can see that the ores are different enough to produce different results during oxidation of the material. This trend continues in the data collected from the reduction as well. First considering the weight change curves. As mentioned the as-received and the 700°C oxidized samples reach the lowest mass loss during reduction, ending at approximately -8.3 %wt change. While the samples oxidized at 800°C and 1000°C reached a weight change of -11.6%. This difference was not due to the different oxygen amounts added by oxidation since it has been accounted for. Which means another reason must be found. The same trend can be found in the O:Fe ratio. The main difference is that the 700°C oxidized sample stays above the as-received line for all reduction times and reaches a value of 0.46, compared to the as-received sample reaching 0.39. The trend of the 700°C sample was also seen for the GCO ilmenite, with it showing slower kinetics than the as-received reduction path. From the TGA results for the KZN ilmenite, one can see that the oxidation kinetics are slow at 700°C. This could indicate that more sintering occurs, closing up pores which in turn decreases gas diffusivity. There is some indication of this in the topology analysis as well. If sintering takes place at this temperature, it may account for the lack of further decrease in O:Fe values observed in the 700°C oxidized sample, as more iron remains in oxide form rather than as metallic iron. The samples oxidized at 800 and 1000°C reach lower values, ending at an O:Fe ratio of 0.05. Furthermore, one can see that the kinetics have improved for these oxidation temperatures compared to the two other samples. The sample oxidized at 1000°C for 15 minutes already having an O:Fe ratio of 0.16, which is close to the 1000°C oxidized GCO sample having 0.1. This indicates that even though the other oxidation temperatures end with different phases present, the highest oxidation temperature of 1000°C follows similar paths of reduction. From these comparisons one can conclude the more weight is gained from oxidation, the clearer one can see the effects it can have on proceeding reduction. This observation was more evident for the KZN ilmenite than for the GCO ilmenite.

When the XRD analysis is considered alongside the weight change data, both results show that the reduction slows significantly for the as-received KZN ilmenite and the 700°C oxidized sample. Considering the as-received sample first. The ilmenite content decreases with increasing reduction time, while the amounts of iron and rutile increase with increasing reduction time, as in the GCO sample. The main difference is that the reduction is not complete. This is also seen in the analysis for the 700°C oxidized sample. The reason for this is clearer in the SEM images. It is believed that a barrier of products is created as the reduction progresses, hindering the diffusion of either reactant- or product gas to and from the reaction interface. This could be similar to what is found in the reduction of magnetite[20], where a dense iron layer is created around the grain that slows the reduction down. In our case, the layer seems to consist of iron and rutile. One other reason for the lower reduction degrees for the KZN samples could be the lower Ti:Fe ratio in the starting material. This could lead to iron oxides making up a larger part of the bulk material, and since the reduction of iron oxides is known to improve with oxidation. It could lead to a lower overall reduction degree. As the oxidation temperature is increased beyond 700°C, this phenomenon is no longer found. From literature[47][51] it is known that higher degrees of oxidation can help improve the specific surface area of the gains as well as create pores allowing for greater gas diffusion of both reactant and product gases. This could be one of the reasons for a larger reduction degree for the KZN samples oxidized at 800 and 1000°C. Without analyzing the pore structure and the surface area of the oxidized grains it becomes difficult to conclude this with certainty. An analysis of these properties could also

answer why the same effects are not seen in the GCO samples, where there was little difference in reduction degree with increasing oxidation temperature.

From the EDS analysis, it becomes clear that the way iron distributes during the initial stages of reduction is widely dependent on the starting phases present. Since the as-received KZN ilmenite had some grains mainly consisting of iron oxides, it follows a different reduction path than the GCO ilmenite where the grains show a more uniform phase distribution. If the iron oxide is present as a separate phase at the beginning, it has been proven to reduce completely before the reduction of ilmenite occurs[49]. This is also seen in the KZN ilmenite. After 5 minutes of reduction, some grains are found to have a high degree of metallic iron. At the same time, others show signs of internal reduction, where small particles of iron are distributed throughout the grain or are contained to the edge of the grains. The amount of internal reduction that occurs also seems to be dependent on the starting phases. Which phases allow a larger extent of internal reduction might pseudorutile created by weathering or phases largely consisting of ferric iron(Fe^{3+}), i.e., ferric pseudobrookite. These phases can either occur naturally from weathering or through oxidation. For the samples oxidized at 1000°C, reduced for 5 minutes, the theoretical O:Fe ratio was 0.75 showing a low degree of metallization. This is reflected in the cross-section of the grains. In a similar fashion as the as-received material, the iron oxides show a greater extent of metallization than the iron titanium oxides. Where the iron titanium oxides were found to have a minimal amount of metallic iron distributed along the edge of the grain and stoichiometric ilmenite at the center. This is on par with the literature, where the first stage of ilmenite reduction, i.e., Fe^{3+} to Fe^{2+}, completes first before the second stage starts[8]. After 60 minutes of reduction, the O:Fe ratios for the as-received and the 1000°C oxidized materials are 0.39 and 0.05, respectively. The exact reason why the as-received KZN ilmenite does not reduce completely is difficult to determine. From the cross-sections of the grains reduced for 60 minutes, one can see that the as-received material still contains ilmenite in the center of the grain. The ilmenite seems to be encapsulated by a Ti-oxide phase with a metallic iron phase. From the literature on the reduction of magnetite, it is known that oxidation helps prevent the formation of a metallic iron layer that hinders the diffusion of hydrogen to the reaction interface[20]. It is possible that similar conclusions can be drawn for the as-received KZN ilmenite. The product layer created by ilmenite reduction likely hinders the diffusion of reactant to the reaction interface, which eventually slows the reaction down or stops it completely. For the samples oxidized at 1000°C, the iron is distributed in much the same way as the GCO ilmenite. A finer distribution where the matrix consists of rutile.

5.4.3 Acid digestion

Comparing the ICP results from the KZN ilmenite to the GCO ilmenite revealed some differences. One still sees an increase in iron and titanium dissolution after 5 minutes of reduction with increasing oxidation temperatures. In the as-received and 700°C oxidized sample, the iron dissolution ends at 55.6%. Since the reduction was not complete for these two runs, it is expected that some of the iron remains in an insoluble state. As for the other oxidation temperatures, 800, and 1000°C, the reduction was completed after 60 minutes. When looking at the ICP results a difference can be seen. The 1000°C oxidized sample reached the highest iron dissolution. After five minutes of reduction, the value is greater than the 800°C oxidized sample. As the oxidation degree increases, more material is added to the ilmenite grains. This in turn leads to a greater mass loss potential when reduction is occurring. As the oxygen is removed and the ilmenite reduces to metallic iron, pores are introduced to the oxide matrix. The porous structure as well as the dissolution of iron could allow the sulphuric acid to penetrate deeper into the grain and dissolve more of the metallic iron. Comparing the different dissolution values of iron with the GCO sample, the reverse trend was not seen for this oxidation temperature. Even still the GCO

sample oxidized at 1000°C reached the highest value, which could be for the same reason as the KZN ilmenite. This could also be the reason why the 800°C oxidized sample did not reach the same dissolution of iron since the oxidation degree is lower compared to the 1000°C sample.

The titanium dissolution was seen to decrease as the reduction time increased. In similarity to the GCO sample one sees that an increase in oxidation temperature leads to an increase in initial titanium concentration. The highest dissolution was for the 1000°C oxidized sample at 65.1%. As the reduction progresses, the titanium decreases. This is believed to be due to rutile making up more of the material. Even though there is still ilmenite present after 60 minutes of reduction for the as-receive and 700°C oxidized sample it does not seem to affect the amount of titanium that gets dissolved. This could mean that the ilmenite is not as soluble as once thought and that another phase is responsible for the initial increase in titanium dissolution. Some of the phases this could be are pseudobrookite, hematite, or pseudorutile. Exactly which one is difficult to say for certain.

5.5 Sources of error

One of the reasons for using a small sample size was to avoid a gradient from the top layer of the sample to the bottom layer during reduction. This was believed to occur if the sample bed was too high and believed to be worsened by the poor airflow conditions generated by using a horizontal tube furnace and rectangular crucibles. A larger sample size could be examined in a fluidized bed reactor.

A substantial XRD and Rietveld analysis was performed on the two ilmenites and the products generated during this project. In as much, it should be mentioned that classifying the quantities of phases present through Rietveld analysis was shown to be especially difficult for the pseudorutile phase, which shares similar peaks with rutile, ilmenite, and hematite. With this in mind, the Rietveld analysis can be used to spot trends in the composition and not used to say anything specific about concentrations.

One of the drawbacks of EDS analysis is that one can not see what is beneath the surface of the cross-section. This can make the exact determination of phase composition difficult. It is especially true for grains, where one has a fine distribution. One example of this is the grains oxidized at 1000°C. The fine phase distribution can lead to the detector picking up signals from phases that are not visible on the SEM and therefore giving a skewed impression of the composition in the phase. Another point to consider when doing EDS analysis on topology is that the surface of the grain is not flat. Since the detector is positioned above the sample, all the signals generated during the analysis will not be picked up. This in turn leads to again a skewed image of the phase composition.

The KZN ilmenite was found to have a much more complex inner structure compared to the GCO ilmenite. It was found that different phases were intermingled to create different patterns, and the amount of grains found with impurities was higher. The increased impurities could lead to slightly inaccurate measurements in regard to mass loss which in turn would shift the O:Fe ratio lower. While the increased complexity of the iron and titanium oxides makes it difficult to draw any major conclusions as to why the ilmenite acted in a certain way.

Abnormalities were found during the ICP analysis of the reduced GCO sample oxidized at 1000°C. A reverse trend was seen in the dissolution of iron and titanium, where it started high and ended low. Though every precaution was taken to ensure good laboratory practice, the observed trend is difficult to explain, and would appear that a series of samples were inverted. Though this is unlikely, the exact reason for the relatively unique trend is uncertain.

5.6 Future work

There are still questions that are left to be answered after the work conducted during this thesis. During the analysis of the cross-section, different iron morphologies were found at different stages of the reduction. Some grains in the as-received material showed a large degree of internal reduction, where the iron is distributed in small globules throughout the grain, while others showed a more connected iron structure. Which phases allow for different iron agglomerations is not yet clear and initial work on elucidating this has been conducted by Salehi et. al.[41], but further investigation is needed to be able to say anything for certain.

A difference in the reduction path was seen in the as-received materials. The KZN ilmenite did not achieve complete reduction after 60 minutes, while the GCO ilmenite did. A preliminary BET analysis was conducted on both of the ilmenites where it was found that the GCO ilmenite had a specific surface area of 2.52 m^2/g while the KZN ilmenite was found to be 1.81 m^2/g. If this is the reason for the difference in reduction path is difficult to say, and a greater investigation is needed to ascertain why they act differently.

6 Conclusion

During this master's thesis, the effects of oxidation on ilmenite reduction with hydrogen have been examined. From the micro-TGA for the GCO ilmenite, it was found that different reactions occurred at different temperatures. It is believed that below 700°C, the formation of pseudorutile occurred. As confirmed by XRD results. At 800°C, hematite in combination with rutile, were the main phases. For oxidation at 1000°C, pseudobrookite was the dominating phase. In the KZN ilmenite, pseudorutile was found in the starting material. However, the pseudorutile phase was not present in the 700°C oxidized KZN ilmenite. Instead, hematite and rutile were found with varying quantities at oxidation temperatures of 700 and 800°C. At 1000°C, pseudobrookite, hematite, and rutile were the main phases.

There were relatively significant dissimilarities during the reduction of the two considered ilmenites. The GCO ilmenite could be reduced fully during reduction at all of the investigated temperatures. An improvement in reduction kinetics was observed for samples oxidized at 800 and 1000°C. The sample oxidized at 700°C showed a decrease in reduction kinetics at reduction temperatures of 800 and 900°C. The O:Fe ratio can be used as a measurement for reduction degree, where 0= complete reduction and negative values indicate the formation of lower titanium oxides. For reduction at 1000°C, the as-received GCO sample showed the greatest degree of reduction with an O:Fe ratio of -0.25, while the oxidized samples reached a ratio of approximately -0.15. The KZN ilmenite oxidization exhibited a greater increase in reduction for the KZN ilmenite. The as-received and 700°C oxidized samples showed an O:Fe ratio of 0.46 and 0.39, respectively, while the 800 and 1000°C samples showed a complete reduction, O:Fe=0. As for the GCO sample, the higher oxidation temperatures of 800 and 1000°C, showed an increase in reduction kinetics. One of the main effects of oxidation was how the metallic iron was distributed in the grain. In the as-received material, the iron was mostly connected and present on the grain rim, while oxidation at 1000°C led to the iron being distributed in small globules throughout the grain.

SEM results showed that acid digestion could not be used to ascertain the metallization degree of ilmenite without further preparation, like milling. SEM revealed inter particle metallic Fe, which could not be solubilized by the implemented acid leaching method. The results showed that increasing the oxidation degree led to a greater dissolution of iron. The titanium dissolution was seen to decrease with increasing reduction times.

Bibliography

[1] J. J. Solheim. The Tyssedal ilmenite smelting process. pages 177–199, 1988.

[2] Eramet Titanium and Iron As. Eramet Titanium and Iron As, 2023. Available at: `http://www.tizir.co.uk/`. Hentet: 17-05-23.

[3] Norwegian Environment Agency. Eramet titanium iron as emmisions, 2022. Available at: `https://www.norskeutslipp.no/en/Miscellaneous/Company/?CompanyID=5118`. Hentet: 26-10-22.

[4] M. Atsushi and H Uemuraand T. Sakaguchi. MIDREX Processes. *KOBELCO TECHNOLOGY REVIEW*, 29:50–57, 2010.

[5] hybritdevelopment.se/. Hybrit, 2023. Available at: `https://www.hybritdevelopment.se/en/`. Hentet: 02-05-23.

[6] Eramet Titanium and Iron As. Eramet Titanium and Iron As, 2023. Available at: `https://www.eramet.com/en/eramet-titanium-iron-pioneer-metallurgy-norway`. Hentet: 17-05-23.

[7] V. Canaguier and E. Ringdalen. Reduction Kinetics of Pre-Oxidized Ilmenite Pellets by H2-H2O Gas Mixtures. *Metals*, 13:1–17, 2023.

[8] S. C. Lobo. *Experimental Investigations and Modelling of Solid-State Ilmenite Reduction With Hydrogen and Carbon Monoxide*. NTNU, 2015.

[9] L. S. Draken and R. W. Gurry. The System Iron-Oxygen. II. Equilibrium and Thermodynamics of Liquid Oxide and Other Phases. *Contribution from the Research Laboratory, U. S. Steel Corporation*, 68:798–816, 1946.

[10] D. Spreitzer and J. Schenk. Reduction of Iron Oxides with Hydrogen - A Review. *Steel Research International*, 90:1–17, 2019.

[11] W. Zhang, Z. Xue, Z. Zou, and H. Saxén. The Ideal and Regular Mechanisms of Hematite Reduction Reactions. *Crystal Research and Technology*, 57:1–7, 2022.

[12] K. Mondal, H. Lorethova, E. Hippo, T. Wiltowski, and S.B. Lalvani. Reduction of Iron Oxide in Carbon Monoxide Atmosphere—Reaction Controlled Kinetics. *Fuel Processing Technology*, 86:33–47, 2004.

[13] M. N. A. Tahari, F. Salleh, T. S. T. Saharuddin, A. Samsuri, S. Samidin, and M. A. Yarmo. Influence of Hydrogen and Carbon Monoxide on Reduction Behavior of Iron Oxide at High Temperature: Effect on Reduction Gas Concentrations. *International Journal of Hydrogen energy*, 46:24791–24805, 2021.

[14] E. T. Turkdogan and J. V. Vinters. Gaseous Reduction of Iron Oxides: Part 1. Reduction of Hematite in Hydrogen. *Metallurgical Transactions*, 2:3175–3188, 1971.

[15] A. Bonalde, A. Henriquez, and M. Manrique. Kinetic Analysis of Iron Oxide Reduction Using Hydrogen- Carbon Monoxide Mixtures as Reducing Agent. *ISIJ International*, 45:1255–1260, 2005.

[16] E. T. Turkdogan and J. V. Vinters. Gaseous Reduction of Iron Oxides: Part III. Reduction-Oxidation of Porous and Dense Iron Oxides and Iron. *Metallurgical Transactions*, 3:1561–1574, 1972.

[17] A. Heidari, N. Niknahad, M. Iljana, and T. Fabritius. A Review on the Kinetics of Iron Ore Reduction by Hydrogen. *Materials*, 14:1–19, 2021.

[18] H. Zuo, C. Wang, J. Dong, K. Jiao, and R. Xu. Reduction Kinetics of Iron Oxide Pellets With H2 and CO Mixtures. *International Journal of Minerals, Metallurgy and Materials*, 22:688–697, 2015.

[19] Z. Wang, J. Zhang, K. Jiao, Z. Liu, and M. Barati. Effect of Pre-Oxidation on the Kinetics of Reduction of Ironsand. *Journal of Alloys and Compounds*, 729:874–883, 2017.

[20] V. L. v. Bogdandy, H. P. Schulz, B. Wiirzner, and I. N. Stranski. Der Mechanismus der Reduktion von porigen Eisenerzen durch Wasserstoff. *Archiv fiir das Eisenhiittenwesen*, 6:401–410, 1963.

[21] S. El Moujahid and A. Rist. The nucleation of iron on dense wustite: A morphologial study. *Metallurgical Transactions B*, 19B:787–802, 1988.

[22] V. Y. Canaguier. *Synthesis of Ilmenite*. NTNU, 2014.

[23] M. Tangstad. *Oksidasjon og Reduksjon av Ilmenittpellets*. NTH, 1988.

[24] F. Chen, W. Lv, G. Zhou, Z. Liu, M. Chu, and X. Lv. Effects of Pre-Oxidation on the Hydrogen-Rich Reduction of Panzhihua Ilmenite Concentrate Powder: Reduction Kinetics and Mechanism. *International Journal of Hydrogen Energy*, pages 1–15, 2022.

[25] G. Zhang and O. Ostrovvski. Effect of Pre-Oxidation and Sintering on Properties of Ilmenite Concentrates. *International Journal of Mineral Processing*, 64:201–218, 2002.

[26] H. Salehi, H. Aghajani, and H. Salimkhani. Isothermal and Kinetic Studies on Oxidation Roasting of Kahnooj Ilmenite Concentrate. *Chemical Engineering Transactions*, 66:397–402, 2018.

[27] S. k. Gupta, V. Rajakumar, and P. Gieveson. Phase Transformations during Heating of Ilmenite Concentrates. *Metallurgical Transactions B*, 22B:711–716, 1969.

[28] X. Goso and K. Bisaka. Improved DC Arc Smelting of Ilmenite Through Pre-Heating and Pre-Reduction. *Mintek, Internal Report*, pages 1–241, 2012.

[29] M. C. Ackland. The Grande Côte Minerals Sand Project. *Eight International Heavy Minerals Conference*, pages 41–60, 2011.

[30] K. Borowiec and T. Rosenqvist. Phase Relations and Oxygen Potentials in the Fe-Ti-Mg-O System. *Scandinavian journal of metallurgy*, 14:33–43, 1985.

[31] K. Boroweic and T. Rosenqvist. Phase Relations and Oxidation Studies in the System Fe-Fe2O3-TiO2 at 700-1100 C. *Scandindinavian journal of metallurgy*, 10:217–224, 1981.

[32] R. E. Johnson, E. Woermann, and A. Muan. Equilibrium studies in the system $mgo\text{-}feo\text{-}tio_2$. *American Journal of Science*, 271:278–292, 1971.

[33] D. G. Jones. Photomicrographic investigation of the reduction of ilmenite. *Izvestiya Akademii Nauk SSSR, Seriya Khimicheskaya*, 2:269–280, 1977.

[34] G. Ôstberg. Solid State Reduction of Ilmenite. *Jernkontorets annaler*, 144(1):46–76, 1960.

[35] I. E. Grey and R. R. Merritt. Stability Relations in the Pseudobrookite Solid Solution FeyTi3-yO5. *Journal of solid state chemistry*, 37:284–293, 1981.

[36] T. P. V. Kaam. *How Ilmenite Reduction by Hydrogen Gas is Affected by the Introduction of Water Vapour*. NTNU, 2020.

[37] P. Waldner and G. Eriksson. Thermodynamic Modelling of the System Titanium-Oxygen. *Calphad*, 23(2):189–218, 1999.

[38] G. G. Michaud and L. M. Pidgeon. The Selective Reduction of Iron in Ilmenite and the Oxygen Pressure of TiO2-x(rutile). *The transaction of the canadian institute of mining*, 57:187–189, 1954.

[39] I. B. Ketteridge. *Selective Reduction of Iron in Ilmenite*. University of Adelaide, 1969.

[40] G. Cheng, Z. Gao, S. Yang, H. Yang, and X. Xue. Microstructure and Chemical Transformation of Natural Ilmenite during Isothermal Roasting Process in Air Atmosphere. *Minerals*, 11:1–11, 2021.

[41] H. Salehi, S. Seim, L. Kolbeinsen, and J. Safarian. Phase Transitions and Microstructural Changes During Oxidation and Reduction of a Weathered Ilmenite Concentrate. *Proceedings of the 59th Conference of Metallurgists*, COM 2020:1–9, 2020.

[42] X. Fu, Y. Wang, and F. Wei. Phase Transitions and Reaction Mechanism of Ilmenite Oxidation. *Metallurgical and Materials Transactions A*, 41A:1338–1348, 2010.

[43] W. Xiao, X. Lu, X. Zou, X. Wei, and W. Ding. Phase Transitions, Micro-Morphology and its Oxidation Mechanism in Oxidation of Ilmenite (FeTiO3) Powder. *Transactions of Nonferrous Metals Society of China*, 23:2439–2445, 2013.

[44] W. Xiao, X. Lu, W. Ding, C. Li, and X. Zou. Pre-oxidation and Hydrogen Reduction of Panzhihua Ilmenite Concentrate. *Rare Metal Technology*, pages 127–131, 2014.

[45] S. Samanta, S. Mukherjee, and R. Dey. Oxidation Behaviour and Phase Characterization of Titaniferous Magnetite Ore of Eastern India. *Transactions of Nonferrous Metals Society of China*, 24:2976–2985, 2014.

[46] R. A. Briggs and A. Sacco. The Oxidation of Ilmenite and Its Relationship to the FeO-Fe203-TiO2 Phase Diagram at 1073 and 1140 K. *Metallurgical Transactions A*, 24A:1–8, 1993.

[47] W. Lv, X. Lv, Y. Zhang, S. Li, K. Tang, and B. Song. Isothermal Oxidation Kinetics of Ilmenite Concentrate Powder From Panzhihua in Air. *Powder Technology*, 320:239–248, 2017.

[48] Y. Zhao and F. Shadman. Reduction of Ilmenite with Hydrogen. *Ind. Eng. Chem. Res.*, 30:2080–2087, 1991.

[49] R. Merk and C. A. Pickles. Reduction of Ilmenite by Carbon Monoxide. *Canadian Metallurgical Quarterly*, 27:179–185, 1988.

[50] P. L. Vijay, R. Venugopalan, and D. Sathiyamoorthy. Preoxidation and Hydrogen Reduction of Ilmenite in a Fluidized Bed Reactor. *Metallurgical and Materials Transactions B*, 27B:731–738, 1996.

[51] X. Zhang, Z. Du, Q. Zhu, J. Li, and Z. Xie. Enhanced Reduction of Ilmenite Ore by Pre-Oxidation in the View of Pore Formation. *Powder technology*, 405:1–12, 2022.

[52] Z. Shi-qing, L. Xiao-dong, Y. Zhi-ming, L. Zue-wei, L. Wei, and B. Chen-guang. Effect of Pre-Oxidation Degree on Gaseous Reduction of Pre-Oxidized Ilmenite Concentrate by CO. *J. Iron Steel Res. Int.*, 29:881–890, 2022.

[53] K. Choi and H. Park. Effect of Pre-oxidation Temperature on the Reduction Kinetics of Ilmenite Concentrate. *The Minerals, Metals Materials Society*, 74:4410–4419, 2022.

[54] G. Cheng, Z. Gao, S. Yang, H. Yang, and X. Xue. Effect of Pre-Oxidation on the Reduction of Ilmenite Concentrate Powder by Hydrogen. *Hydrogen Energy*, 44:4031–4040, 2019.

[55] J. Zhang, Q. Zhu, Z. Xie, C. Lie, and H. Li. Morphological Changes of Panzhihua Ilmenite During Oxidation Treatment. *Metallurgical and Materials Transactions B*, 44B:897–905, 2013.

[56] S. K. Gupta and P. Grieveson. Reduction Behavior of Ilmenite with Carbon at 1240°C. *Metallurgical and Materials Transactions B*, 26B:401–405, 1995.

[57] O. Levenspiel. *Chemical reaction engineering, 3rd edition.* John Wiley & Sons, 1972.

[58] D. G. Jones. Reaction Sequence in the Reduction of Ilmenite. *Transactions of the institution of mining and metallurgy*, 82(805):186–192, 1973.

[59] G. Bardi, D. Gozzi, and S. Stranges. High Temperature Reduction Kinetics of Ilmenite by Hydrogen. *Materials Chemistry and Physics*, 17:325–341, 1987.

[60] C y. Lu, X-L. Zou, X-G. Lu, X-L. Xie, K. Zheng, W. Xiao, H-W. Cheng, and G-S. Li. Reductive Kinetics of Panzhiua Ilmenite with Hydrogen. *Trans. Nonferrous Met. Soc. China*, 26:3266–3273, 2016.

[61] J. Dang, G. Zhang, and K. Chou. Kinetics and Mechanism of Hydrogen Reduction of Ilmenite Powders. *Journal of Alloys and Compounds*, 619:443–451, 2015.

[62] X. Si, X. Lu, C. Li, C. Li, and W. Ding. Phase Transformation and Reduction Kinetics During the Hydrogen Reduction of Ilmenite Concentrate. *International Journal of Minerals, Metallurgy and Materials*, 19:384–391, 2012.

[63] Y. Wang, Z. Yuan, H. Matsuura, and F. Tsukihashi. Reduction Extraction Kinetics of Titania and Iron from an Ilmenite by H2–Ar Gas Mixtures. *ISIJ International*, 49(2):164–170, 2009.

[64] M. Chen and X. Xiao. Investigation on the Reduction of Ilmenite at Lower Temperatures. *Materials Science Forum*, 852:573–578, 2015.

[65] M. L. de Vries, I. E. Grey, and J. D. Fitz Gerald. Crystallographic Control in Ilmenite Reduction. *METALLURGICAL AND MATERIALS TRANSACTIONS B*, 38b:267–277, 2007.

[66] E. Reck and M. Richards. TiO2 Manufacture and Life Cycle Analysis. *Pigment Resin Technology*, 28:149–157, 1999.

[67] T. Hiraki, Y. Maruyama, Y. Suzuki, S. Itoh, and T. Nagasaka. Up-grading of Natural Ilmenite Ore by Combining Oxidation and Adcid Leaching. *International Journal of Minerals, Metallurgy and Materials*, 25:729–737, 2018.

[68] S. Itog, S. Sato, J. Ono, H. Okada, and T. Nagasaka. Feasibility Study of the New Rutile Extration Process From Natural Ilmenite Ore Based on the Oxidation Reaction. *Metallurgical and Materials Transactions B*, 37B:979–986, 2006.

[69] A. V. Dubenko, M. V. Nikolenko, A. Kostyniuk, and B. Likozar. Sulfuric Acid Leaching of Altered Ilmenite Using Thermal, Mechanical and Chemical Activation. *Minerals*, 10:1–19, 2020.

[70] L. Jia, B. Liang, L. Lu, S. Yuan, L. Zheng, X. Wang, and C. Li. Beneficiation of Titania by Sulfuric Acid Pressure Leaching of Panzhihua Ilmenite. *Hydrometallurgy*, 59:92–98, 2014.

[71] A. A. Baba, S. Swaroopa, M. K. Ghosh, and F. A. Adekola. Mineralogical Characterization and Leaching Behavior of Nigerian Ilmenite Ore. *Transactions of Nonferrous Metals Society of China*, 23:2743–2750, 2013.

[72] K. N. Han, T. Rubcumintatara, and M. C. Fuerstenau. Leaching Behavior of Ilmenite with Sulfuric Acid. *Metallurgical Transactions B*, 18B:325–331, 1987.

A Hot acid leaching

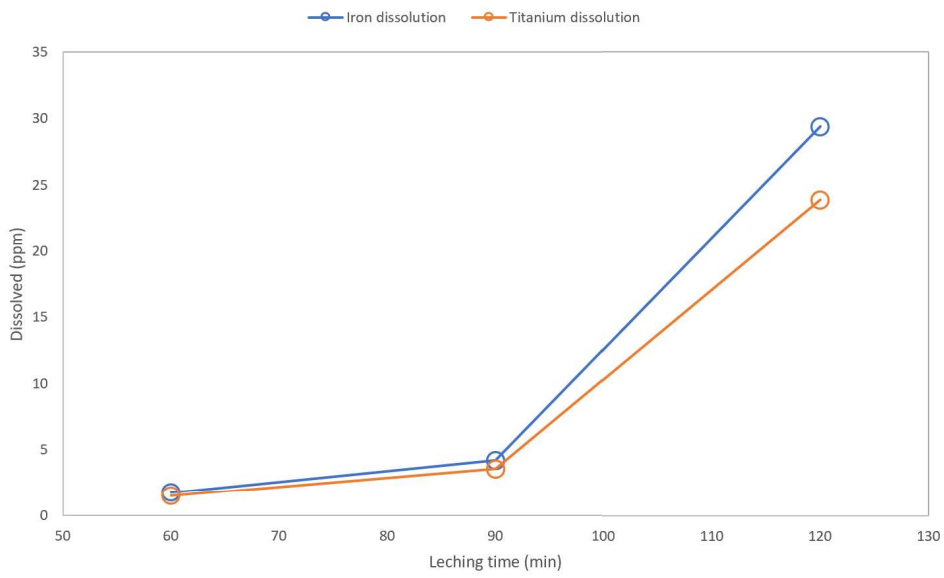

Figure A.1: Iron and titanium dissolution after hot acid leaching of as-received GCO material for different holding times at 80°C.

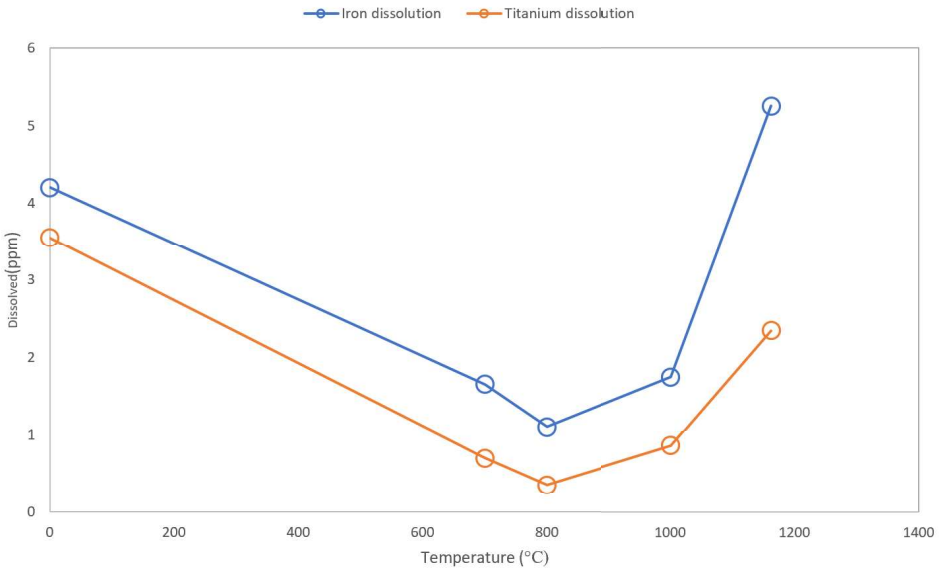

Figure A.2: Iron and titanium dissolution after hot acid leaching of oxidized GCO samples. Holding time was 90 minutes at 80°C.

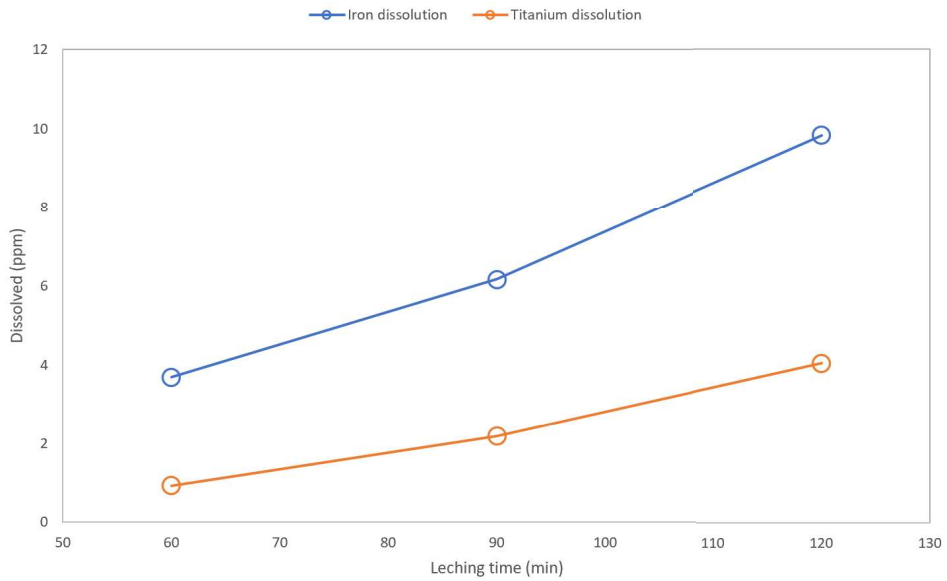

Figure A.3: Iron and titanium dissolution after hot acid leaching of as-received KZN material for different holding times at 80°C.

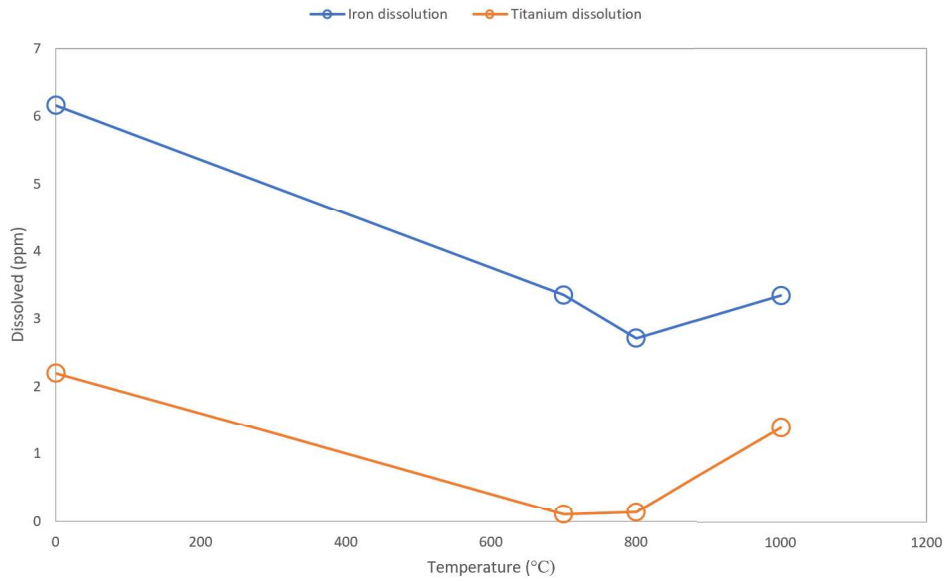

Figure A.4: Iron and titanium dissolution after hot acid leaching of oxidized KZN samples. Holding time was 90 minutes at 80°C.

B XRD-analysis

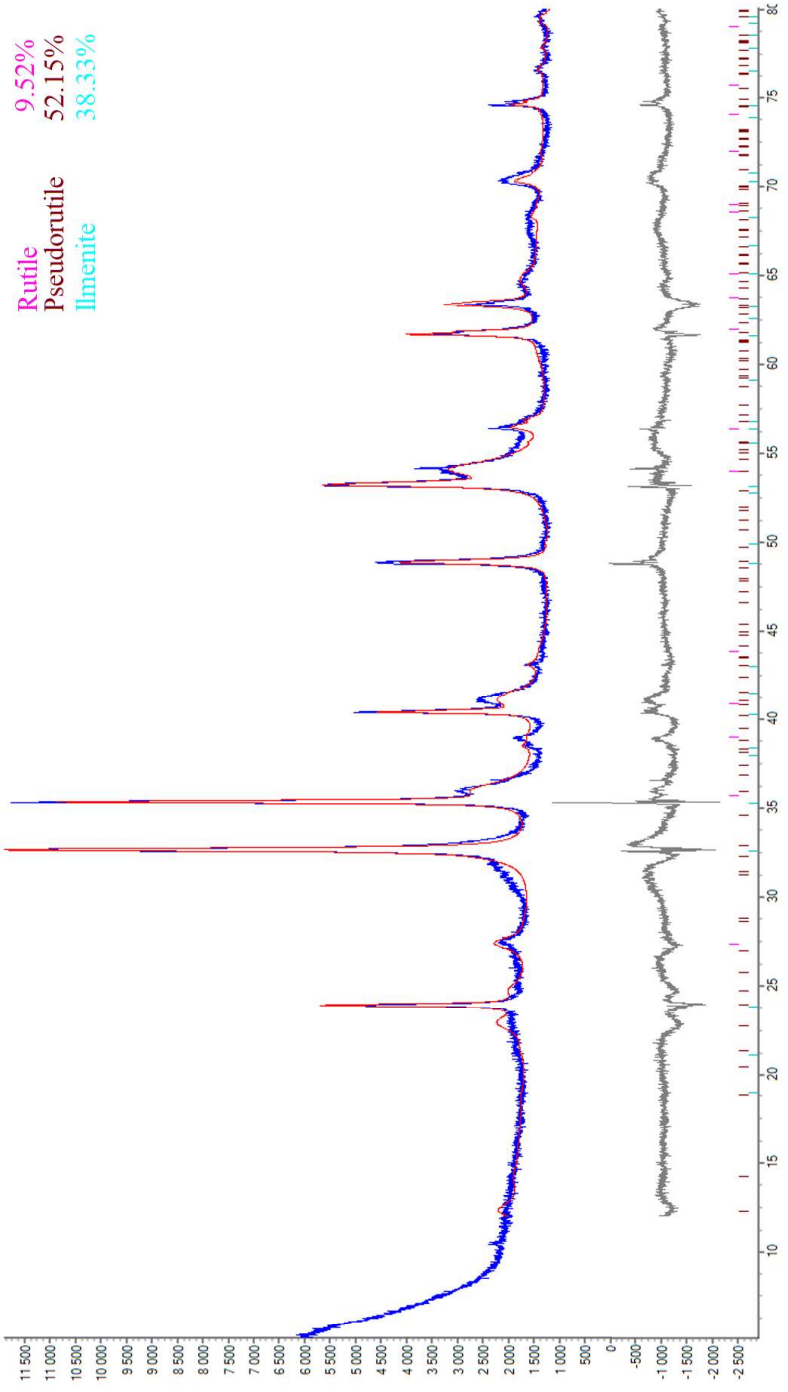

Figure B.1: XRD-results analysed with the PDF-4, for the GCO sample.

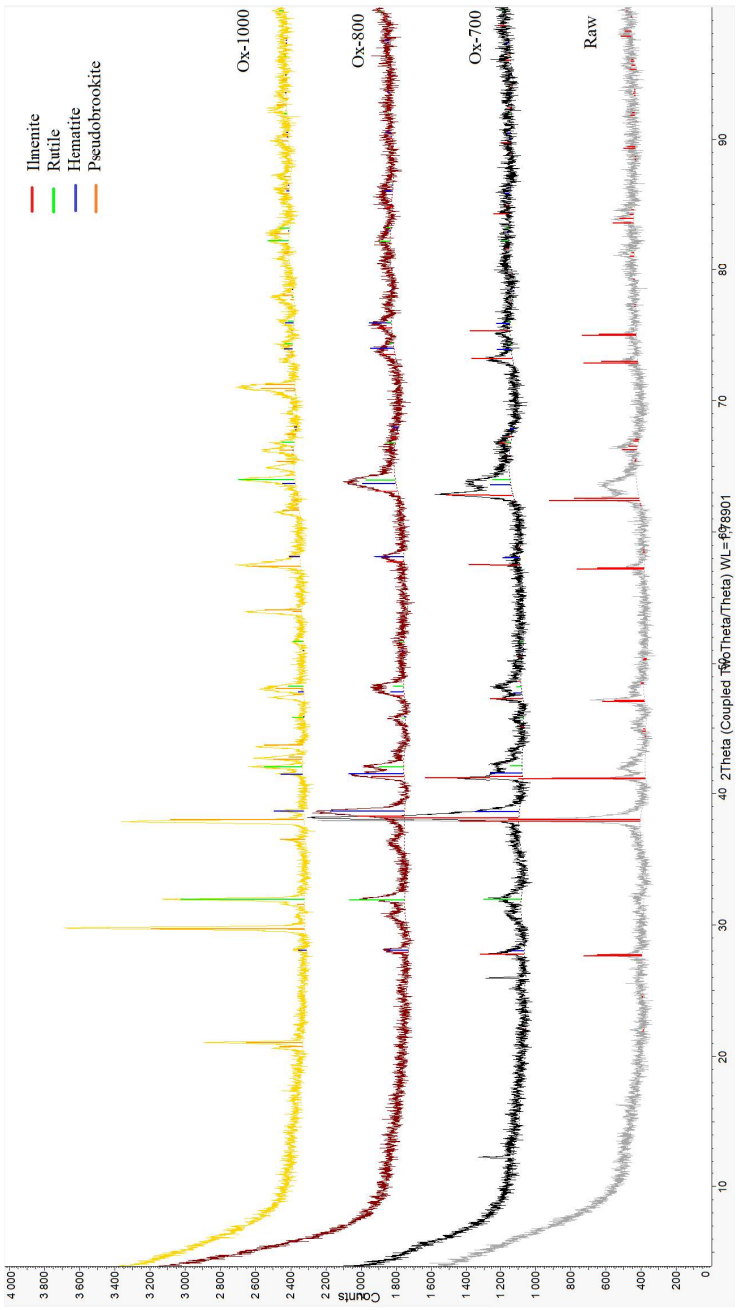

Figure B.2: XRD-results analyzed with the Crystallography Open Database(COD) for as-received GCO sample and different oxidation temperatures.

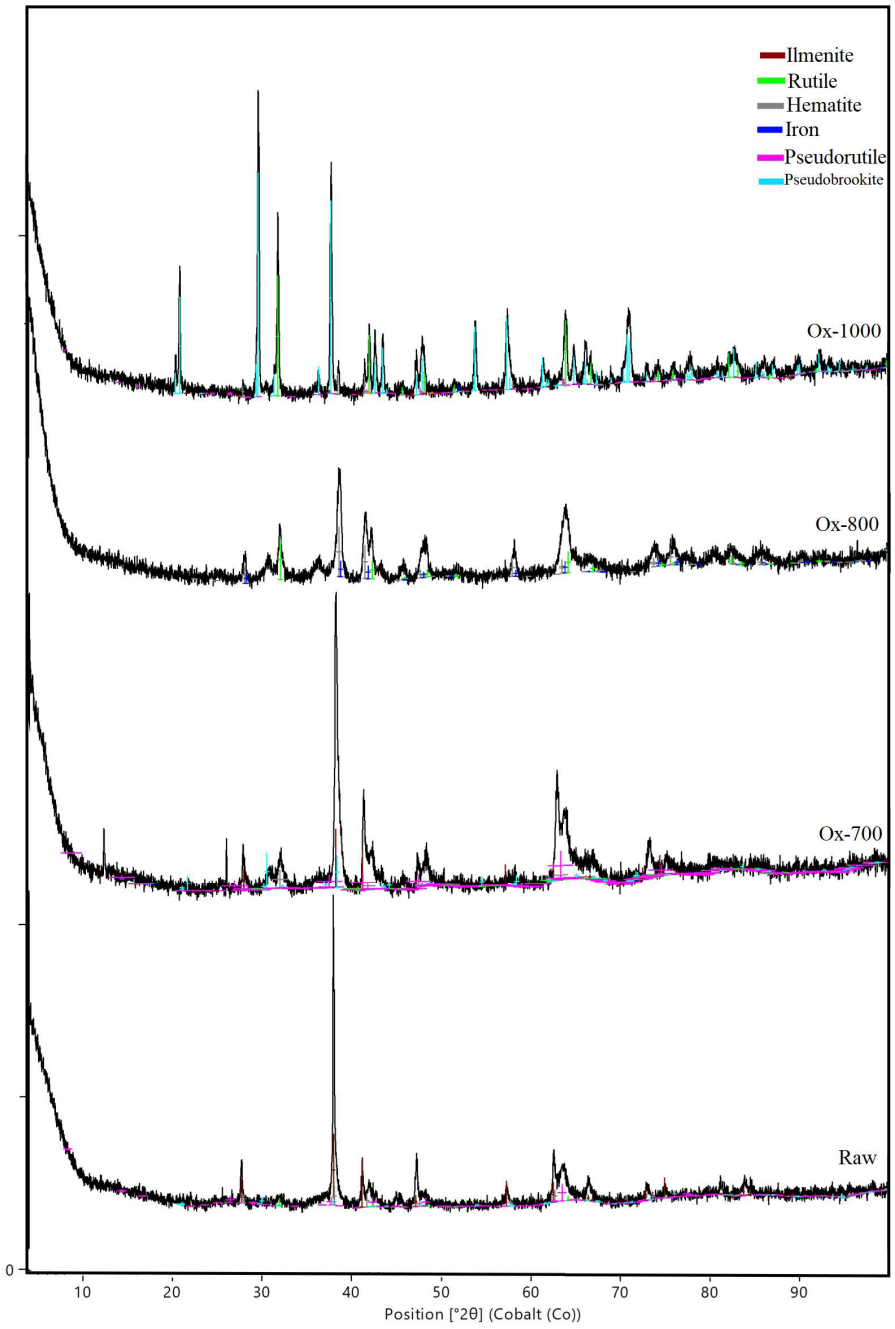

Figure B.3: XRD-results analyzed with the PDF-4), for as-received GCO sample and different oxidation temperatures.

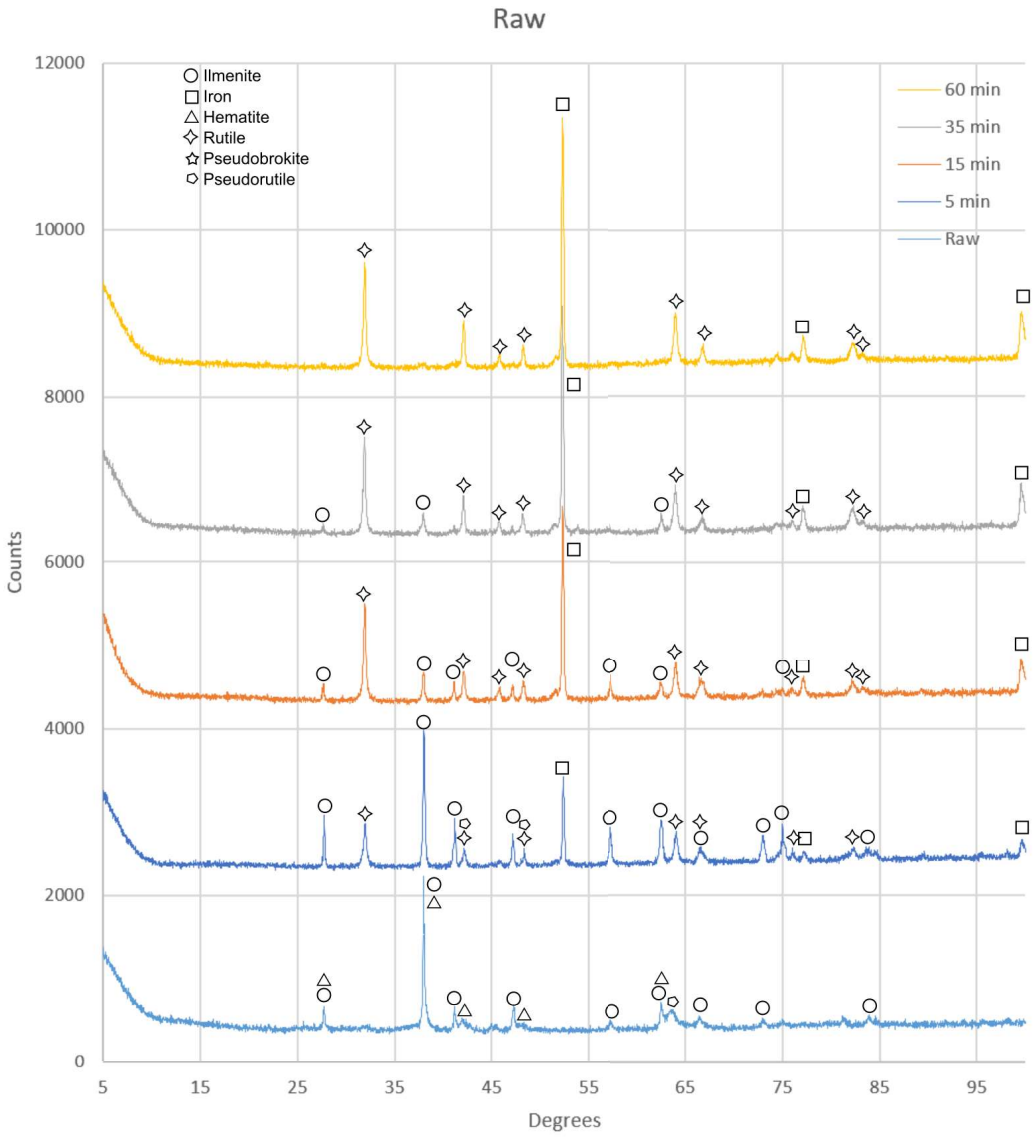

Figure B.4: XRD-results obtained for reduction of as-received GCO sample, reduced at 800°C.

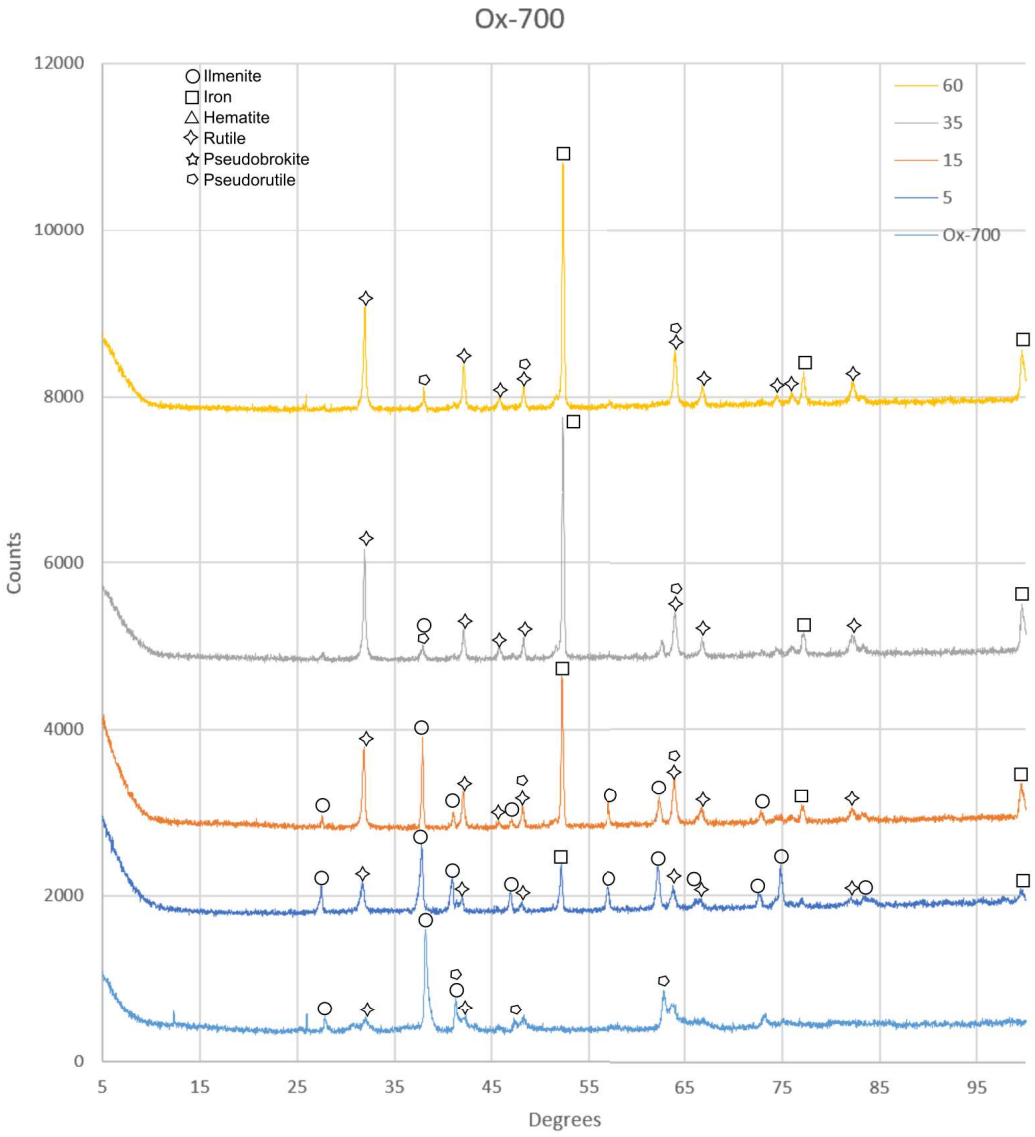

Figure B.5: XRD-results obtained for reduction of GCO sample oxidised at 700°C, reduced at 800°C.

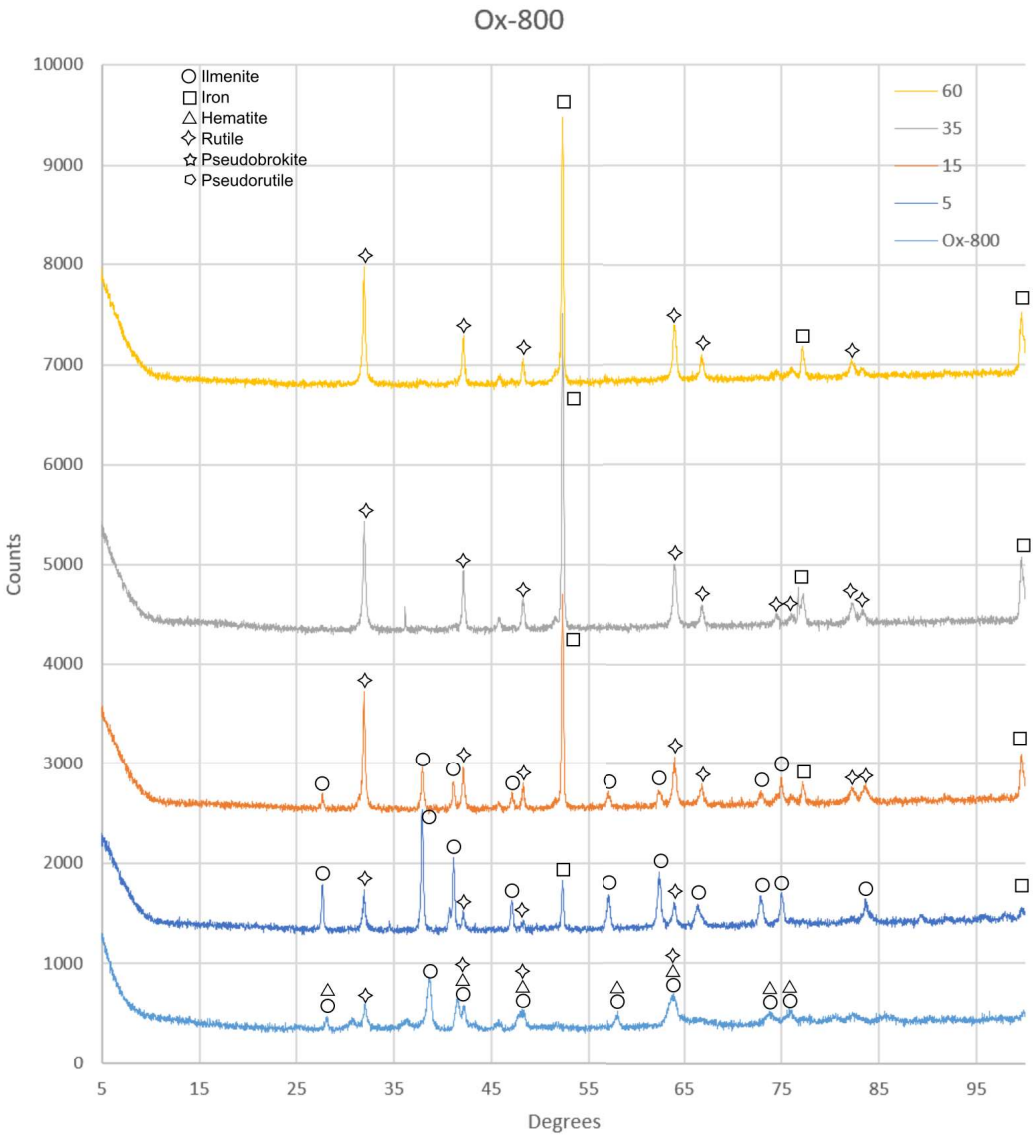

Figure B.6: XRD-results obtained for reduction of GCO sample oxidised at 800°C, reduced at 800°C.

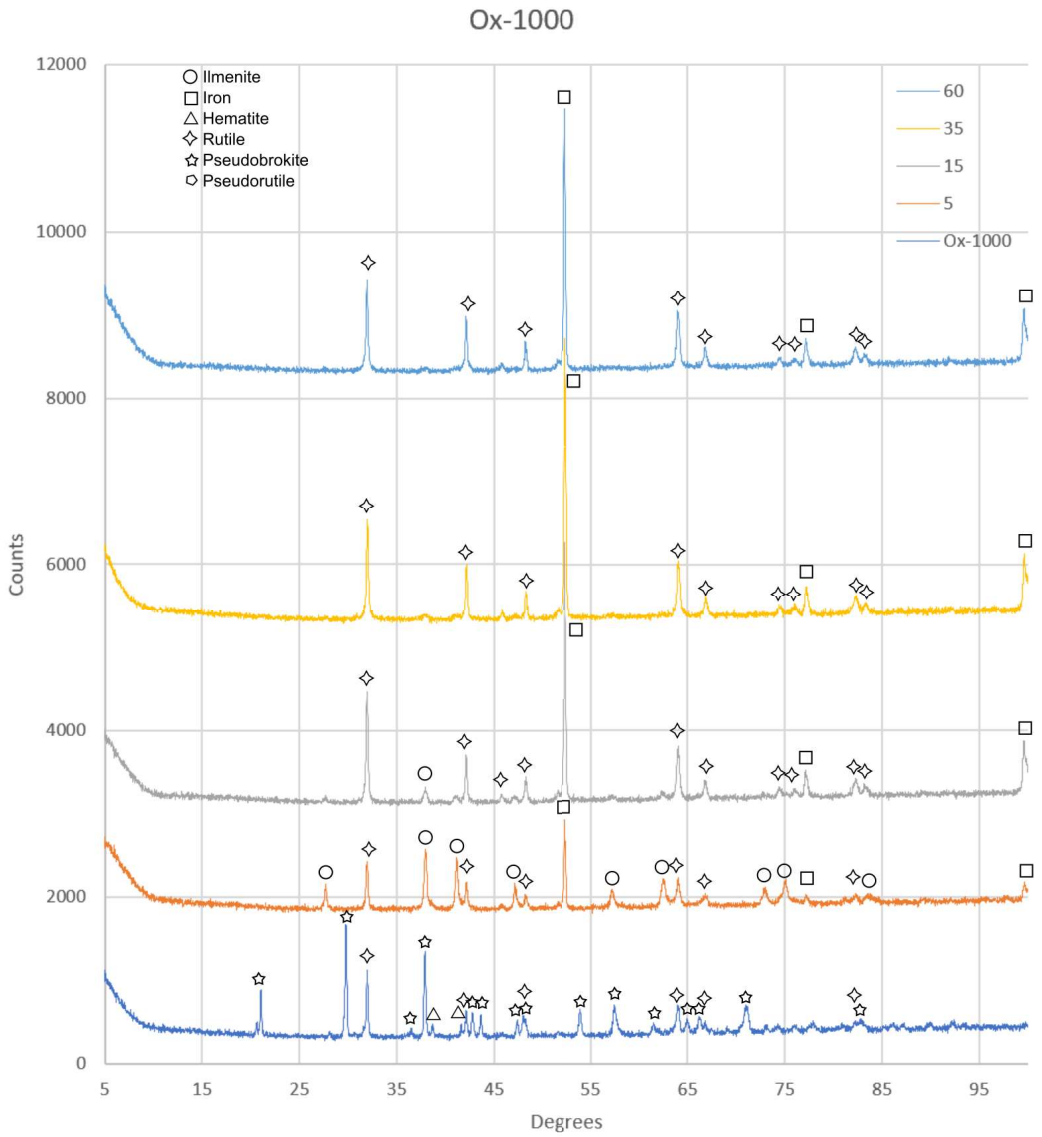

Figure B.7: XRD-results obtained for reduction of GCO sample oxidised at 1000°C, reduced at 800°C.

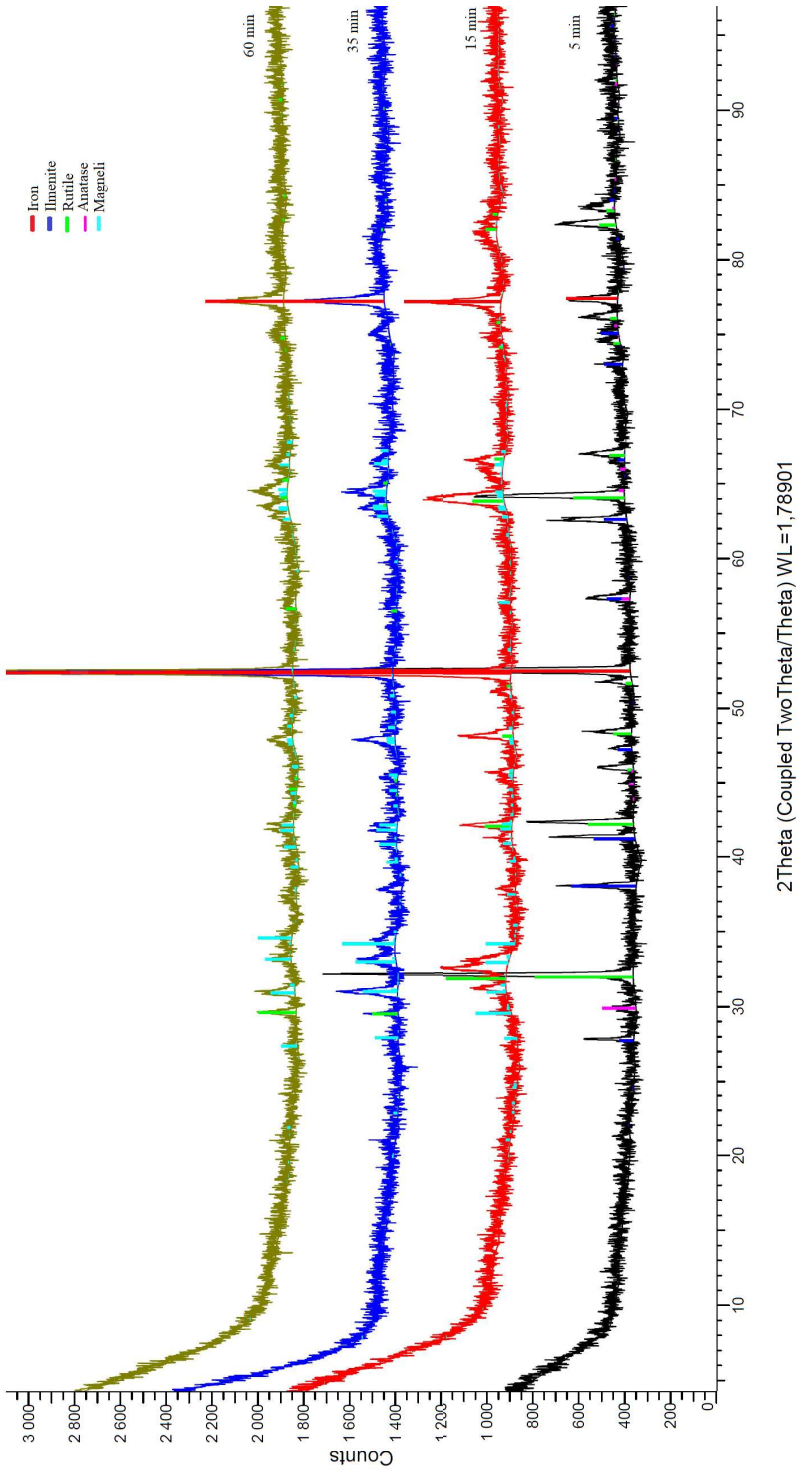

Figure B.8: XRD-results obtained for reduction of as-received GCO sample, reduced at 1000°C.

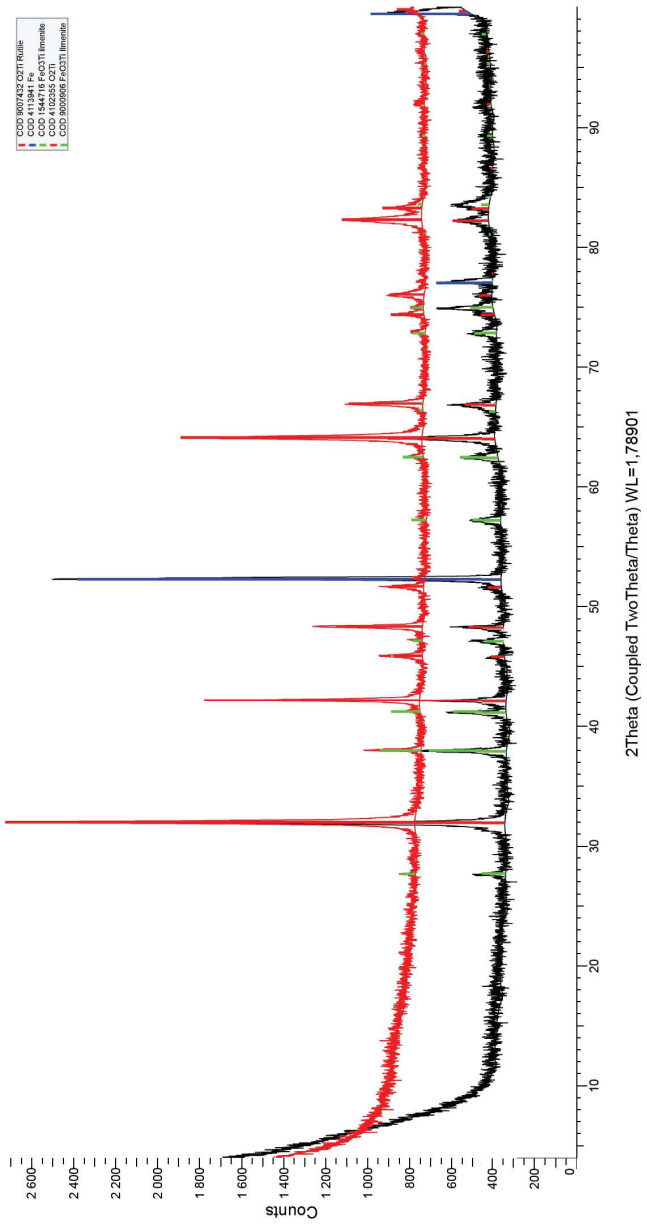

Figure B.9: XRD-results for reduced GCO ilmenite at 800°C for 5 minutes(Black), and leached(Red) for 120 minutes, analysed with the Crystallography Open Database(COD.

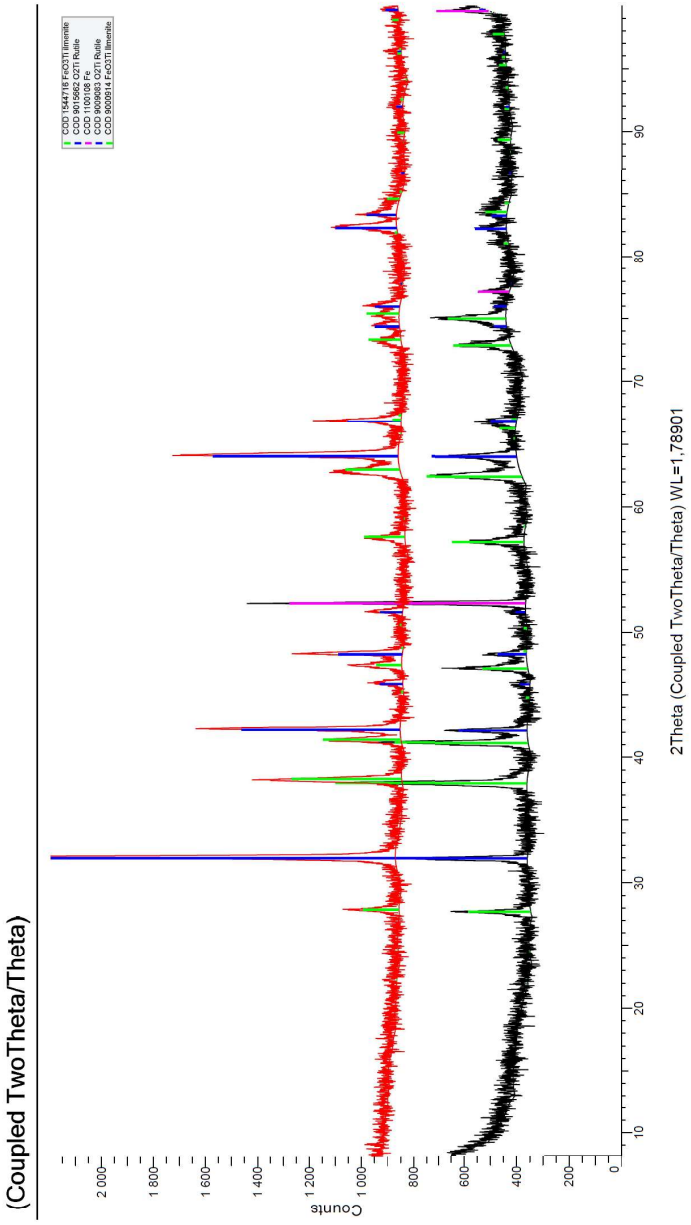

Figure B.10: XRD-results for reduced GCO ilmenite at 1000°C for 5 minutes(Black), and leached(Red) for 120 minutes, analysed with the Crystallography Open Database(COD).

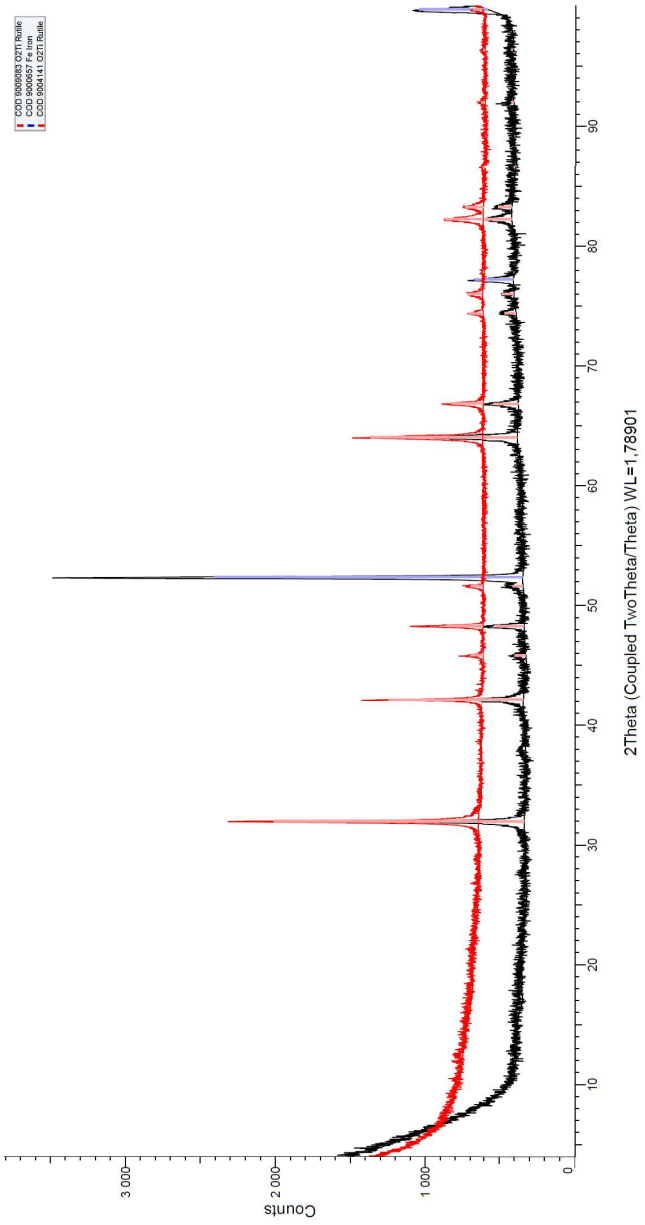

Figure B.11: XRD-results for reduced GCO ilmenite at 800°C for 60 minutes(Black), and leached(Red) for 120 minutes, analysed with the Crystallography Open Database(COD).

C SEM analysis

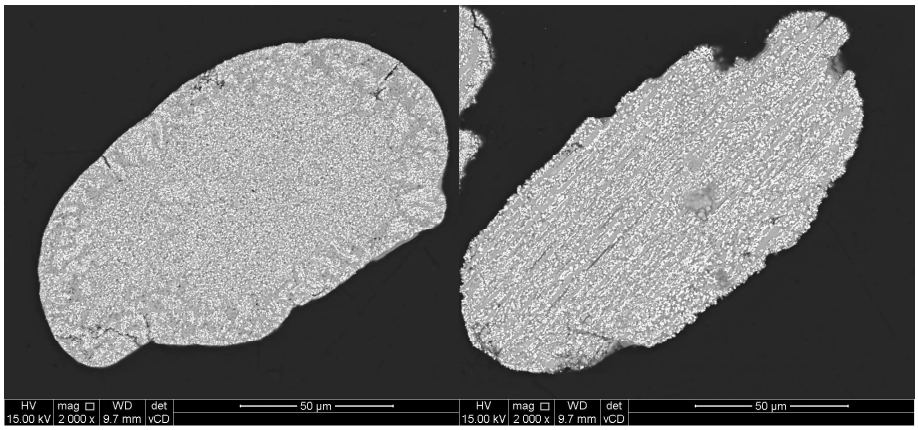

(a) (b)

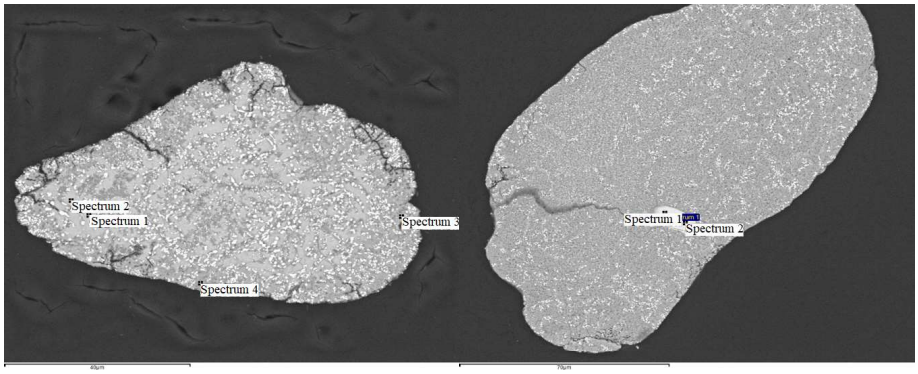

(c) EDS values are shown in Table C.1 (d) EDS values are shown in Table C.2

Figure C.1: Cross-section of grain in GCO ilmenite, oxidised at 1000°, reduced at 800°C for 15 minutes.

Table C.1: EDS analysis for points shown in Figure C.1c).

At%	Ti	Fe	Mn	Mg	Al	O
Spectrum 1	19.8	12.9	0.6	1.2	0.5	65
Spectrum 2	16.75	14.8	0	1.9	0.7	65.9
Spectrum 3	26.2	0.4	0	0	0	73.4
Spectrum 4	29.6	1.5	0	0	0	68.9

Table C.2: EDS analysis for points shown in Figure C.1d).

At%	Ti	Fe	Si	Al	Zr	C	O
Spectrum 1	1	0.4	6.7	0.3	7.1	46.4	38.1
Spectrum 2	0.8	0.2	8	0	8.5	41.5	41.1

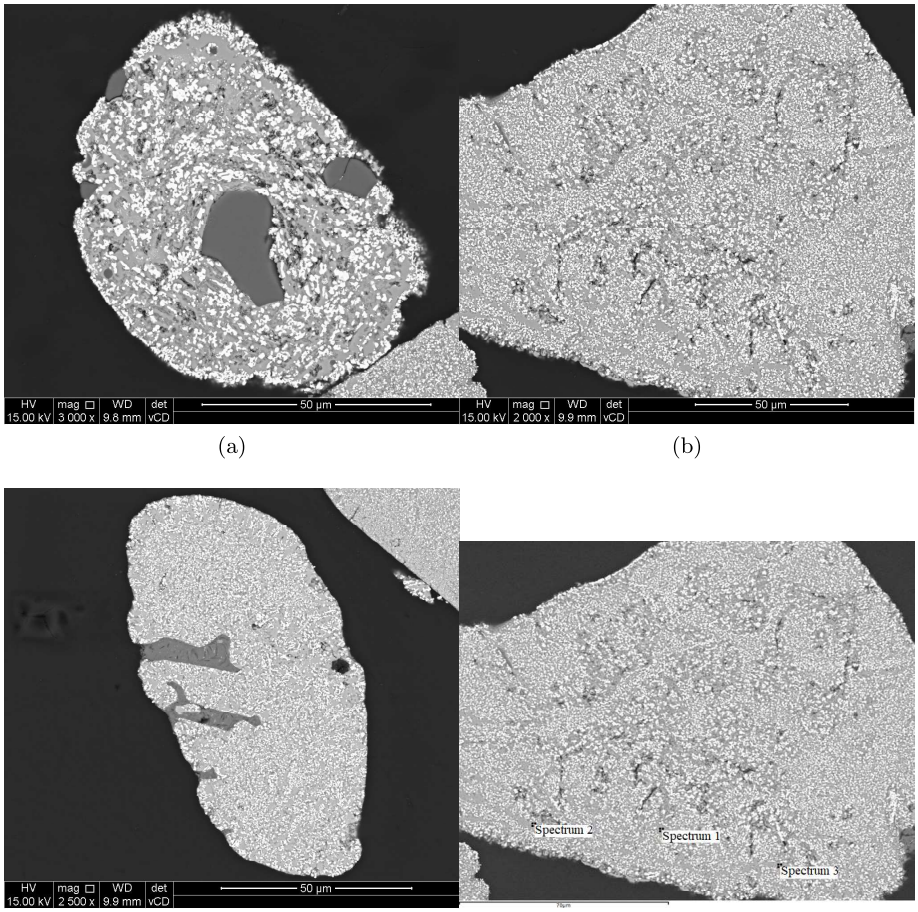

(a) (b)

(c) (d) EDS values are shown in Table C.3

Figure C.2: Cross section of grain in GCO ilmenite, oxidised at 1000°, reduced at 800°C for 28 minutes.

Table C.3: EDS analysis for points shown in Figure C.2d).

At%	Ti	Fe	Mn	O
Spectrum 1	29.3	0.9	0	69.9
Spectrum 2	26.1	5.7	0.5	67.8
Spectrum 3	28.9	0.8	0.2	70.1

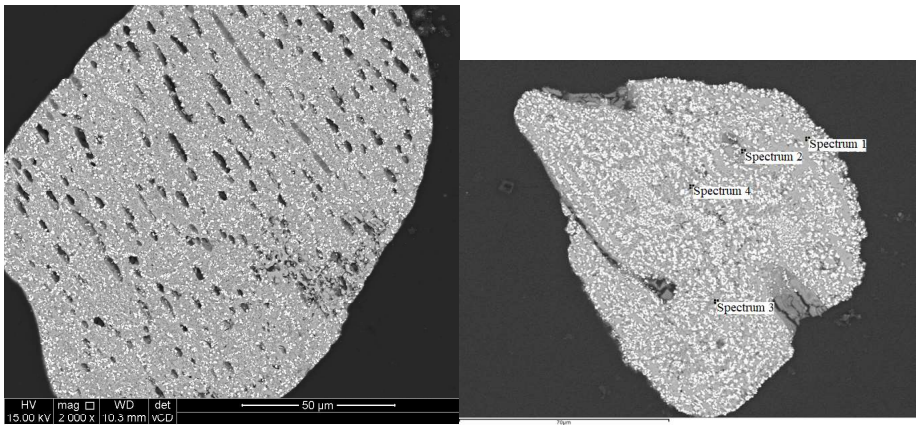

(a) (b) EDS values are shown in Table C.4

Figure C.3: Cross section of grain in GCO ilmenite, oxidised at 1000°, reduced at 800°C for 60 minutes.

Table C.4: EDS analysis for points shown in Figure C.3b).

At%	Ti	Fe	Mn	Mg	Al	Si	K	Na	O
Spectrum 1	29.4	0.4	0	0	0	0	0	0	70.3
Spectrum 2	4.3	8.4	0.5	0.7	7.3	15.6	0.4	0.31	62.6
Spectrum 3	29.2	3.81	0	0	0	0	0	0	67
Spectrum 4	28.6	6.1	0.3	0.4	0	0	0	0	64.7

In Figure C.4, one can see that for the as-received and 700°C oxidation grains the variance is greater than for the 800°C and 1000°C oxidized samples. One particular point of interest can be seen in Figure C.4e) and f), where a lamellar-like structure can be seen. From the EDS analysis, one can see that the brighter phases have a high concentration of iron in relation to the darker phases which have a Ti:Fe ratio of 0.7. Further analysis of the topology of the KZN ilmenite, which is presented in Appendix C, was conducted.

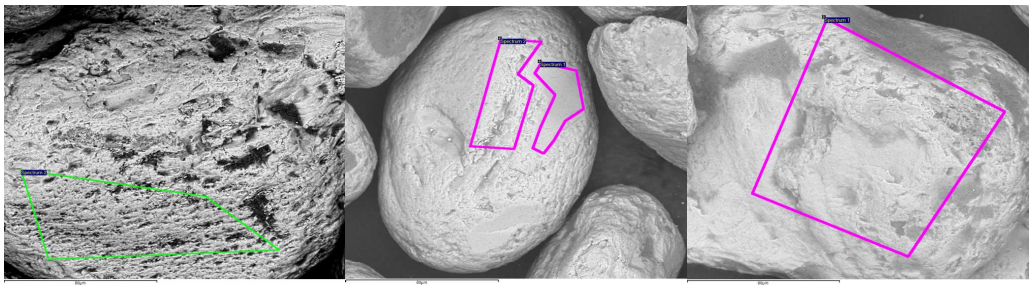

(a) As-received (b) As-received (c) As-received

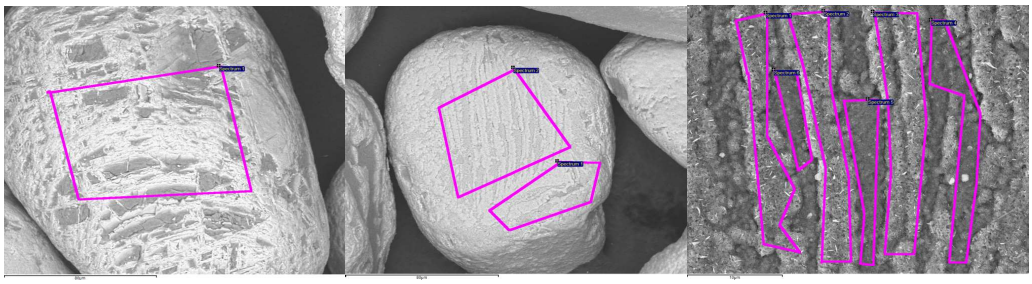

(d) Oxidised at 700°C (e) Oxidised at 700°C (f) Oxidised at 700°C

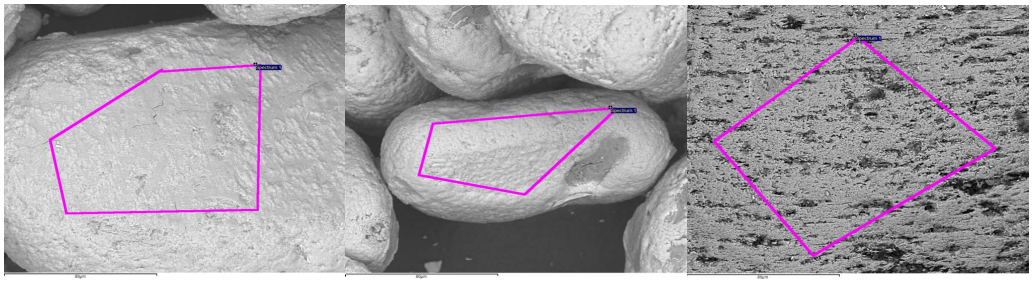

(g) Oxidised at 800°C (h) Oxidised at 800°C (i) Oxidised at 800°C

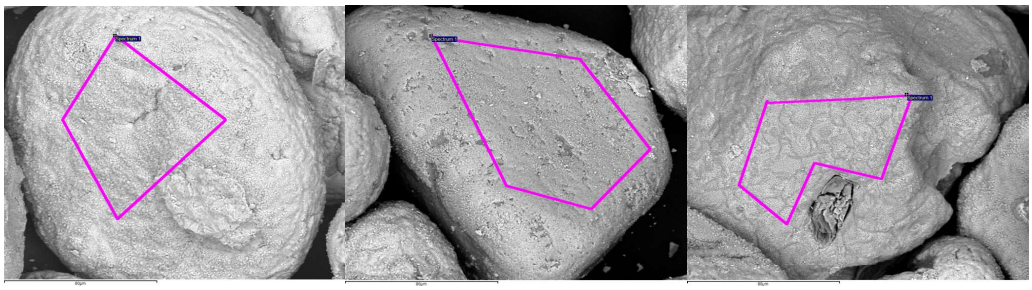

(j) Oxidised at 1000°C (k) Oxidised at 1000°C (l) Oxidised at 1000°C

Figure C.4: Topology changes for KZN ilmenite during oxidation at different temperatures.

Table C.5: EDS analysis of the as-received KZN ilmenite, Figure C.4a)-c).

As-received, At%	Ti	Fe	Si	Al	O
a), Spectrum 1	6.4	29.8	2.9	1.5	59.5
b) Spectrum 1	30.1	13.9	0	0	55.9
b) Spectrum 2	21.7	15.7	1.8	0	60.9
c) Spectrum 1	15.4	15.1	2.1	1.6	65.8

Table C.6: EDS analysis of the 700°C oxidised KZN ilmenite, Figure C.4d)-f).

Ox-700°C, At%	Ti	Fe	Mg	Si	Al	O
d) Spectrum 1	2.5	21.3	1.1	5.0	3.2	67
e) Spectrum 1	6.1	24	0	0.5	0	69.4
e) Spectrum 2	7	25	0	0	0	68
f) Spectrum 1	2.6	30.3	0	0	0	67.1
f) Spectrum 2	2.3	34.1	0	0	0	63.6
f) Spectrum 3	3.7	32.2	0	0	0	64.2
f) Spectrum 4	11.6	17.2	0.6	0.7	0	69.9
f) Spectrum 5	11.6	15.8	0.7	1.0	0	17.9
f) Spectrum 6	12.4	18.3	0	0.5	0	68.8

Table C.7: EDS analysis of the 800°C oxidised KZN ilmenite, Figure C.4g)-i).

Ox-800°C, At%	Ti	Fe	Si	Al	O
g) Spectrum 1	8.3	14.7	0.6	0	76.5
h) Spectrum 1	8.8	23.6	0	0	67.6
i) Spectrum 1	6.1	27	1.9	1.2	63.8

Table C.8: EDS analysis of the 1000°C oxidised KZN ilmenite, Figure C.4j)-l).

Ox-1000°C, At%	Ti	Fe	Si	Al	Mg	O
j) Spectrum 1	21.7	20.7	0	0	0	57.5
k) Spectrum 1	9.5	10.3	0.8	2.7	0	76.7
l) Spectrum 1	0	21.4	5.8	5	8.1	59.8

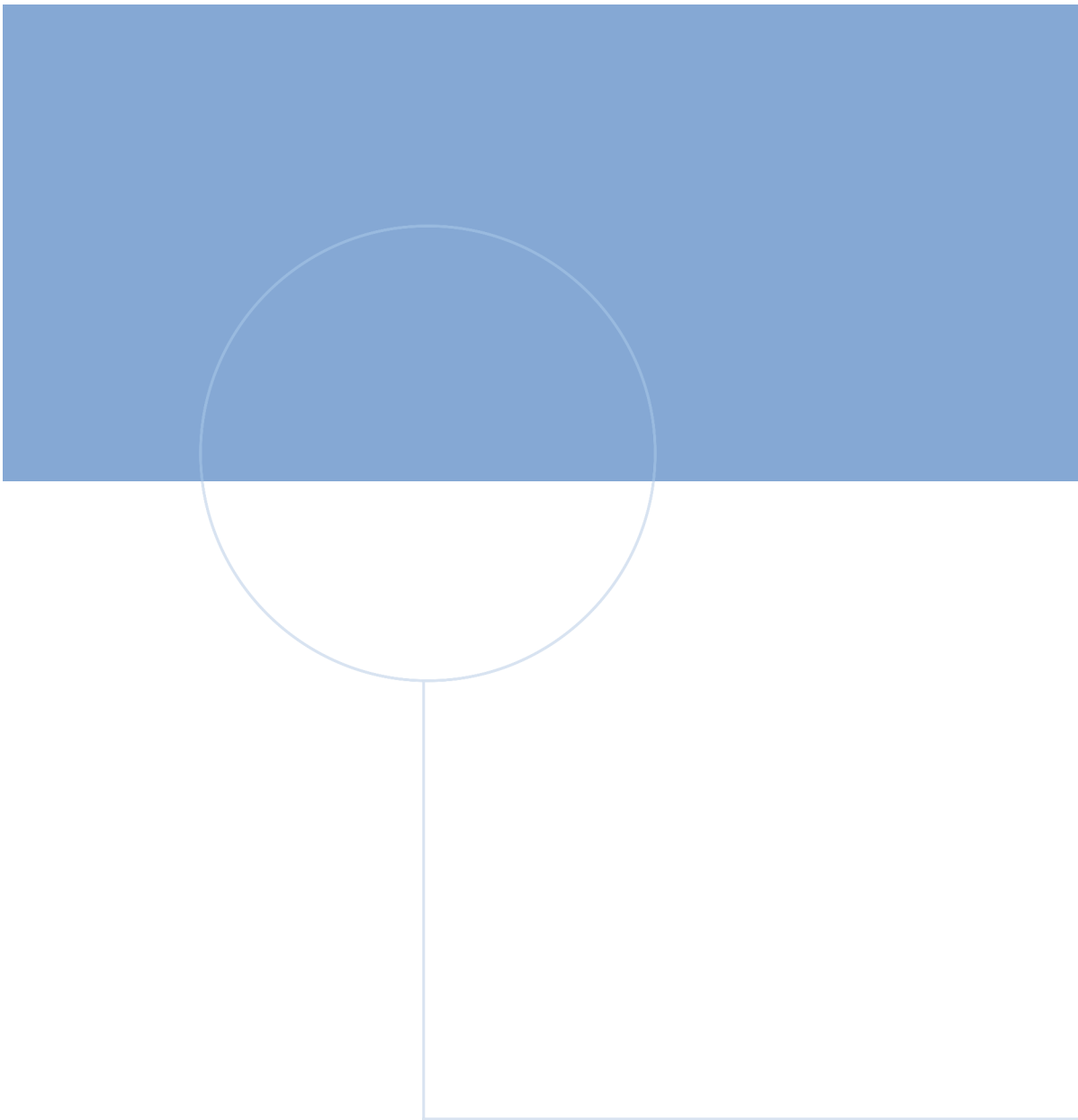

NTNU

Norwegian University of
Science and Technology